UQAC
Université du Québec
à Chicoutimi

A SOUND INSULATION PREDICTION MODEL FOR WOODEN BUILDINGS USING ARTIFICIAL NEURAL NETWORKS APPROACH

BY

MOHAMAD BADER EDDIN

Direction:
Sylvain Ménard, Ph.D., Eng. - Professor, Department of applied sciences, UQAC

Codirection:
Delphine Bard Hagberg, Ph.D. - Associated professor, KU Leuven, Belgium

Codirection:
Jean-Luc Kouyoumji, Ph.D., Eng - Doctor, FCBA, France

THESIS PRESENTED TO THE UNIVERSITY OF QUEBEC AT CHICOUTIMI WITH A VIEW TO OBTAINING THE DEGREE OF PHILOSOPHIAE DOCTOR (Ph.D.) IN ENGINEERING

26 June 2023

Jury members:

Jean Perron	Professor	University of Quebec at Chicoutimi	Jury President
Catherine Guigou Carter	Doctor	CSTB, France	External member
Jianhui Zhou	Associate professor	University of Northern British Columbia	External member
Sylvain Ménard	Professor	University of Quebec at Chicoutimi	Research director
Delphine Bard Hagberg	Professor	KU Leuven, Belgium	Research co-director
Jean-Luc Kouyoumji	Doctor	FCBA, France	Research co-director

Québec, Canada

RÉSUMÉ

Ce projet de recherche vise à développer des modèles de prédiction basés sur des réseaux neuronaux artificiels (ANN) pour estimer les courbes d'isolation acoustique pour différentes structures en bois léger dans des bandes d'un tiers d'octave (50 Hz − 5000 Hz). Deux modèles ont été conçus pour déterminer les performances d'isolation des constructions légères en bois, telles que les planchers et les façades, sur la base de mesures en laboratoire. Le troisième modèle a été développé pour simuler les performances acoustiques des planchers à base de bois lamellé-croisé (CLT) dans des bâtiments réels. Ces modèles intègrent les caractéristiques physiques et géométriques de chaque structure en tant que paramètres d'entrée et utilisent une analyse d'attribution pour déterminer les paramètres les plus importants pour la prédiction de l'isolation acoustique.

Le premier modèle ANN a été créé pour calculer les performances acoustiques des planchers légers en bois pour l'isolation des bruits aériens et des bruits d'impact. Il est basé sur 252 courbes de mesure en laboratoire, qui prennent en compte les caractéristiques physiques et géométriques de chaque plancher. Le modèle le plus précis est celui pour prédire l'indice de réduction des bruits aériens R_w, avec une erreur de 2 dB au maximum, tandis que l'erreur atteignait 5 dB dans le pire des cas pour le niveau de pression acoustique d'impact normalisé pondéré $L_{n,w}$. La précision du modèle a été affectée par les variations à proximité des zones de fréquences fondamentales et critiques. Pour déterminer les facteurs les plus influents dans la prévision de l'isolation acoustique, une analyse d'attribution des caractéristiques a été menée. L'épaisseur des matériaux d'isolation, la densité des dalles en bois lamellé-croisé et des chapes flottants en béton, ainsi que la densité totale des structures de plancher se sont révélées être les paramètres les plus importants.

Le deuxième modèle basé sur un réseau neuronal artificiel a été développé pour évaluer les performances acoustiques des murs de façade en bois en ce qui concerne l'isolation contre les bruits aériens. Il est basé sur 100 mesures de courbes d'isolation de laboratoire comme paramètres d'entrée. Le modèle s'est avéré précis dans la prévision de la réduction des bruits aériens, avec une différence maximale de 3 dB dans l'indice pondéré de réduction des bruits aériens (R_w). Une analyse de sensibilité a été menée, qui a révélé que l'épaisseur des façades et la densité totale des couches extérieures étaient des facteurs clés pour la précision du modèle.

Le troisième modèle de réseau de neurones a été développé pour prédire les différences de niveau normalisées et les niveaux de pression acoustique d'impact normalisés des systèmes de planchers multicouches en CLT, à l'aide de données provenant de 104 mesures acoustiques effectuées dans 15 bâtiments différents en Europe. Ce modèle tient compte de divers paramètres structurels tels que les composants du plancher, les types de murs environnants, les types de jonctions et leurs couches intermédiaires viscoélastiques, ainsi que le volume de la pièce réceptrice et la surface de séparation. Le modèle a démontré une précision satisfaisante dans la prévision des courbes normalisées

d'isolation aux bruits aériens et aux bruits d'impact pour toutes les fréquences, avec une variation maximale de 1 dB pour les différences de niveau normalisées pondérées D_{nTw} et jusqu'à 2 dB pour le niveau de pression acoustique d'impact normalisé pondéré L'_{nTw}. Une étude de sensibilité a révélé que le trajet direct du son à travers le sol était le facteur le plus influent, suivi par les trajets latéraux, le volume de la pièce réceptrice s'avérant être un facteur critique pour les estimations.

ABSTRACT

This research project aims to develop prediction models based on artificial neural networks (ANN) to estimate the sound insulation curves for different wood assemblies in one-third octave bands (50 Hz – 5000 Hz). Based on laboratory measurements, two models have been designed to determine the insulation performance of lightweight wooden constructions, such as floors and façades. The third model was developed to simulate the acoustic performance of CLT-based floors in field conditions in real buildings. These models incorporate each structure's physical and geometric characteristics as input parameters and use feature attribution analysis to ascertain the most important parameters for sound insulation prediction.

The first ANN model was created to calculate the acoustic performance of lightweight wooden floors for airborne and impact sound insulation. It is based on 252 laboratory measurement curves considering each floor's physical and geometric characteristics. The model is more precise in predicting the airborne sound reduction index R_w, with an error of 2 dB at maximum, while the error was up to 5 dB in the worst case for the weighted normalized impact sound pressure level $L_{n,w}$. The variations near fundamental and critical frequency areas affect the model's accuracy. A feature attribution analysis is conducted to determine the factors most influential in predicting sound insulation. The thickness of insulation materials, the density of cross-laminated timber slabs and concrete floating floors, and the total density of floor structures are the most notable parameters that follow the mass law.

The second artificial neural network-based model is developed to evaluate the acoustic performance of lightweight wooden façade walls for airborne sound insulation. It is based on 100 insulation curve measurements and uses laboratory data from the façade walls as input parameters. The model proves to be accurate in predicting airborne sound reduction, with a maximum difference of 3 dB in the weighted airborne sound reduction index (R_w). Then a sensitivity analysis is conducted, revealing that the thickness of the façades and the total density of the exterior layers are critical factors for the model's accuracy.

The third neural network model was developed to predict the standardized level differences and standardized impact sound pressure levels of multi-layered, cross-laminated timber (CLT)-based floor systems, with data taken from 104 acoustic measurements from 15 different buildings in Europe. The network model accounted for various structural parameters such as floor components, surrounding wall types, junction types, visco-elastic interlayers, the volume of the receiving room, and the surface separating area. The model demonstrated satisfactory accuracy in predicting the standardized airborne and impact sound insulation curves across all frequencies, with a maximum variation of 1 dB for the weighted standardized level differences D_{nTw} and up to 2 dB for the weighted standardized impact sound pressure level L'_{nTw}. The sensitivity study revealed that the direct sound path through the floor is the most influential factor, followed by flanking paths, with the volume of the receiving room being found to be a

critical factor for estimations.

TABLE OF CONTENTS

LIST OF TABLES

LIST OF FIGURES

LIST OF ABBREVIATIONS

AI	Artificial Intelligence
ANN	Artificial Neural Networks
ASTM	American Society for Testing and Materials
CEN	European Committee for Standardization
CLT	Cross-Laminated Timber
DL	Deep Learning
FEM	Finite Element Method
IG	Integrated Gradients approach
ISO	International Organization for Standardization
ML	Machine learning
MSE	Mean-Square-Errors
RMSE	Root-Mean-Square-Errors
ReLU	Rectified Linear Function
SEA	Statistical Energy Analysis

LIST OF DISCRIPTORS

Symbol	Description	Unit
τ	Sound power transmission coefficient	$--$
P_S	Incident sound power	Watt
P_E	Transmitted sound power	Watt
$\tilde{P}_S$	Sound pressure in the receiving room	Pa
S	Surface area of the partition	m^2
ρ	Air density	kg/m^3
c	Sound velocity	m/s
A_E	Equivalent absorption area	m^2
R	Sound transmission loss	dB
L_S	Sound pressure level in the source room	dB
L_E	Sound pressure level in the receiving room	dB
V	Volume of the receiving room	m^3
T_{60}	Reverberation time in the receiving room based upon the first 60 dB of decay	s
T_{30}	Reverberation time in the receiving room based upon the first 30 dB of decay	s
T_{20}	Reverberation time in the receiving room based upon the first 20 dB of decay	s
α_i	Absorption coefficient	$--$
$R^{'}$	Apparent sound reduction index	dB
D	Difference in the sound pressure level between source and receiving rooms	dB
D_{nT}	Standardized level deference	dB
D_{nTw}	Weighted standardized level deference	dB
T_0	The reference reverberation time	s
R_w	Weighted sound reduction index	dB
C	A-weighted pink noise spectrum	dB
C_{tr}	A-weighted urban traffic noise spectrum	dB
P_r	Reflected sound power	Watt
K_B	Bending wave number	m^{-1}
m	Mass per unit area	kg/m^2
υ	Partition velocity	m/s
t	Sound transmission coefficient	$--$
r	Sound reflection coefficient	$--$
λ	Incident sound wave length	m
λ_B	Bending sound wave length of a partition	m
f_{cr}	Critical frequency of a partition	Hz
ϑ_{cr}	Critical incident sound wave angle	degree

Symbol	Description	Unit
$B^{'}$	Bending stiffness per length	N /m
η	Material loss factor	−−
$\overline{\tau}$	Average sound power transmission coefficient	−−
s	Static stiffness	N/m
$\tilde{P}_i$	Sound pressure between partitions	Pa
ω_0	Natural frequency	degree/s
f_0	Resonance frequency	Hz
L_n	Normalized impact sound pressure level	dB
M_s	Surface density	kg/m^2
h	Thickness of a slab	m
ρ_s	Density material	kg/m^3
E	Young's modulus of elasticity	N/m^2
$L_{n,w}$	Weighted normalized impact sound pressure level	dB
A_0	Reference equivalent absorption area	m^2
L_{nT}	Standardized impact sound pressure level	dB
$L^{'}_{nT}$	Weighted standardized impact sound pressure level	dB
TL	Sound transmission loss	dB
STC	Sound transmission class	−−
IIC	Impact insulation class	−−

ACKNOWLEDGEMENTS

I wish to express my graduate to my supervisor Prof. Sylvain Ménard and my co-supervisors Prof. Delphine Bard, and Dr. Jean-Luc Kouyoumji without whose continual encouragement, interest, and guidance this dissertation would never have been completed. I would like to express my appreciation to Dr. Nikolaos-Georgios Vardaxis for his guidance and involvement at the very beginning of my research project. Many thanks to Dr. Klas Hagberg for providing an opportunity to participate in on-site acoustic measurements in Sweden. I would also like to thank the member of the jury Prof. Duygu Kocaefe and Prof. Jean Perron, Dr. Catherine Guigou Carter, Prof. Jianhui Zhou for their guidance and evaluation of my thesis.

I am grateful to Prof. Pierre Blanchet, director of CIRCERB, Pierre Gagné, Jenny McKenzie, and Guylaine Bélanger, CIRCERB, and MRQ, for their administrative procedure support. Many thanks also go to MFFP for financing my participation in several conferences. I want to thank Yannick Bidon and Myriam Drouin for their collaboration and assistance in writing scientific vulgarization articles.

Special thanks to the industrial partners Sylvain Gagnon Dr. Cheng Qian, and Anes Omeranovic at FPInnovations for allowing me to be part of their experimental tests and for sharing their acoustic reports and industrial perspectives to complete this project.

I had the pleasure of collaborating with Jonathan Michael Broyles and Samantha Leonard, The Pennsylvania State University, USA, to publish conference papers and have informative meetings about sustainability and acoustics. I would like to recognize the valuable discussion with Erik Nilsson about my research project during his stay in Quebec.

Thanks should also go to my colleagues in our research team, Cheng, Minh-Van, Axel, Etienne, Erik, and Marie-Laure at Chicoutimi. I am also thankful to my friends in Syria and Europe for their continuous support and encouragement.

My worm thanks and jasmine-linden-scented kisses to the one in whose eyes my blue haven of peace and tranquility lies: my dear mother. I would like to express my love and gratitude to you until the seas dry up. To my first English teacher and the ocean of knowledge who has long been quenching my thirst of knowledge, my father. I am most grateful to my brothers for their keenness in assisting me and sharpening my desire to work hard.

Thank you all !

SCIENTIFIC PUBLICATIONS

Peer-reviewed journal articles

-Bader Eddin M, Ménard S, Bard Hagberg D, Kouyoumji J-L. Modeling Field Measurements of Sound Insulation For Multi-layered CLT-based Floor Systems: A Means of a Prediction Model Using Artificial Neural Networks. Building and Environment. 2023. https://doi.org/10.1016/j.buildenv.2023.110561.

-Bader Eddin M, Vardaxis N-G, Ménard S, Bard Hagberg D, Kouyoumji J-L. Prediction of Sound Insulation Using Artificial Neural Networks—Part II: Lightweight Wooden Façade Structures. Applied Science. 2022, 12, 6983. https://doi.org/10.3390/app12146983.

-Bader Eddin M, Ménard S, Bard Hagberg D, Kouyoumji J-L, Vardaxis N-G. Prediction of Sound Insulation Using Artificial Neural Networks—Part I: Lightweight Wooden Floor Structures. MDPI Acoustics 2022, 4, 203-226. https://doi.org/10.3390/acoustics4010013.

Conference articles

-Bader Eddin M, Ménard S, Bard Hagberg D, Kouyoumji J-L. Acoustic Sensitivity Analysis and Modeling of Sound Insulation Performance of Lightweight Wooden Structures. In WCTE 2023 June 19.-22. Oslo, Norway.

-Leonard S, Bader Eddin M, Prichard M, Broyles J, Brown N, Ménard S. Trade-off Between Embodied Carbon and Acoustic Insulation for Mass Timber Floor Assemblies. In WCTE 2023 June 19.-22. Oslo, Norway.

-Bader Eddin M, Menard S, Bard Hagberg D, Kouyoumji J-L, Vardaxis N-G. Acoustic Modeling of Airborne Sound Insulation of Wooden Façade Systems using artificial Neural Networks. In Woodrise Conference Proceedings 2022, Portoroz, Slovenia.

-Bader Eddin M, Menard S, Bard Hagberg D, Kouyoumji J-L, Vardaxis N-G. Sound Insulation of Lightweight Wooden Floor Structures: ANN Model and Sensitivity Analysis. In INTER-NOISE and NOISE-CON Congress and Conference Proceedings 2022, Institute of Noise Control Engineering: Glasgow, United kingdom.

-Bader Eddin M, Broyles J, Menard S, Bard Hagberg D, Kouyoumji J-L. A Comparison of Numerical Approaches to Quantify Sound Insulation of Lightweight Wooden Floor Structures. In INTER-NOISE and NOISE-CON Congress and Conference Proceedings 2022, Institute of Noise Control Engineering: Glasgow, United Kingdom.

-Bader Eddin M, Menard S, Bard Hagberg D, Kouyoumji J-L, Vardaxis N-G. A Sound Insulation Prediction Model for Floor Structures in Wooden Buildings Using Neural Networks Approach. In INTER-NOISE and NOISE-CON Congress and Conference Proceedings 2021, 583 Institute of Noise Control Engineering: Reston, VA, USA.

Scientific vulgarization

-Bader Eddin M, Bidon Y. Le Bois et la Performance Acoustique. Scientific vulgarization, Le portal du batiment durable au Québec (VoirVert.ca) 2023 January 24.

-Bader Eddin M, Bidon Y. Une Analyse de la Performance Acoustique des Bâtiments en Bois et les Possibilités d'amélioration de ces Performances. Scientific vulgarization, Le journal de la construction commerciale en bois, Cecobois 2022 November 23.

Chapter 1

INTRODUCTION

1.1 Overview

Sound is the omnipresent companion during our entire life. It is everywhere, from the beginning of our day with the alarm clock to the end of it. Even in the quietest place, it is not free of sound. Complete silence is rare, instead gives unpleasant feelings and even could be unbearable. However, noise can be annoying and harm our health and hearing, especially when exposed to high sound pressure levels. Even sound of medium or low density could damage our nerve system caused by sleep irregularity, elevated blood pressure, etc. [1]. A noisy environment has been publicized as one of the most critical risks to health [2]. Although there is no bright-line distinction between noise and another sound, the undesired sound can be defined as noise.

Sound environment plays an essential part in human daily life where people practice their daily routine in their working place or home. In recent years there has been a significant increase in the number of office buildings, factory spaces, and dwellings where acoustics are often concerned. It is acknowledged that reducing noise levels in people's living environment improves life quality. Hence building acoustics science appeared. It refers to the propagation of sounds in buildings and ways to obstruct their transmissions between adjacent rooms or to prevent external noise from penetrating [1]. Legal requirements are defined to cover a wide range of characteristics such as noise levels, airborne, impact sound insulation, and reverberation time. In order to enforce such requirements, relevant measuring procedures must be provided and formulated in

national or international standards. The international standards provided by International Organization for Standardization (ISO) are increasing both in number and covering broader aspects. In Europe, the European Committee for Standardization (CEN) has been very active in developing standards [3]. The cooperation between ISO and CEN under the Vienna Agreement has contributed substantially to the creation of standards of general acceptance.

Controlling the acoustical conditions, including sound insulation, reverberation time, or noise levels in the building, may be a complicated task even for qualified experts. Another challenging task is to have an accurate prediction tool for building acoustics especially in the design stage. Nowadays, several computer-based tools are at the disposal of the building acoustics expert. Those tools are based on standards and experimental tests to estimate the acoustical performance of different assemblies. However, some of these tools have demonstrated non-negligible deviations in the results, each with limitations. Since an appropriate estimation tool is vital, especially in the design stage, the demand for developing a reliable prediction model becomes crucial.

Machine learning and neural network approaches are being acclaimed as the future wave in predictions. They are applied in various fields and sought after in different industries. Their strength lies in being a self-learning mechanism without exclusively being modeled, and the need for human operators is avoidable [5–7].

1.2 Statement of the problematic

Since Canada is primarily forested, wood construction has been one of the most significant interests of the industrial sector. Recently, higher multi-story wooden buildings were allowed by the Canadian building code. Although wooden constructions have many advantages, they are still under development, especially in the noise control aspects when they are compared to heavy structures.

To maintain sufficient indoor acoustic quality, it is essential to use appropriate prediction tools to estimate structural elements' acoustic behavior to improve the indoor climate's quality. Some estimation approaches have been developed to forecast the

sound transmission through multiple structures using different approaches: theoretical ones [8–11], numerical tools [12–16], or artificial intelligent applications [17, 18]. However, significant gaps in results exist in some of those tools [13, 19–22], that need to be considered to improve their reliability.

Developing a reliable prediction tool is a laborious task due to many factors. Uncertainties and variations in sound insulation measurements are usually related to the construction system, workmanship, and measurement implementations. This could be a potential problem for building contractors that require a high safety margin during project decision-making to meet the sound insulation requirements. Qian has investigated the uncertainties in the constructional material properties, such as Young's modulus and shear modulus, and how they could affect the Finite Element Method (FEM) modeling [15]. Zimmermann [23] employed the transfer matrix method to construct a model to calculate airborne sound insulation of single and double walls with interrupted cavities. The results of this model were compared to the most widely used analytical models [23]. The outcomes of the comparison showed agreement in results; however, the developed model only applies to certain types of walls with limited components and, therefore, cannot be generalized to various assemblies.

Moreover, the acoustic performance of tested structures is sometimes varied between laboratory to on-site measurements [26]. Direct sound transmission paths generally control sound insulation measurements in laboratories. However, there will be energy transmitted by walls, ceilings, through cracks, or by common junctions in real buildings [27]. The latter is called sound flanking transmission paths, which could mainly contribute to decreasing the acoustic performance in constructions [3]. Such challenges could limit the potential of developing a reliable prediction model. Nilsson [24, 25] has addressed the flanking airborne transmission by developing models that deal with certain cases of sound reduction for ventilation ducts through walls. Therefore, developing a general and reliable tool capable of overcoming these difficulties is vital.

A direct prediction tool is based on theory-based analytical expressions, including stiffness, mass, and damping [3]. This is reasonable for a single-leaf element but

more complicated for lightweight multi-layered structures. Accurate forecasting of sound isolation performance of multi-layered elements is still a challenging task [3]. Specific details, i.e., structural connections between elements, can scarcely be involved in prediction tools, particularly in analytical approaches [28]. In addition, the diversity of construction materials makes predictions even more complicated since each new assembly must be tested to quantify its acoustic performance. Moreover, the standardized method, which is indicated in ISO 12354 Part 1 [29], is extracted using insulation data of heavy monolithic elements [30]. This is currently not appropriate for lightweight and multi-layered structures [30].

1.3 Aims and objectives

The scope of the research project is to develop Artificial Neural Networks (ANN) models to forecast the sound insulation performance of floor and façade structures. This thesis aims to develop prediction tools to estimate the acoustic performance of floors and façades (based on laboratory measurements) and to predict the insulation curves of different floor structures considering field conditions. The isolation data comprises laboratory and on-site measurements on various lightweight wooden elements.

The first model (Model-I) is developed to forecast the insulation performance of lightweight floor structures using 252 lab-based acoustic curves. Moreover, the second model (Model-II) is utilized to predict the acoustic spectra of façades based on 100 measurements that were implemented in the laboratory. In addition, Model-III is utilized to simulate the field sound insulation of multi-layered CLT-based floor systems. The insulation data comprises 104 on-site measurements (airborne and impact sound insulation) implemented in different real buildings in Europe. Finally, a sensitivity analysis is conducted to explore the relationships between the simulated parameters in the models and how they can contribute to sound insulation estimations.

1.4 The originality of the research

Sound insulation in building acoustics has been considered a matter of public interest. However, many prediction tools have been developed in order to estimate the accurate acoustics performance of wooden structures, but notable gaps in the results are evident. Developing an appropriate prediction tool in building acoustics has always been a crucial issue. Since the estimation of the acoustic performance in building acoustics has gained the attraction of both industrial and research sectors. The literature review at the time of this study did not find any research that attempted to develop an ANN-based model to simulate the field or laboratory sound insulation for wooden structures in the frequency range from 50 Hz to 5000 Hz.

This study will focus on developing a new alternative method for calculating airborne and impact sound insulation based on the artificial neural network approach. The first part of the study focuses on developing a model to simulate the lab-based measurements for floor and façade structures. Then, another network model is developed to model field sound insulation measurements considering different structural parameters.

1.5 Thesis outline and chapters organization

This thesis includes eight chapters; the majority centered around three peer-reviewed articles produced during the research project to attain a Doctorate of Philosophy in Engineering. It commences with an abstract in both English and French (résumé) which outlines the essential findings and is followed by scientific publications (peer-reviewed, conference, and scientific vulgarization articles).

Chapter 1 discusses the thesis overview and the statement of the research project's problematic. The purpose and goals of the project, which are to create a dependable forecasting tool using an artificial neural networks approach, are also established. Additionally, the project's originality, the chapters' arrangement, and the research funding are discussed.

Chapter 2 provides an overview of building acoustics, explaining the principles and

concepts of sound insulation in buildings. It tackles the physics beyond sound propagation and airborne and impact sound insulation measurements. In addition, it reviews the different acoustic prediction tools that were found in the literature, such as theory-based analytical expressions, FEM tools, artificial intelligence models, etc. Since two primary standards are used worldwide: the American Society for Testing and Materials (ASTM) and the International Organization for Standardization (ISO), Chapter 1 briefly reviews both and sheds light on their main differences.

Chapter 3 discusses the concept of artificial intelligence and its branches, along with the supervised and unsupervised learning techniques. Additionally, the fundamentals of artificial neural networks, the process of developing an ANN model, and the overfitting/underfitting issues will be addressed. Furthermore, the sensitivity analysis approach used to evaluate the parameters of ANN models is detailed.

Chapter 4 covers the experimental sound insulation measurements conducted during the research project. Part of the measurements was conducted in the laboratory of Lund University in Sweden and FCBA in France. In addition, the tests consist of field measurements conducted in the research center of FPInnovations in Quebec, Canada, and the north of Sweden. Furthermore, Chapter 4 details the database organization, the sources of the measurements used to develop ANN models, and the standards they followed.

Chapter 5 deals with developing an artificial neural network model to predict the sound insulation performance of different lightweight wooden floors. It starts with a general introduction followed by a detailed explanation of how the database is organized, insulation measurement types, and the standards used to implement those tests. Chapter 5 depicts the prediction results for airborne and impact insulation curves. It demonstrates the relationship between the structural parameters used to develop the model and the estimated results using the feature attribution technique (sensitivity analysis).

Chapter 6 focuses on a neural network model for predicting sound insulation in lightweight wooden façades. It provides information on the sound insulation curves used to create the network model and the database structure for the wall parameters.

Additionally, it displays the sensitivity analysis results and identifies which variables the model depends on for accurate predictions.

In Chapter 7, a field sound insulation prediction tool for CLT-based floors is developed through an artificial neural network approach. The Chapter provides an in-depth look into the field of sound insulation modeling. It shows how laboratory and on-site measurements differ, which had an apparent effect on the outcomes of the sensitivity analysis.

Chapter 8 brings the thesis to a close with a summary of the main findings and the scientific contributions that have been achieved. It also outlines the possible steps to be taken to enhance the network models' accuracy.

1.6 Research funding

This research Is funded by the Natural Sciences and Engineering Research Council (NSERC) of Canada through its IRC and CRD programs (IRCPJ 461745-18 and RDCPJ 524504-18), the Region Nouvelle-Aquitaine (ref. 2017-1R10223) and the industrial partners of the NSERC industrial chair on eco-responsible wood construction (CIRCERB).

Chapter 2

LITERATURE REVIEW

2.1 Building acoustics

Building acoustics is the science of controlling noise inside buildings. It includes minimizing noise transmission from one space to another and controlling sound characteristics within spaces. Sound transmission is a critical nonstructural design consideration for designing walls and floors in multistory buildings, whether designed for residential or commercial purposes. This topic has significant practical importance, which concerns noise control. Noise can penetrate a room from the exterior could have two possible reasons:

1. The airborne sound in a room, such as a speech or operating machine, with respect to the surrounding walls and ceiling, also represents an exciting spatially distributed force. The vibration is also generated in the structures, which eventually radiate sound. That can be summarized by airborne sound - structure-borne sound - airborne sound, which is defined as airborne sound (Figure 2.1 (a)).

2. Direct external forces affect walls and ceilings, such as a neighbor walking on a floor in the apartment above or operating a machine in a building. Such forces induce vibrations, and structure-borne sound develops, which is transported to other floors. These vibrating structures excite the surrounding air and radiate sound. This sound development can be summarized by the term "force - structure-borne sound - airborne sound", which is defined by impact sound (Figure 2.1 (a)).

The afore-mentioned forms of excitation in the rooms of buildings that radiate sound are not necessarily transmitted via the direct path (which leads from the partition wall or ceiling to the adjacent room), see Figure 2.1 (b). The propagation of vibrations can take multiple paths because adjacent ceilings can exchange vibration energy. In addition to the direct transfer path, there are many other transfer paths, called flanking paths (Figure 2.1 (b)). It should be mentioned that it is only possible to determine the dominant path by carrying out measurements first. For example, in a partition wall with high sound insulation, the dominant transmission path is flanking. Therefore, an additional acoustic improvement on the partition wall will not necessarily achieve better results in the total sound insulation.

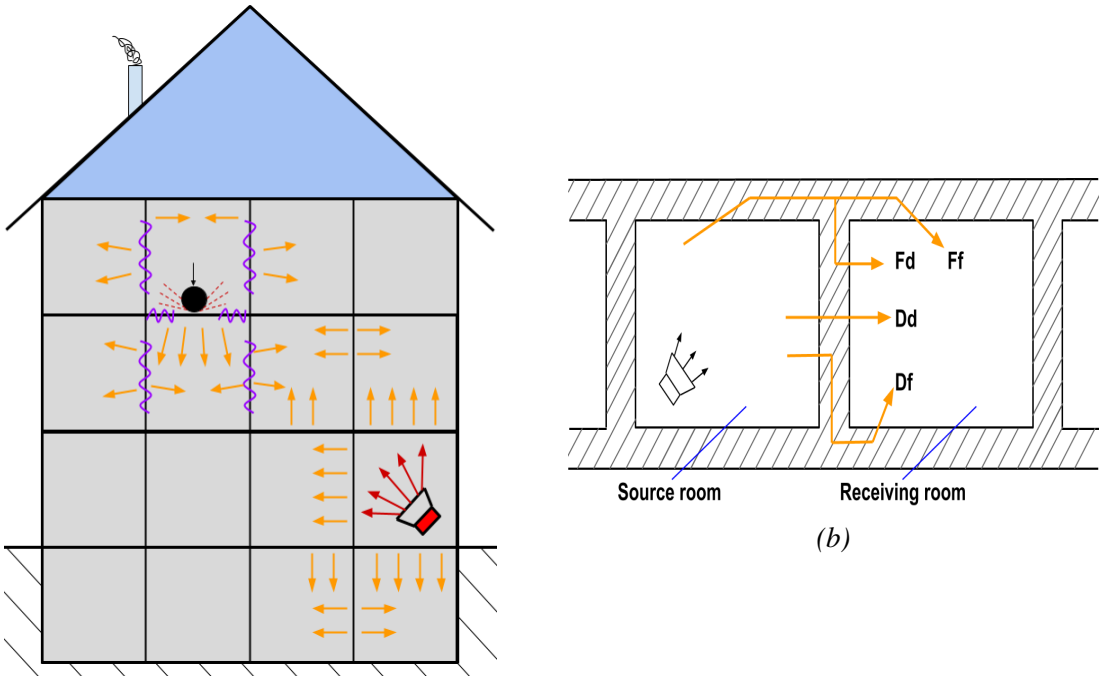

Figure 2.1: The propagation of a sound flux through partitions. (a) Sound generation and its paths inside the building. (b) Sound transfer paths: Ff: flanking–flanking, Fd: flanking–direct, Dd: direct–direct, Df: direct–flanking.

2.2 Measurements of airborne sound insulation

In measuring airborne sound insulation, the measured element is constituted by a partition between two rooms. Airborne sound insulation can be measured directly in a

laboratory or the field. Laboratory measurements follow the procedures that are indicated in ISO 10140-2 (2010) [89] and American Society for Testing and Materials (ASTM) E90-09 (2016) [32], while field ones are implemented according to ISO 16283 (Part 1 & 2) [33, 34] and to ASTM E336 and ASTM E1007 [35, 36]. For laboratory measurement, the lab consists of two adjacent rooms that are separated by a common surface or partition. In airborne measurements, a sound source (speaker) is used in the source room as a source for emitting the noise. White or pink steady noise is usually used for such measurements. The sound pressure levels are measured in several microphone positions with at least four positions, which is implied in two rooms; see Figure 2.2.

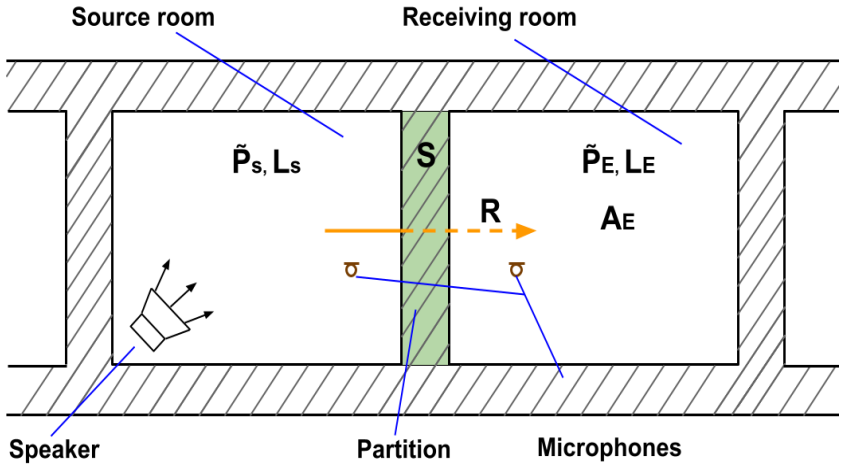

Figure 2.2: Experimental setup for measuring the transmission loss of a partition wall between two rooms.

The sound level pressure in a specific room depends on the sound power incidence and the room's acoustic design. Supposing that only the level differences between the source and receiving room were used as an indicator for sound insulation of a wall (in airborne case), the resulting value would characterize not only the wall attributes but also the room properties. For this reason, the sound power transmission coefficient τ is principally used to describe the wall properties.

$$\tau = P_E / P_S . \tag{2.1}$$

The transmission coefficient represents the power P_E ratio, passing through the receiving side, and the power incidence P_S on the source side. When a diffuse sound field

is assumed on both sides of the partition element, the incident sound power is given by:

$$P_s = \frac{\tilde{P}_S^2 S}{4\rho c}, \tag{2.2}$$

where $\tilde{P}_S$ represents the rms-value (root mean square) of the sound pressure in the source room, S, the surface area of the partition, ρ air density and c is sound speed. Under steady-state conditions, the power inflow in the receiving room is equal to the absorbed sound power:

$$P_E = \frac{\tilde{P}_E^2 A_E}{4\rho c}, \tag{2.3}$$

where A_E represents the equivalent absorption area of the receiving room. So the sound power transmission coefficient:

$$\tau = \frac{\tilde{P}_E^2 A_E}{\tilde{P}_S^2 S}. \tag{2.4}$$

τ is a component of the transmission loss R (also known as the sound reduction index)

$$R = 10log1/\tau = L_S - L_E + 10\,log\,\frac{S}{A_E} \tag{2.5}$$

By definition, a large value of R represents good sound insulation. L_S and L_E are the sound pressure levels in the source and receiving room, respectively. The equivalent absorption area A_E can be derived from Sanbine's fundamental equation as:

$$A_E = \frac{0.161V}{T_{60}}. \tag{2.6}$$

According to Sabine's principle, for an empty room of volume V, the reverberation time (T_{60}) in the receiving room is given by (in SI units). A_E id given by:

$$A_E = \sum_i \alpha_i A_i. \tag{2.7}$$

The summation expresses the total surface area of the room, each element of area A_i characterized by an absorption coefficient α_i. The absorption coefficient is determined

with various components of wall coverings and from the requirement that $\alpha_i = 1$ for an open window.

The reverberation time (T_{60}) is one the most important quantities in building acoustics. If the sound energy in a random room is switched off, the room is gradually emptied. The duration of this process depends on the outlet surface area. Large outlet surface areas result in a quick empty of sound energy, whereas small areas result in a slow empty with a long duration. Reverberation time is defined by the time elapsed for the sound pressure level to decrease by 60 dB or equivalent. In field measurements, and due to high background noise, T_{30}, T_{20} (decay time for 30 and 20 dB respectively) are used [1, 3].

2.2.1 Apparent sound reduction index

As different from the measuring situation in the laboratory and imitating the actual phenomena, the actual situation in a building is the existence of many flanking paths for the sound energy. The sound could be transmitted via flanking constructions, cable ducts, cracks, etc. Certain limiting values of the sound reduction index give the requirements for airborne sound insulation in building acoustics in most countries. The same laboratory procedures are applied for on-site measurements. Instead of equation 2.5, we write:

$$R^{'} = D + 10log\frac{A_E}{S}, \tag{2.8}$$

where $D = L_S - L_E$ is the difference in the sound pressure level between rooms. In this case, $R^{'}$ is called the apparent sound reduction index. However, the measurement of sound insulation for on-site measurement is described in ISO 16283-1 (2014) [116] depending on a given standardization reverberation time for dwellings $T_0 = 0.5$ sec. In addition, D_{nT} is donated standardized level deference. The $R^{'}$ and D_{nT} are measured in 1/3 octave bands. After measuring the sound reduction index as curves, those curves are converted to a single number value instead of a sound reduction curve, and the word weighted is added to their definition, whether for laboratory or on-site measurements.

$$D_{nT} = D + 10log\frac{T_{60}}{T_0}. \tag{2.9}$$

2.2.2 Weighted sound reduction index:

Usually, in building codes, when indicating the sound insulation capability for a specific construction, it is reasonable to specify a single number instead of the whole frequency curve. In addition, the last number is usually composed of data in one-third-frequency bands from 100 Hz to 3150 Hz and could be extended down from 50 Hz to 5000 Hz. The idea of indicating a single number to refer to the acoustic performance of a specific assembly is based on the use of what is called a reference curve [3]. That means there is unanimous consent on a specific sound reduction curve to be compared with measurement data. There are reference curves for airborne and impact sound insulation, which is internationally accepted in ISO 717 Part 1 [37] and Part 2 [38]. The single numbers or weighted indices are acquired by calculations as follows. The reference curve is shifted in 1 dB steps towards the measured curves unite the sum of unfavorable deviation is as large as possible but not exceeding 32 dB, regarding all frequency bands available between 100 Hz to 3150 Hz. Finally, the weighted value is the value of the shifted reference curve at 500 Hz; see Figure 2.3. In ASTM E413-16 [39], the same procedures are carried out to calculate the rating number value, called sound transmission class STC, with some differences that will be discussed in Section 2.5.

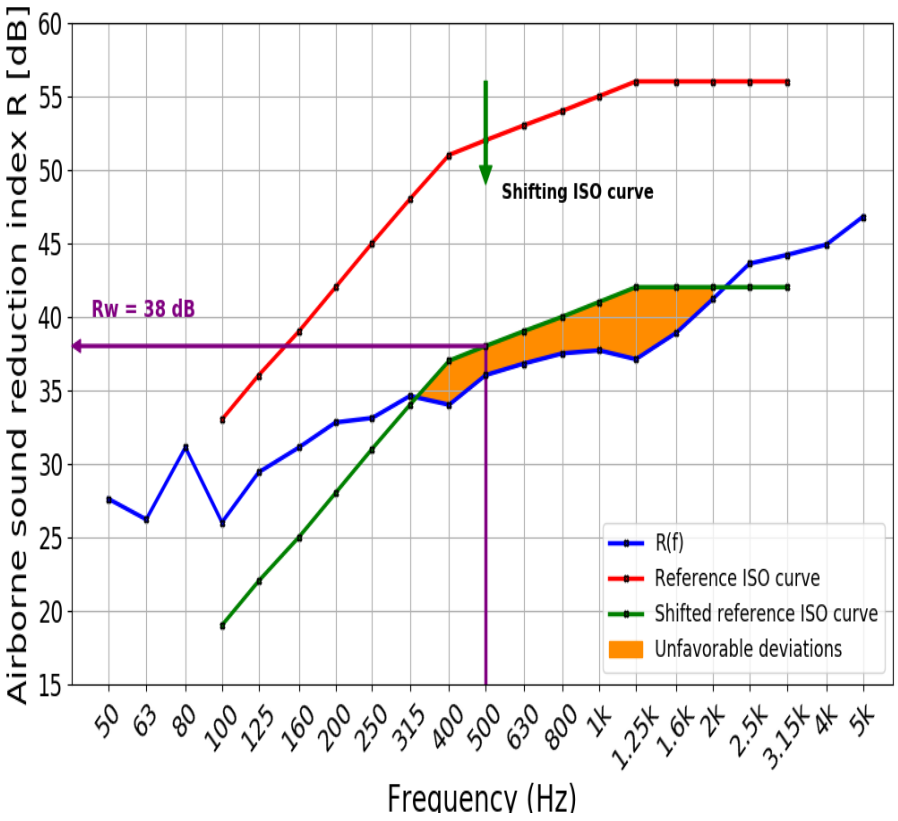

Figure 2.3: Calculating the weighted sound reduction index R_w *for an insulation curve according to ISO standards.*

Acoustic descriptors:

Acoustic descriptors are called for indices that describe the acoustic properties of the tested structures, such as weighted airborne and impact sound insulation or reverberation time. In addition, spectrum adaption terms C and C_{tr} are defined in ISO 717 Part 1 [37]. Those terms are given to consider the influence of spectrum characteristics on the final weighted value for the cases of airborne sound insulation [40]. C terms are calculated according to the frequency range, and C_{tr} is the A-weighted urban traffic noise spectrum. Then the single rating number can be written $R_w(C; C_{tr}; C_{50-3150}; C_{tr,50-5000})$ if two frequency bands (100-3150 Hz and 50-3150 Hz) are used, see Annex B of ISO 717 part 1 [37]. The latter is called the weighted standardized sound reduction index with correction spectra in the frequency range of 50 to 3150 Hz. The calculation of the

spectrum adaption terms is given in ISO 717 part 1 [37]:

$$C_{50,3150} = -10log(\sum_{i}^{19} 10^{(L_i - R_i)/10}) - R_w, \tag{2.10}$$

$$C_{tr} = 10log(\sum_{i} 10^{(L_i - R_i)/10}) - R_w. \tag{2.11}$$

2.2.3 Sound transmission loss of single-leaf partitions

The sound transmits through a wall through successive events. The incident sound wave elasticity bends the wall. The latter vibrates and then acts as a sound source that emits sound to the adjacent room. Figure 2.4 illustrates a simple description of the airborne sound transmission through a single leaf partition.

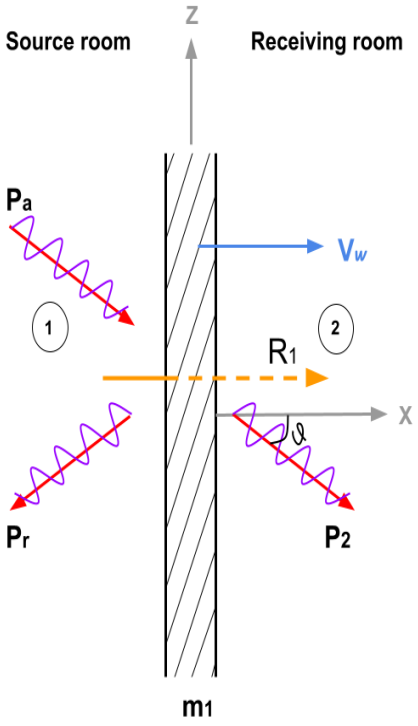

Figure 2.4: The sketch is used to calculate the transmission loss of a single-leaf partition. P_a : incident sound field, P_r : reflected sound field, $P_1 = P_a + P_r$: total sound field in front of the wall, P_2 : transmitted sound field.

Some elements can be identified in Figure 2.4:

The source room. A half space that is filled with air is assumed for this case. The

sound field is donated by a wave incident from the angle ϑ:

$$P_a = P_0 e^{-jkxcos\vartheta} e^{jkzsin\vartheta}, \tag{2.12}$$

while the reflected sound field is expressed by:

$$P_r = rP_0 e^{jkxcos\vartheta} e^{jkzsin\vartheta}. \tag{2.13}$$

The sound field in the source room consists of two waves:

$$P_1 = P_a + P_r = P_0 e^{jkzsin\vartheta}(e^{-jkxcos\vartheta} + re^{jkxcos\vartheta}). \tag{2.14}$$

Therefore, the sound field in the source room consists of two elements:

$$P_1 = P_a + P_r = P_0 e^{jkzsin\vartheta}(e^{-jkxcos\vartheta} + re^{jkxcos\vartheta}). \tag{2.15}$$

Both room spaces are assumed to be a half-space filled with air. Therefore, the sound power is described as:

$$P_2 = \tau P_0 e^{-jkxcos\vartheta} e^{jkzsin\vartheta}, \tag{2.16}$$

where τ is the sound power transmission coefficient.

The applied pressure difference $P_1(0,z)$ - $P_2(0,z)$ excite the wall to vibrates. However, the solutions of the bending wave equation by:

$$\frac{1}{k_B^4}\frac{d^4 \upsilon_W}{dz^4} - \upsilon_W = \frac{j}{m_1 \omega}(P_1(x=0,z) - P_2(x=0,z)), \tag{2.17}$$

where υ_W is wall velocity, K_B is bending wavenumber, m_1 represents the mass per unit area of the partition, and ω is the angular frequency. A detailed description of the bending wave solution can be found in [41].

Then the incident sound wave reaches the wall, and the latter vibrates in the same

direction of sound incidence (with respect to the z-axis by assumption):

$$\upsilon_W = \upsilon_0 e^{jkzsin\vartheta}. \tag{2.18}$$

Utilizing (2.15) and (2.16),

$$\upsilon_0 = \frac{1 + r - t}{\frac{k^4}{k_B^4} sin^4\vartheta - 1} \frac{jP_0}{m_1\omega}, \tag{2.19}$$

where υ_0 is the wave amplitude of υ_W. t represents the sound pressure transmission coefficient. The reflection coefficient r is a value to be known. Assuming that velocities on both sides of the partition are equal to its velocity υ_W:

$$\upsilon_1(x = 0) = \frac{j}{\omega\rho} \frac{\partial P_1}{\partial x}|_{x=0} = \upsilon_W, \tag{2.20}$$

$$\upsilon_2(x = 0) = \frac{j}{\omega\rho} \frac{\partial P_2}{\partial x}|_{x=0} = \upsilon_W. \tag{2.21}$$

Both equations 2.21, and 2.22 can be expressed by:

$$\frac{P_0}{\rho c} cos\vartheta(1 - r) = \upsilon_0. \tag{2.22}$$

Since

$$t = 1 - r \quad or \quad r = 1 - t, \tag{2.23}$$

Equation 2.22 can be written as:

$$t\frac{P_0}{\rho c} cos\vartheta = \upsilon_0. \tag{2.24}$$

By utilizing Equations 2.19 and 2.24:

$$tcos\vartheta = \frac{j\rho c}{m_1\omega} \frac{1 + r - t}{\frac{k^4}{k_B^4} sin^4\vartheta - 1}. \tag{2.25}$$

Replacing the reflection coefficient r with the sound pressure transmission coefficient t.

The latter is given by:

$$t = \frac{\frac{2j\rho c}{m_1\omega}}{(\frac{k^4}{k_B^4}sin^4\vartheta - 1)cos\vartheta + \frac{2j\rho c}{m_1\omega}}. \tag{2.26}$$

The sound pressure transmission coefficient is used to determine the sound power transmission coefficient as follows:

$$\tau = |t|^2 . \tag{2.27}$$

Therefore, airborne transmission loss is given by:

$$R = 10log1/\tau \tag{2.28}$$

The interpretation of equation 2.26 highlights a significant relationship between the bending wavelength λ_B and the air wavelength λ. Equation 2.26 can also be written:

$$(\frac{k^4}{k_B^4}sin^4\vartheta - 1) = (\frac{\lambda_B^4}{\lambda^4}sin^4\vartheta - 1) = (\frac{f^2}{f_{cr}^4}sin^4\vartheta - 1). \tag{2.29}$$

At frequencies below the coincidence frequency $\lambda_B << \lambda$ (comparable to $f << f_{cr}$), terms in brackets in Equation 2.29 are almost independent of the incidence angel ϑ. However, within the frequency ranges $f > f_{cr}$ ($\lambda_B > \lambda$), the sound transmission is strongly linked to ϑ. Therefore, the two cases ($f << f_{cr}$ and $f > f_{cr}$) can be identified in the sound insulation.

Frequency range below the critical frequency $f << f_{cr}$

The sound pressure transmission coefficient t is given by:

$$t \approx \frac{\frac{2j\rho c}{m_1\omega}}{\frac{2j\rho c}{m_1\omega} - cos\vartheta}. \tag{2.30}$$

The ratio c/m_1 has a small number in all cases [41]. Therefore, the sound power transmission coefficient can be donated by:

$$\tau = |t|^2 \approx (\frac{2\rho c}{m_1 \omega})^2 \frac{1}{cos^2 \vartheta}, \tag{2.31}$$

and the transmission loss by:

$$R = 10log(\frac{m_1^2 \omega}{2\rho c})^2 + 10log cos^2 \vartheta. \tag{2.32}$$

Assuming diffuse sound incidence and an average incidence angle of $\vartheta = 45^0$. Then the transmission loss can be expressed using Equation 2.32 as:

$$R = 10log(\frac{m_1^2 \omega}{2\rho c})^2 - 3\text{dB}. \tag{2.33}$$

The latter equation is known as the mass law or Berger's law. This mass law states that the transmission loss increases by 6 dB per octave and by 6 dB per doubling the mass [41]. Equation 2.33 shows the inefficiency of the bending stiffness of the partition at frequencies $f << f_{cr}$. Therefore walls are called flexible when the critical frequency is above the range of interest.

Frequency range above the critical frequency $f > f_{cr}$

In this case, the incidence angle is called critical incidence angle ϑ_{cr}, resulting in a total sound power transmission t roughly equal to 1. When $\vartheta = \vartheta_{cr}$, it is true that:

$$sin\vartheta_{cr} = \frac{k_B}{k} = \frac{\lambda}{\lambda_B} = \sqrt{\frac{f_{cr}}{f}}. \tag{2.34}$$

Therefore, the wall is referred to as acoustically transparent due to the match between the incidence sound wave and the partition vibration ($\vartheta = \vartheta_{cr}$). The wavelength of the incident sound wave is given by:

$$\lambda_b = \lambda / sinc\vartheta. \tag{2.35}$$

At the matching (where $\vartheta = \vartheta_{cr}$), the coincidence effect is obvious when:

$$\lambda_s = \lambda / sinc\vartheta_{cr}. \tag{2.36}$$

The simplified sound transmission loss model indicates a transmission coefficient t equals 1 when $\vartheta = \vartheta_{cr}$, which is not satisfying in practice [41]. This is because of the presence of inner partition damping. However, the losses of the partition can be described by a complex bending stiffness:

$$B^{'} \rightarrow B^{'}(1 + j\eta), \tag{2.37}$$

where η is the loss factor of the partition (which is material dependent, see table 2.1). Therefore, the wavelength becomes:

$$K_B^4 = \frac{m_1}{B'}\omega^2 \rightarrow \frac{m_1}{B'(1 + j\eta)}\omega^2 = \frac{k_B^4}{1 + j\eta}. \tag{2.38}$$

Then, the sound pressure transmission becomes:

$$t = \frac{\frac{2j\rho c}{m_1\omega}}{(\frac{\lambda_B^4}{\lambda^4} sin^4\vartheta(1 + j\eta) - 1)cos\vartheta + \frac{2j\rho c}{m_1\omega}}. \tag{2.39}$$

At coincidence angle, where $\vartheta = \vartheta_{cr}$. Equation 2.39 is transferred to:

$$t(\vartheta = \vartheta_{cr}) = \frac{\frac{2j\rho c}{m_1\omega}}{\frac{2j\rho c}{m_1\omega} + \eta cos\vartheta_{cr}}. \tag{2.40}$$

Equation 2.40 states that the sound transmission depends on the loss factor of the partition at high frequencies. When a diffuse sound field is considered, the average sound power transmission coefficient $\overline{\tau}$ is given by:

$$\overline{\tau} = \frac{1}{\pi/2}\int_0^{\pi/2} \tau(\vartheta)\partial\vartheta = \frac{1}{\pi/2}\int_0^{\pi/2} |t(\vartheta)|^2\, \partial\vartheta. \tag{2.41}$$

Then,

$$R = -10log\bar{\tau} \tag{2.42}$$

The integration in Equation 2.41 can only be integrated analytically using an approximation, which is a lengthy procedure. The average sound power transmission coefficient becomes (using an approximation in the calculation):

$$\bar{\tau} = (\frac{2\rho c}{m_1\omega})^2 \sqrt{\frac{f_{cr}}{f}\frac{1}{2\eta}}, \tag{2.43}$$

and the transmission loss R above the critical frequency $f > f_{cr}$ is donated by:

$$R = 10log(\frac{m_1\omega}{2\rho c})^2 + 5log\frac{f}{f_{cr}} + 10log2\eta. \tag{2.44}$$

The transmission is influenced by the loss factor η of the wall, which could be due to the material damping of the wall or transmitted energy to the adjacent elements.

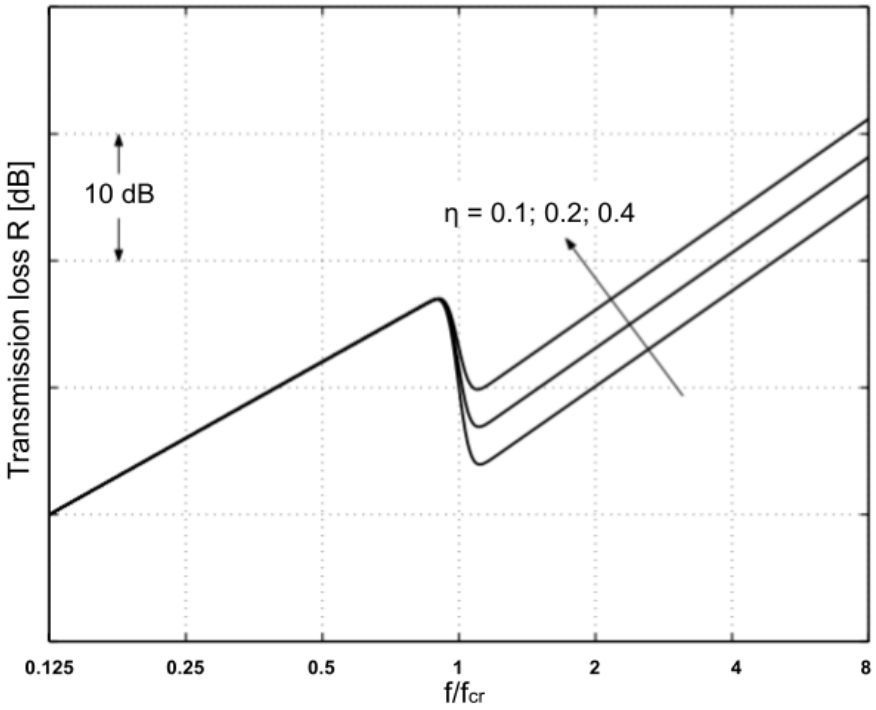

Figure 2.5: The effect of the loss factor on the characterization of the the transmission loss curve of single-leaf partitions [41].

Figure 2.5 illustrates the transmission loss characteristics for single-leaf elements

below and above the critical frequency. The transmission loss depends on the effect of the loss factor [41]. The results in practice do not always meet the theories for different reasons, such as the sound leakage (in windows and doors), the inhomogeneities in the materials, and porous materials [41].

Table 2.1: Typical loss factors for various materials [42].

Material	**Loss factor η**	**Material**	**Loss factor η**
Aluminum	10^{-4}	Magnesium	10^{-4}
Brass, bronze	$< 10^{-4}$	Masonry blocks	$5 - 7 \times 10^{-3}$
Brick	$< 1 - 2 \times 10^{-2}$	Oak, fi	$0.8 - 1 \times 10^{-2}$
Concrete		Plaster	5×10^{-3}
Light	$< 1.5 \times 10^{-2}$	Plexiglass, Lucite	$2 - 4 \times 10^{-2}$
Porous	$< 1.5 \times 10^{-2}$	Plywood	$1 - 1.3 \times 10^{-2}$
Dense	$< 1.5 \times 10^{-2}$	Sand, dry	0.6 – 0.12
Copper	$< 2 \times 10^{-3}$	Steel, iron	$1 - 6 \times 10^{-4}$
Glass	$< 0.6 - 2 \times 10^{-3}$	Wood fiberboard	$1 - 3 \times 10^{-2}$
Gypsum board	$< 0.6 - 3 \times 10^{-2}$	Lead	$0.5 - 2 \times 10^{-3}$

2.2.4 Sound transmission loss of double-leaf partitions

Usually, to enhance the acoustic performance of a specific partition, an additional lining is added. The supplemented layer could be fabricated of plasterboard or any other material that is expected to fulfill the acoustic requirements. The additional layer is mounted separately from the first partition by leaving a distance between the latter d. The distance d should be small compared to the incident wavelength. An air gap acts as a spring in the mass-spring wall system. The stiffness of the cavity per unit area is given by:

$$s = \frac{\rho c^2}{d}. \tag{2.45}$$

The pressure P_i in the cavity between the two partitions can be described by:

$$P_i = \frac{s}{j\omega}(\upsilon_1 - \upsilon_2), \tag{2.46}$$

This states that the transverse coupling of the elements in the cavity parallel to the partitions can be neglected. The cavity can also be damped with mineral wool or other insulation material. In general, the lining is thin, so its critical frequency is higher than the range of interest. The resulting pressure in the cavity can be donated by:

$$P_i = j\omega m_2 \upsilon_2, \tag{2.47}$$

where m_2 is the mass per unit area of the additional lining. Figure 2.6 illustrate the sound incident on double-leaf partitions. The sound pressure in the receiving room P_2 is smaller by magnitude to the right of the lining than the pressure in cavity P_i.

$$|P_2(x = 0))| << |P_i|\,. \tag{2.48}$$

If the double-leaf system consists of a solid heaving wall, it can be assumed that the additional lining would not influence the wall's vibration. Therefore, the results for single-leaf can be adopted in this case. From 2.24 and 2.18, it can be found:

$$\upsilon_1 = \frac{P_0}{\rho c} t_1 cos\vartheta e^{jkzsin\vartheta}. \tag{2.49}$$

And according to Equation 2.26:

$$t_1 = \frac{\frac{2j\rho c}{m_1\omega}}{(\frac{k^4}{k_B^4} sin^4\vartheta - 1)cos\vartheta + \frac{2j\rho c}{m_1\omega}}\,. \tag{2.50}$$

The vibration of the additional lining υ_2 can be calculated by inserting Equation 2.47 into Equation 2.48:

$$\upsilon_2 = \frac{\upsilon_1}{1 - \frac{\omega^2 m_2}{s}} = \frac{\upsilon_1}{1 - \frac{\omega^2}{\omega_0^2}}\,. \tag{2.51}$$

The resonance frequency ω_0 is given the cavity air spring s and the mass of the additional lining m_2 as:

$$\omega_0^2 = \frac{s}{m_2}.$$

Theoretically, the additional lining performs infinitely large vibrations when $\omega = \omega_0$. The latter is because of a lack of damping which can reduce its effect by adding a loss factor η. Inserting 2.49 in (2.51) gives:

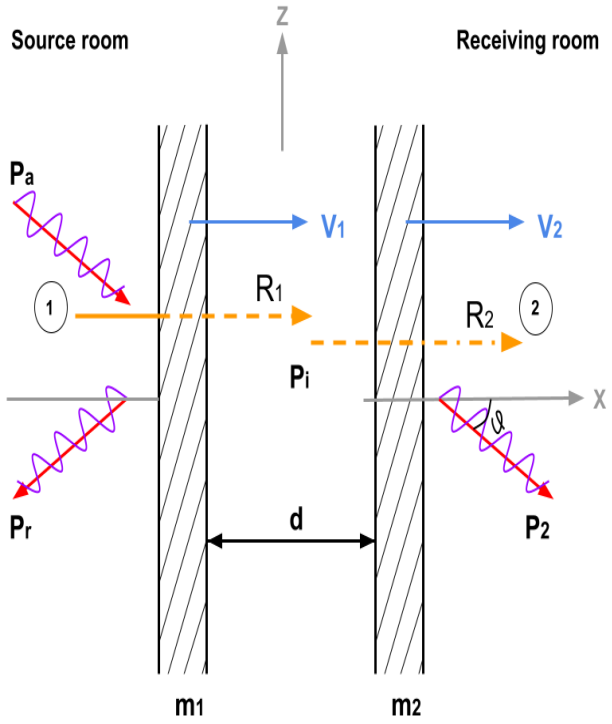

Figure 2.6: The sketch is used to calculate the transmission loss of a double-leaf partition. P_a: incident sound field, P_r: reflected sound field, $P_1 = P_a + P_r$: total sound field in the front of the wall, P_2: transmitted sound field, P_i: sound pressure in the filled cavity.

$$\upsilon_2 = \frac{P_0}{\rho c} \frac{t_1}{1 - \frac{\omega^2}{\omega_0^2}} cos\vartheta e^{jkzsin\vartheta}. \tag{2.52}$$

The sound pressure that is radiated from the additional lining can be written as:

$$P_2 = tP_0 e^{-jkxcos\vartheta} e^{jkzsin\vartheta}, \tag{2.53}$$

where t represents the sound pressure transmission coefficient of the double-leaf partition

that is delivered from the condition:

$$\frac{j}{\omega\rho}\frac{\partial P_2}{\partial x}|_{x=0} = \upsilon_2.$$

And then,

$$t = \frac{t_1}{1 - \frac{\omega^2}{\omega_0^2}}. \tag{2.54}$$

Therefore,

$$R = 10log\frac{1}{\tau} = 10log\frac{1}{t^2} = 10log(1 - \frac{\omega^2}{\omega_0^2})^2 + 10log\frac{1}{\tau_1}, \tag{2.55}$$

or in another way:

$$R = R_1 + 10log(1 - \frac{\omega^2}{\omega_0^2})^2, \tag{2.56}$$

where R_1 is the transmission loss of the single-leaf partition. The transmission loss of double-leaf consists of the summation of the transmission loss of the heavier wall and the improvement R_2 that results from the additional lining:

$$R = R_1 + R_2, \tag{2.57}$$

where R_2 is given by:

$$R_2 = 10log(1 - \frac{\omega^2}{\omega_0^2})^2. \tag{2.58}$$

Form Equations 2.57 and 2.58, the followings are true concerning the additional lining [41]:

- the effectiveness of the additional lining below the resonance frequency $\omega << \omega_0$ where $R_2 = 0$,
- at the resonance $\omega = \omega_0$, the transmission loss decreases, and it depends on the loss factor,
- at resonances above $\omega >> \omega_0$, the transmission loss $R_2 \approx 40log(\omega/\omega_0)$ rising at a

gradient of 12 dB per octave.

Moreover, from the noise control perspective, the resonance frequency f_0 should be as low as possible,

$$f_0 = \frac{1}{2\pi}\sqrt{\frac{\rho c^2}{m_2 d}} \approx \frac{60Hz}{\sqrt{m_2 d}}.$$

Therefore, it is recommended to utilize an additional heavy lining with a large gap distance d to achieve better insulation. Figure 2.7 shows the measurement improvements that are achieved by damping the cavity with mineral wool. Avoiding the physical connections (known also sound bridges) between the two partitions could increase the improvements. Sound bridges could create a way for sound to transfer through the two linings, which can affect the sound insulation negatively [3].

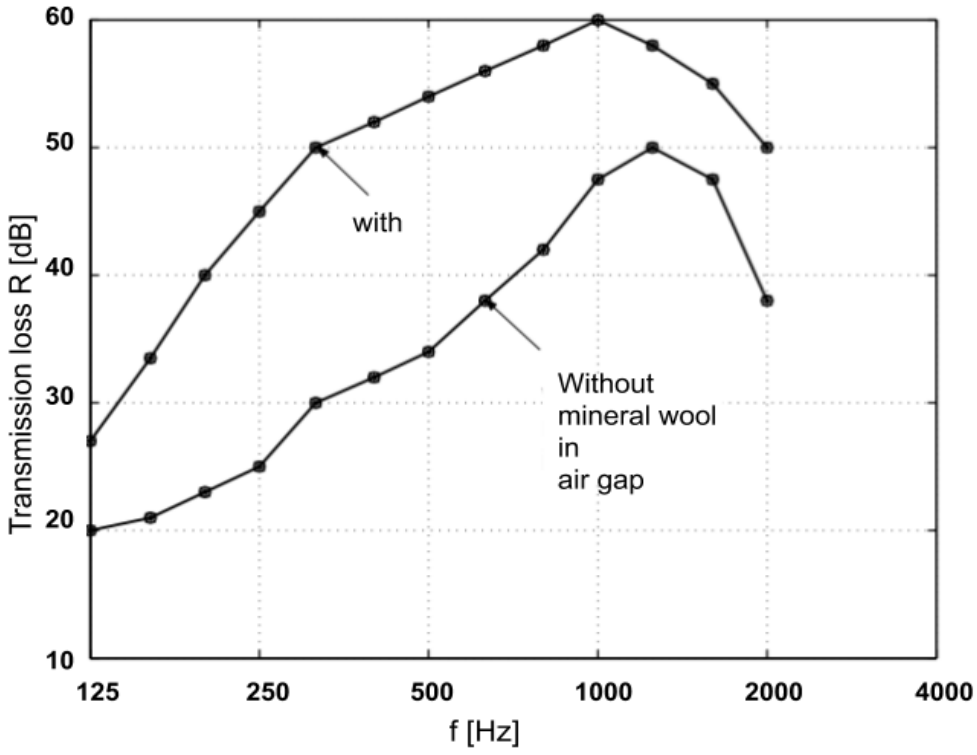

Figure 2.7: The effects of damping the cavity with mineral wool. The critical frequency f_{cr} of the double-leaf plaster partition is (f_{cr} = 3000 Hz). Figure from [41].

However, to obtain a higher sound insulation performance of double-leaf partitions, it is important to [41]:

– use a non uniformly distributed overall mass of the two partitions,

– utilizing a large cavity width d between the partitions,

– utilizing absorbent materials to damp the cavity,

– avoids the leakage that can result due to window or door installations,

– avoid sound bridges or structure-borne sound in the design of the partitions.

2.3 Measurements of impact sound insulation

The impact noise can be described as the noise that is radiated by a ceiling or a wall from another room floor that is excited by footsteps, moving chairs, or similar exciters. When the floor is excited, it performs structure-borne vibrations (which is also called impact sound) and emits airborne sound to the below or adjacent room. It is common to have an impact sound annoying in a room above a noisy, non-acoustically treated space function, such as a restaurant.

The measurements of impact sound in a laboratory are performed on a floor with 10 m^2 opening in the middle by a certain source, and the impact sound pressure level is measured below in a room below the floor see Figure 2.8. The radiated sound power can only be measured in the receiving room using several microphone positions. The measurement procedures are described in detail by ISO 10140-3 (2010) [43] and ASTM E492-09 (2016) [44]. The latter standards considered a frequency range of 100 Hz – 3150 Hz (ISO) or 125 Hz – 4000 Hz (ASTM). Recently, ISO Standards attempted to enlarge the evaluation low-frequency range down to the 50 Hz one-third octave band. For on-site measurements, the impact noise depends on the directly transmitted noise from the bottom surface of the floor/ceiling and on flanking transmitted sound paths by the linked walls to the separating floor.

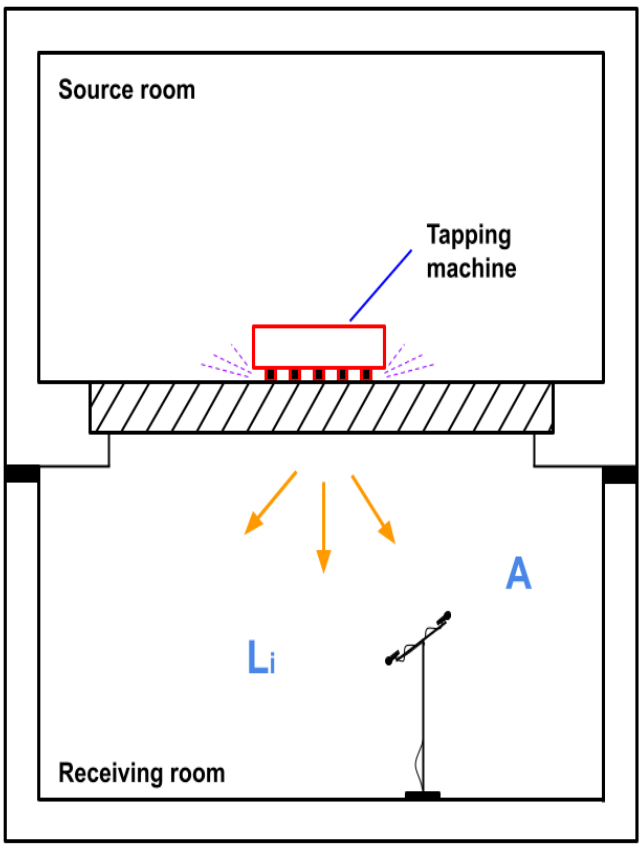

Figure 2.8: Measure the impact sound pressure levels in the laboratory using the standardized taping machine as an excitation source.

In laboratory, the normalized impact sound pressure level L_n is given by:

$$L_n = L_i + 10\,log\,(A/A_0), \tag{2.59}$$

where L_i is the energy average sound pressure level in the one-third octave band in the receiving room when the impact source excites the floor. A is the equivalent absorption area, and A_0 is the reference equivalent absorption area equal to 10 m^2. It can be noticed that the impact sound level is sensitive to the absorption in the receiving room. This means that the room criteria will highly affect the measurements of impact sound. Therefore, it is advisable to standardize the measurement by the reverberation time. The standardized impact sound pressure level is given by:

$$L_{nT} = L_i + 10logT/T_0, \tag{2.60}$$

where T is the reverberation time in the receiving room, and T_0 is the reference reverberation time equals 0.5 *sec*.

Theoretically, for massive floor, the impact sound level for 1/3 octave bands is given by [114]:

$$L_n = 10log(\frac{f_c}{\eta M_s^2}) + 10log(\frac{4\eta f}{\pi f_c} + \sigma) + 82.3, \tag{2.61}$$

where L_n is the sound pressure level in the receiving room, and it is normalized to a 10 m^2 absorption area, M_s is the surface density, and σ the radiation factor of the plate. Equation 2.61 is valid for an isotropic and homogenous plate without topping. The last term in Equation 2.61 considers partly the near-field contribution and partly the radiation efficiency of the reverberant field in the plate. When the loss factor η is relatively small, the near field contribution is often neglected, and Equation 2.61 can be written as:

$$L_n = 10log(\frac{f_c}{\eta M_s^2}) + 10log(\sigma) + 82.3. \tag{2.62}$$

Further simplification can be carried out in [114], and the normalized impact sound pressure level becomes:

$$L_n \approx 131 - 30logh - 15log\rho_s - 5logE - 10log\eta + 10log\sigma, \tag{2.63}$$

where h is thickness of the plate(m), ρ_s the density of the plate material (kg/m^3), E the Young's modulus of elasticity of the plate (N/m^2).

2.3.1 Impact sound sources

Using an impact source aims to mimic the walking step sound. However, the standardized tapping machine is used to quantify the impact insulation performance of a particular floor structure. It is a standardized measurement device consisting of five hammers, each weighing 500 g, which fall onto the floor from a defined height (40 mm) one after another with a tapping frequency of 5 Hz [3]. The distance between the center of each hammer is 100 mm [45]. Warnock [46] compared real footsteps and ISO tapping machine. The measurement data shows that the ISO tapping machine force spectrum

roughly equals the real walk steps spectrum. However, the tapping machine generates a poor impact sound spectrum in low frequency as it was initially developed to imitate the impact sound of high-heeled shoes [27]. In order to induce this kind of sound in low frequency, some countries use a rubber tire and a rubber ball that is purposed in [47]. The rubber tire is used as an impact source which weighs 3 kg, and it is dropped from a height of 0.5 m to generate a peak force from 1250 to 2400 N [48]. Another device is the Japanese rubber ball. It weighs 2.5 ± 0.1 kg with a diameter of 183 mm, dropping from 1 m height to imitate human activities and to generate an impact noise spectrum.

2.3.2 Weighted normalized impact sound pressure level

Similarly to the weighted airborne sound index, the weighted impact sound index can be calculated using the impact sound reference curve described in ISO 717 Part 2 [38]. Again, the curve is shifted in 1 dB steps towards the measured curve until the sum of deviation is as large as possible but not exceeding 32 dB. Then the weighted impact sound index $L_{n,w}$ is the value of the reference curve at 500 Hz, see Figure 2.9. The rating impact number in ASTM E989-06 is notated by IIC (impact insulation class). The better impact insulation gives higher IIC values but lower $L_{n,w}$. Section 2.5 explains a better comparison between both standards.

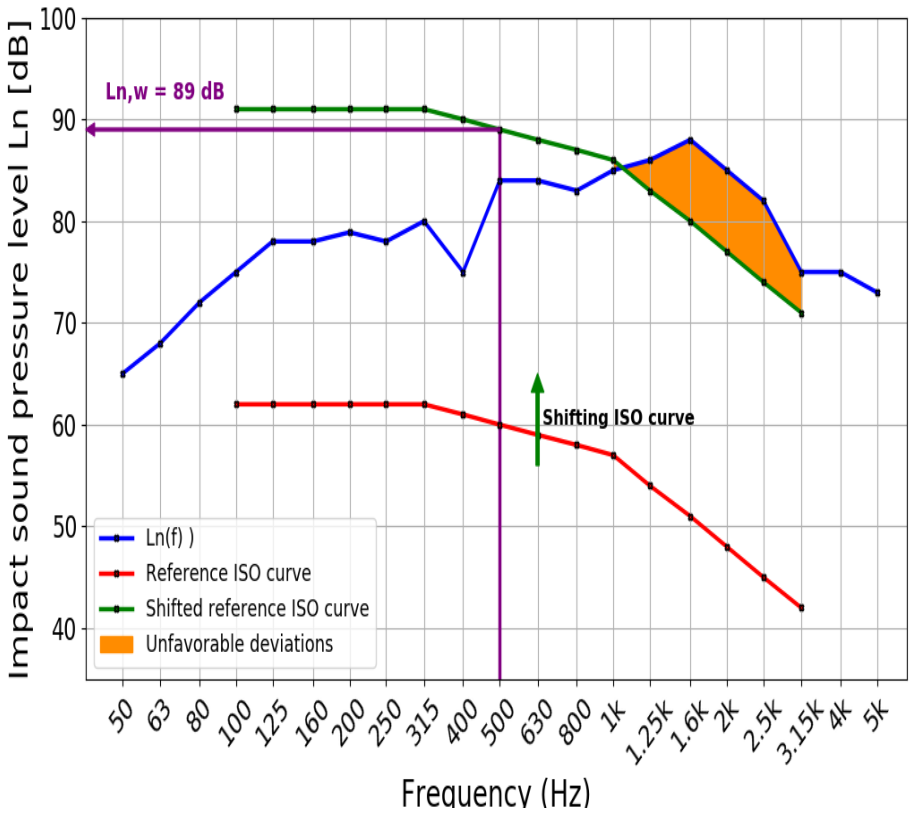

Figure 2.9: The Calculation of weighted sound pressure level $L_{n,w}$ *for an insulation curve according to ISO standards.*

Spectrum adaption term

Similarly to airborne sound insulation, the spectrum adaption term for impact sound insulation is defined in ISO 717 Part 2, which is C_I. It is a value, in decibels, added to the single number quantity to take account of the unweighted impact sound level. Usually, it is calculated according to the frequency range, and for instance, there is C_I (for the frequency range 100-2500 Hz) or for the enlarged range $C_{I,50-2500}$ (for 50-2500 Hz). Then it can be written $L_{n,w,100} = L_{n,w} + C_{I,50-2500}$, which is the standardized impact sound pressure level index with spectrum adaption terms in the frequency range of 50 Hz to 3150 Hz. The calculation of the spectrum adaption term is given in ISO 717 part 2:

$$C_{I,50-2500} = 10log(\sum_{50}^{2500} 10^{L_{n,i}(f)/10}) - 15 - L_{n,w}\,. \tag{2.64}$$

2.4 Different acoustic prediction tools

Since the beginning of the 20th century, acousticians have been interested in computing sound transmission through solid structures [22]. Different analytical and empirical formulations have been developed for structures ranging from simple monolithic homogeneous isotropic thin partitions to more complex and double-leaf systems. Despite these tools, limitations remain due to the range of technological solutions involved in building partitions - from non-homogeneous massive walls to lightweight double-leaf systems. Thus, more advanced models are needed. Heck [49] provided a thorough theoretical understanding of sound transmission in buildings. Additionally, Pellicier and Trompette [50] reviewed the prediction methods based on the wave approach for estimating sound transmission through specific partitions. However,

In 1942, Cremer investigated sound transmission through a homogeneous single-leaf partition [51]. This theory was also discussed in other works [52, 53]. The sound transmission coefficient is generally defined as the ratio of the transmitted to the incident sound power, which can also be calculated as the square of the ratio of the sound pressure [22]. This concept has been explained in numerous textbooks [52, 54, 55].

2.4.1 Sound transmission for homogeneous panels

The mass law [57] states that, in the case of a simple homogeneous panel, the most significant factor to consider when predicting its transmission loss is the mass per unit area:

$$R = 20log(mf) - 47, \tag{2.65}$$

where m is the superficial weight (kg/m^2) and f the frequency (Hz). However, Cremer [51] modified Equation 2.65 of mass law to account for the change in transmission at the critical frequency and higher:

$$R = 20log(mf) - 10log(2\eta w/\pi\omega c) - 47. \tag{2.66}$$

The latter equation provides a reasonable estimate for high-frequency ranges but is limited regarding low frequencies. For typical structures that measure 10-20 m^2, the radiation efficiency of forced waves must be considered for frequencies below 200 Hz. Sewell [192] has investigated that for an infinite area panel by providing a certain correlation:

$$\Delta R = -log_{10}[ln(kA^{1/2})] + 20log_{10}[1 - (\omega/\omega_c)^2], \tag{2.67}$$

where A is the partition surface area, and k is the wave number. Equation 2.65) and (2.66) with the Sewell correlation is not sufficient to describe very thick and heavy panels, such as concrete. For these panels, flexural waves become the dominant waves at high frequencies [58]. This causes the transmission loss to be decreased by 6 dB/octave [59] instead of 12 dB/octave for thin panels above the critical frequency.

2.4.2 Sound transmission for double Panels

Sharp [60] suggests using a thin lining with an air gap in between, such as two homogeneous panels without interconnections separated by an air gap. This helps to improve the acoustic performance since the air gap acts like an acoustically absorbing blanket. Sharp [60] developed an expression for transmission loss across three frequency domains for this purpose.

$$R = 20log(f(m_1 + m_2)) - 47 \qquad f < f_0, \tag{2.68}$$

$$R = R_1 + R_2 + 20log(fd) - 29 \qquad f_0 < f < f_1, \tag{2.69}$$

$$R = R_1 + R_2 + 6 \qquad f_1 < f, \tag{2.70}$$

where m_1 and m_1 the surface mass for each panel, d is the air gap depth, and f_0 is the resonance frequency, f_1 is equal to 55/d Hz. R_1 and R_2 are the transmission loss for each

panel. Sharps' expressions do not consider the acoustical variation in the whole system due to the air gap. Fahy [54] took that effects into account in high-frequency domain as:

$$R = R_1 + R_2 + 8.6\alpha d + 20log_{10}(\beta/k) \qquad f > f_1, \tag{2.71}$$

where α and β are the real and imaginary parts of the propagation coefficient of the absorption.

In addition, the wave approach can be used to calculate the sound transmission loss for infinite thin single or double-leaf partitions (using Kirchhoff theory) as follows [50]:

$$R(f) = 10log(\frac{1}{\tau(f)}), \tag{2.72}$$

where $\tau(f)$ is the sound transmission coefficient, at the frequency f, in a diffuse incident sound field that is obtained by the summation of all angles of incidence:

$$\tau(f) = \frac{\int_0^{\theta max} \tau(\omega, \theta) cos(\theta) sin(\theta) d\theta}{\int_0^{\theta max} cos(\theta) sin(\theta) d\theta}. \tag{2.73}$$

2.4.3 Prediction tools for impact sound insulation

It is essential to estimate an assembly's impact sound insulation performance, particularly during the design stage. Prediction tools must consider the sound transmission system and the excitation source [61]. In dwellings, the source of the impact sound can be footsteps or objects dropped onto the floor. As described in ISO standards, a standardized tapping machine is used to evaluate the impact sound levels experimentally. Several authors have investigated this problem concerning particular floors, considering the interaction between the hammers and the floor. Cremer [62] derived an impact source spectrum on a homogeneous floor caused by a tapping machine, assuming the impact to be elastic; the results proved applicable for several frequencies. Vér [63] described the force spectrum caused by a tapping machine on hard surfaces. He also suggested ways to improve the insulation on high-impedance surfaces, such as using elastic layers on the surface or floating floors.

Brunskog and Hammer [64] developed a theoretical-based model to estimate the impact of sound pressure levels for lightweight floor assemblies (mainly based on two boards, joists, and with/without mineral wool). However, disagreements were found in the middle to higher frequencies due to the air cavity's influence, which is not entirely neglected when the cavity is not filled with mineral wool. In high frequency and above 800 Hz, the deviation between measurements and the calculations was approximately 5 dB.

In [65], more than forty types of materials were studied to assess the effect of various floor toppings on sound performance. The results indicated that the effect of the floor topping materials is not solely dependent on the mass density but also on the nature of the material and the internal and external damping mechanisms. Caniato et al. [66] conducted field measurements of a four-story building with a Cross-Laminated Timber (CLT) floor. By utilizing equations, they determined the average equivalent impact sound in different frequency domains for bare CLT floors:

$$L_{n,eq,avg} = -0.15(f) + 77.7 \quad \text{(dB)} \qquad 50 < f < 80\text{Hz}, \tag{2.74}$$

$$L_{n,eq,avg} = -7.26(f) + 35.6 \quad \text{(dB)} \qquad 100 < f < 630\text{Hz}, \tag{2.75}$$

$$L_{n,eq,avg} = -0.006(f) + 84.4 \quad \text{(dB)} \qquad 800 < f < 5000\text{Hz}. \tag{2.76}$$

Developing an accurate model is challenging due to the lack of knowledge about the dynamic behavior of timber constructions. In order to predict the sound insulation performance, two methods are currently utilized: Statistical Energy Analysis (SEA) and Finite Element Method FEM.

Statistical energy analysis (SEA) is a method used to predict a complex structure's vibration or noise levels. This method divides the system into subsystems and considers the exchange of energy between them via resonant vibration modes [67]. The basic concepts of SEA are as follows [68]: 1) The power flow between subsystems corresponds

to the energy in each subsystem. 2) The transmitted power in a subsystem is either dissipated in the subsystem or transmitted to the adjacent one. 3) Energy only exists at resonant modes. Therefore, the greater capacity of the subsystem implies that more energy modes are excited. A disadvantage of SEA is that it is more applicable to heavy constructions, such as masonry and concrete. Additionally, it is used to predict sound insulation in mid and high frequencies. Unfortunately, SEA is not as effective in predicting sound insulation in low-frequencies, as this is often where noise issues in wooden structures arise.

The Finite Element Method (FEM) is a widely used computational technique for obtaining approximate solutions to boundary value problems in engineering. A boundary value problem is a mathematical problem with one or more dependent variables that must satisfy a differential equation everywhere within a known domain of independent variables, under specific conditions on the boundary of the domain [69]. One of the disadvantages is the difficulty in handling the boundary conditions in the modelling. Another challenge of the FEM is selecting the proper mesh element, as there is a strong relationship between frequency and finite element size [70]. Furthermore, long computation times and hardware problems such as storage capacity are other limitations of this method.

However, each developed prediction tool deals with a specific case of study [71] or a certain frequency band. For example, some of them do not consider the joists in a double-leaf structure [60, 72, 73]. However, others include the joists in the calculations [64, 74–77]. In addition, they cannot be generalized for a certain kind of structure. Moreover, significant deviations are shown in the results. Such limitations make developing a reliable estimation tool a difficult task, and therefore, innovative tools such as machine learning applications should be adapted.

2.4.4 Models based on artificial neural networks approach

Machine learning algorithms have paved the way for technological achievements in various fields that have been challenging since a few years ago. It is the science that allows

algorithms to learn and predict based on sample data. Big and diverse data is essential to enhance the predictive power of these models, especially artificial neural networks (ANN). The latter is widely used in different acoustic applications and will be discussed in detail in Chapter 3.

A few studies have been conducted in the literature concerning building acoustics using artificial neural networks. For instance, Shin et al. developed a convolutional neural network model to classify inter-noise floors between apartment houses by recording noise for 24 hours [78]. Garg et al. employed ANN to predict weighted sound reduction index (R_w) and sound transmission class (STC) for sandwich partition panels within ±3 dB deviations [79]. Additionally, Buratti et al. used ANN to predict R_w for wooden windows using limited technical parameters [80]. However, these models can only predict single-number-quantities (SNQ) and do not predict full-spectrum insulation curves.

Several studies have used an ANN approach to predict 1/3-octave-band curves based on sound insulation measurements. For example, a model was developed for monolithic brick walls based on 34 sound insulation measurements [17], and 49 types of aramid honeycomb sandwich panels were studied in the frequency range of 100 Hz − 6300 Hz [81]. Additionally, two studies [82–84] that used lab-based measurements were published to consider a wider frequency range (50 Hz − 5000 Hz) and for lightweight wooden structures. These two studies will be discussed more in Chapters 5 and 6. The models developed from 252 and 100 lab-based acoustic measurements for floors and façades, respectively, gave reasonable results with maximum differences of 1 and 3 dB in the estimation of R_w. However, the deviation was up to 5 dB in the prediction of $L_{n,w}$ (weighted normalized impact sound pressure level). Moreover, Another network model was developed to estimate the field sound insulation of multi-layered cross-laminated timber (CLT) floor systems using 104 field sound insulation curves (will be discussed in Chapter 7). The results were reasonable, with a maximum error deviation of 1 dB in the estimation of weighted standardized differences D_{nTw} and 2 dB for the weighted standardized impact pressure level L'_{nTw}.

2.5 Acoustic Standards - ISO & ASTM

International standards published by ASTM and ISO are adapted for sound insulation measurements in building acoustics. Airborne and impact sound insulation measurements are standardized through several international standards, which are used depending on the geographical region. For example, ASTM standards are used in the United States and Canada, whereas in Europe, Asia, and other parts of the world, ISO standards are employed. Since the acoustic measurements (that are used in this thesis) have been carried out according to ISO and ASTM standards, a comparison relating to building acoustics measurements will be presented in this section. This comparison will highlight the similarities and differences between the two standards and their equivalent parts.

The airborne sound transmission in ASTM standards is developed by the E33 committee "Building and Environmental Acoustics" [85], and subcommittee E33.03 "Sound transmission". However, for impact sound insulation, it is developed by subcommittee E33.10 "Sound Acoustics and Vibrations". In ISO standards, airborne and impact sound transmission are developed by committee 43, subcommittee 2 (ISO/TC43/SC 2) [86, 87]. SC 2 is responsible for developing standards related to building acoustics, such as the measurement of sound absorption, the measurement of flanking sound transmission, and the prediction of apparent sound insulation based on the performance of building elements. Tables 2.2 and 2.3 show the equivalent parts for ASTM and ISO standards.

Table 2.2: The ISO equivalent of ASTM standards for sound transmission committee [87].

ASTM	**Year**	**Title**	**ISO equivalent**
ASTM E90	2016	Standard Test Method for Laboratory Measurement of Airborne Sound Transmission Loss of Building Partitions and Elements	ISO 10140-2
ASTM E336	2017	Standard Test Method for Measurement of Airborne Sound Attenuation between Rooms in Buildings	ISO 16283-1
ASTM E413	2016	Classification for Rating Sound Insulation	ISO 717-1
ASTM E596	2016	Standard Test Method for Laboratory Measurement of Noise Reduction of Sound-Isolating Enclosures	ISO 15667 & ISO 11546
ASTM E966	2018	Standard Guide for Field Measurements of Airborne Sound Attenuation of Building Facades and Facade Elements	ISO 16283-3
ASTM E1289	2016	Standard Specification for Reference Specimen for Sound Transmission Loss	ISO 10140-5
ASTM E1332	2016	Standard Classification for Rating Outdoor-Indoor Sound Attenuation	ISO 717-1
ASTM E1414	2016	Standard Test Method for Airborne Sound Attenuation Between Rooms Sharing a Common Ceiling Plenum	ISO 10848-2
ASTM E1704	2010	Standard Guide for Specifying Acoustical Performance of Sound-Isolating Enclosures	ISO 15667 & ISO 11546
ASTM E2249	2016	Standard Test Method for Laboratory Measurement of Airborne Transmission Loss of Building Partitions and Elements Using Sound Intensity	ISO 15186-1
ASTM E2964	2014	Standard Test Method for Measurement of the Normalized Insertion Loss of Doors	ISO 16283-1

Table 2.3: ASTM standards for structural acoustics and vibration committee and their equivalent in ISO standards.

ASTM	Year	Title	ISO
ASTM E492	2016	Standard Test Method for Laboratory Measurement of Impact Sound Transmission Through Floor-Ceiling Assemblies Using the Tapping Machine	ISO 10140-3
ASTM E756	2017	Standard Test Method for Measuring Vibration-Damping Properties of Materials	ISO 18437-3
ASTM E989	2012	Standard Classification for Determination of Impact Insulation Class (IIC)	ISO 717-2
ASTM E1007	2016	Standard Test Method for Field Measurement of Tapping Machine Impact Sound Transmission Through Floor-Ceiling Assemblies and Associated Support Structures	ISO 16283-2
ASTM E1123	2016	Standard Practices for Mounting Test Specimens for Sound Transmission Loss Testing of Naval and Marine Ship Bulkhead Treatment Materials	—
ASTM E2179	2016	Standard Test Method for Laboratory Measurement of the Effectiveness of Floor Coverings in Reducing Impact Sound Transmission Through Concrete Floors	ISO 16251-1
ASTM E2963	2016	Standard Test Method for Laboratory Measurement of Acoustical Effectiveness of Ship Noise Treatments Laboratory Measurement of Acoustical Effectiveness for Marine Bulkhead and Deck Treatments	—
ASTM E3133	2018	Standard Test Method for Laboratory Measurement of Floor Impact Sound Radiation Using the Tapping Machine	—

2.5.1 Sound insulation requirements in ASTM and ISO

The laboratory measurement of the airborne sound insulation of structure elements follows the same principles in ASTM and ISO standards. The tested element is mounted between two reverberation rooms (source and receiving chambers), and the average level differences between the two rooms are detected by sampling the sound field in both rooms. The measurements are normalized, and they consider the structure surface area S and the equivalent absorption area A_E. In receiving room, transmission loss TR (ASTM terminology) or sound reduction index R (ISO standards) is determined by:

$$TL(f) = L_s(f) - L_R(f) + 10log(\frac{S}{A_E}), \tag{2.77}$$

$$R(f) = L_s(f) - L_R(f) + 10log(\frac{S}{A_E}). \tag{2.78}$$

Although the principles of the laboratory measurements of airborne sound insulation are the same, there are some differences in the laboratory requirements between ASTM and ISO standards [87]:

- **reverberation time procedures:** the reverberation time measurements are indicated in ISO 10140-4 [88] using two procedures (interrupted noise and response methods). While in ASTM E90, only the interrupted noise method is permitted. However, in ISO 10140-2 [89], the ideal room reverberation time should be between 1 and 2 sec. If the value falls outside of this range, then the room must be modified by: $1 \leq RT \leq 2(V/50)^(2/3)$.

- **volume of the receiving room:** in ASTM E90 [32], the minimum required room volume is 80 m^3, while it is 50 m^3 in ISO 10140-5 [90]. More eigenmodes at lower frequencies can be excited with higher room volume as a condition of a diffuse sound field [87]. Moreover, in ISO, the weighted single number, weighted sound reduction index R_w covers lower frequency ranges than a single number, sound transmission class STC, in ASTM standards. Although ISO standards have smaller

minimum requirement room volume and consider lower frequencies, several recommendations are adapted for better mode distribution.

- **requirements for specimen area:** According to ISO, the recommended size of the specimen area for walls is 10 m^2, while for floors, it is between 10 m^2 to 20 m^2, with a minimum length of 2.3 m for the shorter edge. However, ASTM does not set a minimum size for the specimen area but specifies a minimum dimension of 2.4 m.

- **loss factor value:** ISO 10140-5 [90] precises the minimum loss factor for heavy structures should be $\eta_{min} = 0.01 + 0.3/\sqrt{f}$. However, no such requirement for the loss factor has been indicated in ASTM E90 [32].

- **precision:** ISO 10140-2 [89] requires a rounded sound reduction index R to the nearest 0.1 dB, ASTM E90 [32] indicates that the transmission loss TL must be reported in integers.

2.5.2 Airborne and impact sound rating numbers

The process for calculating the weighted single number R_w (in ISO) or the sound transmission class STC (in ASTM) is essentially the same in both standards, with some differences outlined in Table 2.4. The reference curve in ASTM E413-16 [39] is from 125 Hz to 4000 Hz, while it covers lower ranges in ISO 717-1 [37]. The STC value is rounded to the nearest whole dB value, and it is rounded to the nearest 0.1 dB for R_w [23]. The same procedures are carried out in both standards for calculating the single number values. However, an additional criterion is required in ASTM, known as the 8 dB rule. The latter indicates that the reference curve and the measured one must be as big as possible but not exceed 32 dB as long as the maximum deficiency allowed during the fitting procedure is 8 dB at a single frequency band. The result is written as STC XX (without dB notation), where it is in dB for R_w. Usually, the R_w and STC are close, but significant differences could be found in resonance dip cases [152]. However, no adaption terms are indicated in ASTM in contrast to ISO standards.

Table 2.4: Differences between airborne rating single number in ISO and ASTM standards.

Notes	ISO 717-1	ASTM E413-16
Precision	rounded to the nearest 0.1 dB	rounded to the nearest 1 dB
Reference curve	100 Hz – 3150 Hz	125 Hz – 4000 Hz
Curve shifting rules	sum of deviations ≤ 32	in additions to the 8 dB
Adaptation terms	such as C and C_{tr}	no adaption terms

Calculating the weighted impact sound pressure level $L_{n,w}$ using a standard reference in one-third-octave bands (100 Hz – 3150 Hz) is indicated in ISO 717-2 [38]. For calculating the STC value, ASTM E989-06 [91] is a relative standard to ISO 717-2 with the same reference curve. Moreover, both standards are essentially the same and use the same standardized tapping machine. There is a significant difference in the interpretation of the results. The IIC value is given by: 110 dB - $L_{n,w}$ if the 8 dB rule is not invoked. The letter means the higher impact sound insulation donates a higher IIC value but a lower $L_{n,w}$. Additionally, some differences can be highlighted between the standards in representing the single number quantities. ASTM E989-06 rounds the IIC value to the nearest 1 dB while it is to the nearest 0.1 dB in ISO. The additional criterion regarding the 8 dB rule is also applied in calculating the IIC value. In ASTM, The result is written as ICC XX (without dB notation), where it is in dB for $L_{n,w}$. Table 2.5 summarized the calculation method of impact single number quantities in ASTM and ISO.

Table 2.5: Differences between impact rating single number in ISO and ASTM standards.

Notes	ISO 717-2	ASTM E989-06
Precision	rounded to the nearest 0.1 dB	rounded to the nearest 1 dB
Reference curve	100 Hz – 3150 Hz	100 Hz – 3150 Hz
Curve shifting rules	sum of deviations ≤ 32	in additions to the 8 dB
Higher rating number means	lower impact insulation	higher impact insulation

Chapter 3

ARTIFICIAL NEURAL NETWORKS APPROACH

3.1 Artificial intelligence: history and techniques

Recently, Artificial Intelligence (AI) and data science have gained tremendous popularity. AI was developed in the 1950s when a handful of pioneers in the computer science field started wondering whether the machine could be coded to think [92]. AI is a general field that encompasses both Machine learning (ML) and Deep Learning (DL), but some approaches are not quantified as a learning approach (Figure 3.1 (a)). For instance, simple chess programs only involved hard code, which is written by programmers, and did not classify as machine learning. Not long ago, experts believed they could achieve human-level intelligence by utilizing a large set of rules. The latter approach is known as symbolic AI, and it was the dominant AI archetype from the 1950s to the late 1980s [92]. Although the symbolic AI is suitable for solving logical and well-defined problems, solving many complex problems, such as image classification or speech recognition, is intractable using symbolic AI. However, a new approach arose to replace it, which is called machine learning (Figure 3.1 (b)).

Machine learning arises to deal with a specific task without being explicitly programmed by looking at the data. With this approach, doors are opened to a new programming paradigm. The main differences between AI and ML are how rules are created. In the AI method, humans put rules, and data proceeds depending on those rules to find the answer for a specific task. While in ML, the rules are extracted from the

given data to automate the task without being explicitly programmed see Figure 3.1 (b). Although ML techniques only started in the 1990s, they became AI's most popular and flourishing branch.

Deep learning is a particular subfield of ML, a new view on the learning representation of data that emphasizes successive layers. Artificial neural networks are a specific approach to DL algorithms. It was motivated by the structure of the human biological brain [6]. The Artificial Neural Networks approach uses simple computational operations (multiplication, additions, and fundamental logic elements) to solve complex and ill-defined tasks [93]. Furthermore, it allows for very low-level programming to solve complex problems in a self-organizing manner.

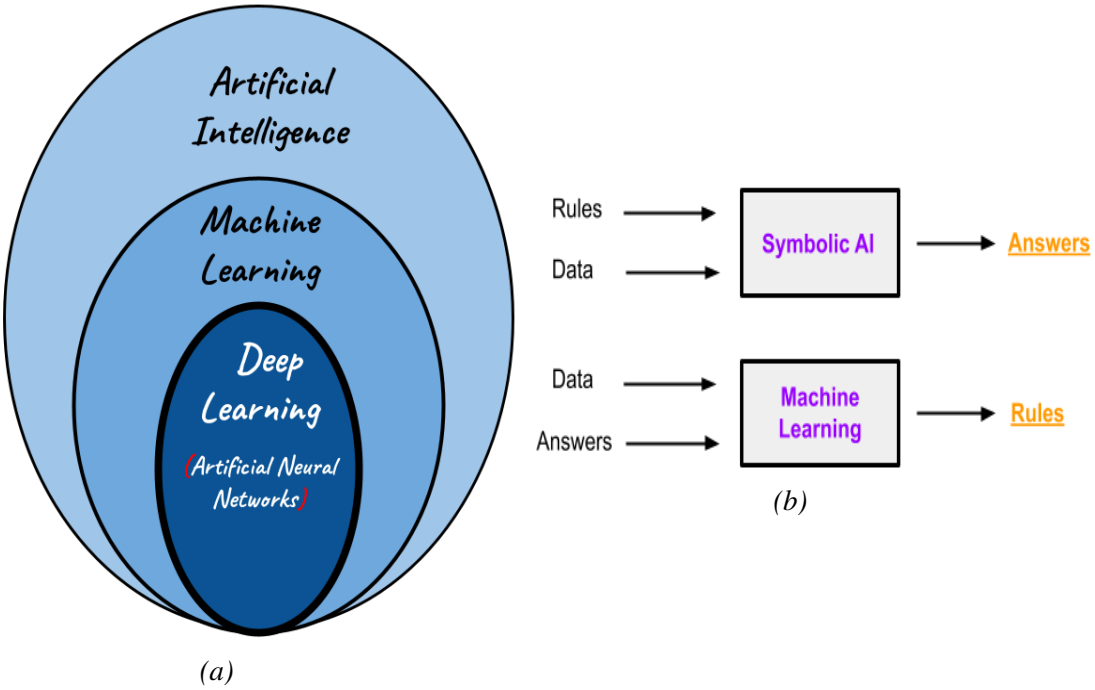

Figure 3.1: Artificial intelligent division. (a) AI, ML, and DL. (b) The paradigm of machine learning.

3.2 Main artificial neural networks learning modes

The primary purpose of training the network model is to tune the intermediate connections (weights) between layers by respecting the neural-based algorithm. This modifies the weight values to achieve the desired accuracy, called the adaption function

or learning mode. There are two types of modes: supervised and unsupervised learning. Supervised learning needs an external observer. The latter could be a data training set or an observer who rates the performance of a network model. However, in unsupervised learning, no external observer is needed, and the system must organize itself by some designed criteria in the network [94].

3.2.1 Supervised learning

The vast bulk of the ANN tasks has been trained with supervised learning. In this mode, inputs and output values are provided to the network system. Then the ANN processes the inputs and compares the predictions against the desired outputs (actual values) to initiate weight values. The system reviews errors, and weights are adjusted to increase the reliability of the predictions. Several iterations repeat this process, and weights are continually tweaked until the system finds optimal values. The latter is called training the ANN. However, some network models can never learn. This is probably because the input data does not contain the specific information from which the desired output is derived. In addition, networks also do not converge if insufficient data is provided. Therefore, a big and wide range of data should be available to develop a reliable model.

3.2.2 Unsupervised learning

The other type of training mode is called unsupervised training. In this type, the network is fed with inputs but not with desired outputs. The system must identify what features it needs to group the input data. This is often referred to as self-organization or self-adaption. This adaption to the environment is the promise that would enable science fiction types of robots to learn independently as they encounter new situations and environments continually. This promising field of unsupervised learning is also known as self-supervised learning. In those networks, there is no external influence to adjust weight values, and they monitor their performance by themselves. However, most neural network applications are trained with supervised learning.

In both learning modes, if a specific network model is not able to solve the problem, the designer then has to review the inputs and the outputs (in the supervised training case), the number of layers, the number of units per layer, the summation, and the training functions, and even the initial weights themselves. In addition, the designer's creativity also governs the rules of training. There are many laws (algorithms) used to implement adaptive feedback. The most common technique is backward-error propagation, more commonly as back-propagation, which will be explained in section 3.3.4.

3.3 Developing an ANN model

The architecture of ANN consists of layers, and each layer contains computation units referred to as neurons [95]. Those units are connected through weights, which take the same role as the strength of the connections in biological organisms. Weights are utilized to scale each input to a neuron, affecting the function computed at that unit. ANN computes a function of the inputs by propagating computed values from the input neurons to the output neuron(s) and using weights as intermediate parameters [96]. Training data contains examples of input-output pairs of the function to be learned. It provides feedback on the correctness of the weights depending on how well the network can predict output values. Errors made by ANN are viewed to evaluate the weights between neurons through what is called back-propagation. Then the weights are adjusted in a network model (this is how ANN learns). Features of ANN (weights and bias) are adjusted during the learning phase of the network. A data set flows through each neuron in an input-output manner. In other words, each neuron receives a signal, manipulates it, and forwards an output signal to the other connected neurons in the adjacent layer, see Figure 3.2.

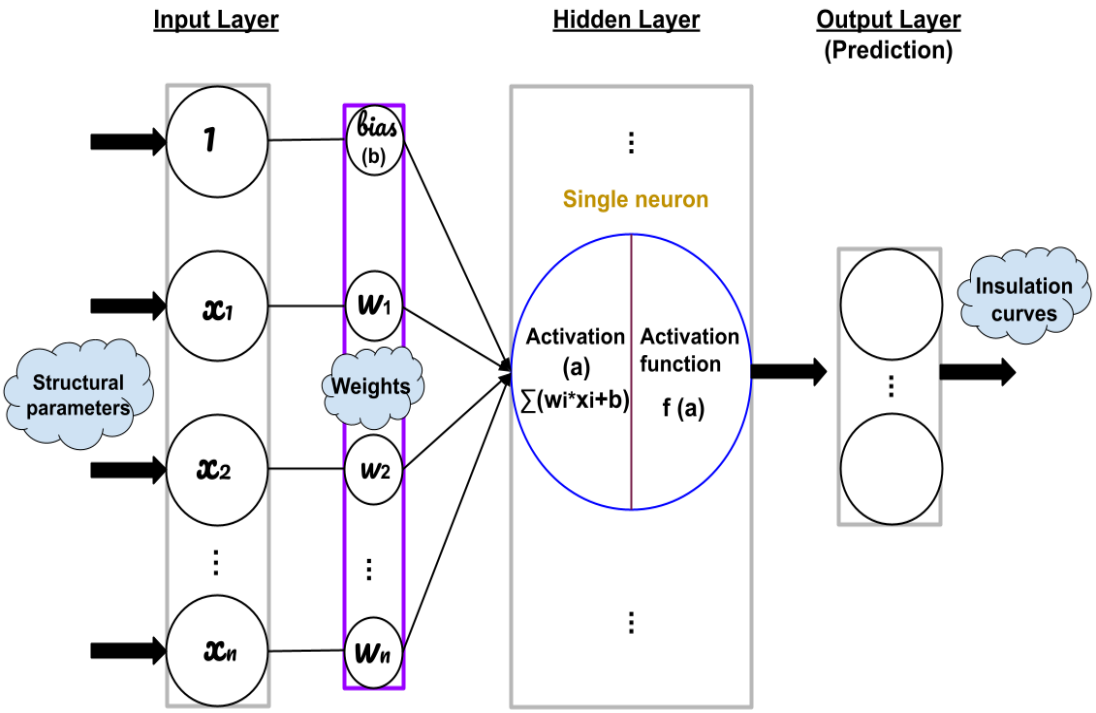

Figure 3.2: The architecture of an ANN model shows how input data propagates to calculate the predicted values.

A single neuron can be defined as a mathematical function that takes one or more input values and outputs them as a single numerical value. The neuron is identified as follows:

$$y = f(\sum(w_i x_i + b)), \tag{3.1}$$

where y, w_i, x_i, and b represent a neuron's output, weight value, input, and bias, respectively. Output values from neurons are known as activation values, used as input to the activation function. The activation functions most commonly used are sigmoid, hyperbolic, tangent, ReLU, and LeakyReLU functions [97].

3.3.1 Different types of activation functions

The choice of activation function is a critical part of an ANN design. Multi-layered networks can be classified as linearly inseparable classes. Therefore, they need to satisfy more than one condition. If the neurons do not have activation functions, their outputs would be the weighted sum of the inputs $\sum(w_i x_i)$, which is a linear activation function.

Then the entire neural network becomes a composition of linear functions. In addition, when hidden layers are added, the network will still be equivalent to a simple linear regression model as long as a linear activation function is used for all hidden layers. In order to use the network model in non-linear problems, non-linear activation functions need to be utilized. Each layer could have different activation functions according to the purposes of the model. The most activation functions are as follows:

– **identity function**. This function lets the activation value go through without any modification.

$$f(a) = a, \tag{3.2}$$

– **threshold activity function**. This function activates the neuron, whereas the activation is above a certain value.

$$f(a) = \begin{cases} 1 & if \quad a \geqslant 1 \\ 0 & if \quad a < 1 \end{cases}, \tag{3.3}$$

– **logistic function**, or the **logistic sigmoid**. It is also called the S-shaped activation function. It is one of the most commonly used in AI field, as it basically converts values into probabilities between 0 and 1 (Fig. 3.3), and can be interpreted scholastically as the probability of the neuron activity.

$$f(a) = \frac{1}{1 + exp^{-a}}, \tag{3.4}$$

– **bipolar sigmoid**. It is simply a logistic sigmoid rescaled and translated to have an output in a $(-1, 1)$ range.

$$f(a) = \frac{2}{1 + exp^{-a}} - 1 = \frac{1 - exp^{-a}}{1 + exp^{-a}}. \tag{3.5}$$

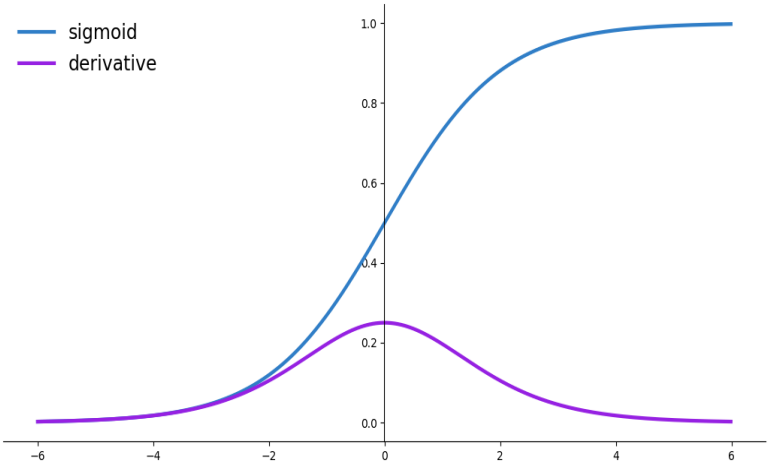

Figure 3.3: Graphical representation of the sigmoid activation function.

– **hyperbolic tangent** (or **tanh**). This is also sigmoidal (S-shaped), and the range of this function is between $(-1, 1)$, see Fig.3.4. The main advantage of this activation function is that the negative values can be dealt with more easily.

$$f(a) = \frac{exp^{a} - exp^{-a}}{exp^{a} + exp^{-a}} = \frac{1 - exp^{-2a}}{1 + exp^{-2a}}. \tag{3.6}$$

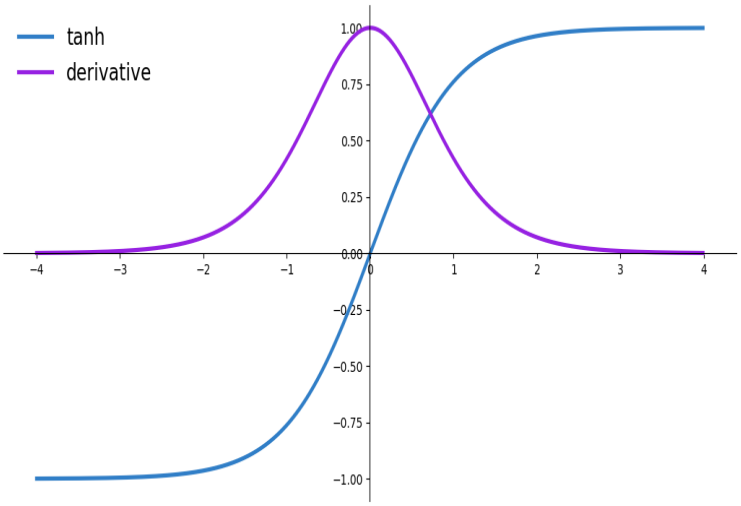

Figure 3.4: Graphical representation of the tan activation function.

– **ReLU function**. The Rectified Linear Function (ReLU) is a mix of the identity and the threshold function (Fig. 3.5). There are variations on the ReLU, such as Noisy ReLU, Leaky ReLU, and ELU (Exponential Linear Unit).

$$f(a) = \begin{cases} a & if \quad a > 0 \\ 0 & if \quad a \leq 0 \end{cases}. \tag{3.7}$$

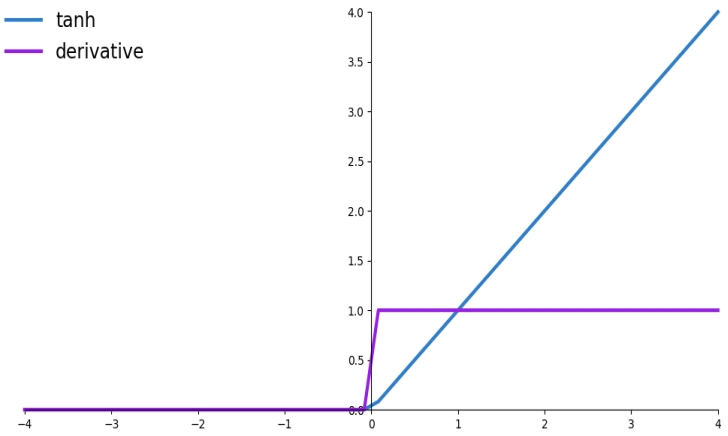

Figure 3.5: Graphical representation of the ReLU activation function.

– **Leaky-ReLU**. It is an improvement of the main default ReLU. It is similar to ReLU but relaxes sparsity constraints by allowing small negative activation values [5]; see Figure 3.6. It has two benefits which could face ReLU and other activation functions. Firstly, it fixes the dying ReLU problem, as it does not have a zero-slop part. In addition, it speeds up the training phase, as the mean activation values are close to zero.

$$f(a) = \begin{cases} a & if \quad a \geqslant 0 \\ 0.01a & if \quad a < 0 \end{cases}. \tag{3.8}$$

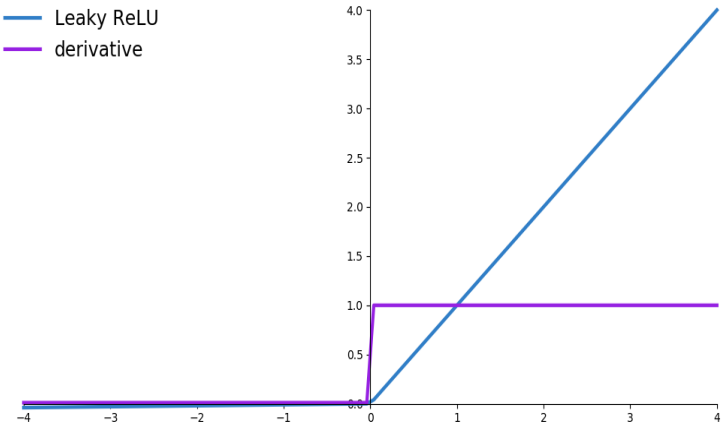

Figure 3.6: Graphical representation of the Leaky ReLU activation function.

The range for the logistic function is $(0, 1)$, which is one reason why it is a preferred function for stochastic networks. The hyperbolic function is similar to the logistic function, but its range is $(-1, 1)$. In contrast, the ReLU has a range of $(0, \infty)$. The derivative (or the gradient) of activation functions such as logistic sigmoid, hyperbolic tangent, and ReLU is essential for the training process of the network, as will be explained in sections 3.3.2 and 3.3.3.

The derivative of the logistic activation function f is:

$$f * (1 - f), \tag{3.9}$$

while the hyperbolic tangent function is:

$$(1 + f) * (1 - f). \tag{3.10}$$

Moreover, the decoration of the ReLU activation function is much simpler as:

$$f^{'}(a) = \begin{cases} 1 & if \quad a \geqslant 0 \\ 0 & if \quad a < 0 \end{cases}. \tag{3.11}$$

The purpose of artificial neural networks is to transfer inputs to outputs using

intermediate values (weights) through the activation functions. In each iteration, weights are evaluated depending on errors in the predicted values. Then, the aim is to minimize the errors utilizing a cost function. The cost function is a mathematical expression used to evaluate the model's performance. The latter procedure is training the network model. There are two algorithms to train the ANN model: linear and logistic regression, depending on the data. Regression algorithms are supervised algorithms that use input data to predict the desired values. Regression analysis works on finding the best network parameters that fit the input dataset.

3.3.2 Linear regression

In a linear regression algorithm, the goal is to minimize the cost function by finding appropriate parameters. A popular cost function is the Mean-Square-Errors (MSE) or the Root-Mean-Square-Errors (RMSE), where they take the square (or root-square) of the mean differences between the predicted and the desired values. Once the cost function is calculated for each epoch, the gradient descent algorithm updates the weights to minimize the cost function. The gradient descent starts working when weight values are initialized with random values. Then the cost function (in this case MSE) is calculated for all trained samples. Let us donate MSE by J, where J is given by:

$$J = MSE = \frac{1}{n}\sum_{i=0}^{n}(a^i - \hat{y})^2 = \frac{1}{n}\sum_{i=0}^{n}(x^i * w - \hat{y})^2, \tag{3.12}$$

n is number of training sample, a is the neuron activation value ($x^i * w$), and $\hat{y}$ is the target value. In the next iteration, weight values are reviewed and tuned by calculating the derivative of J and choosing an appropriate learning rate α. The learning rate determines the ratio by which the weights are adjusted. The last process is repeated until the cost function falls below the threshold or reaches the minimum.

$$w := w - \alpha \bigtriangledown (J(w)). \tag{3.13}$$

Since y^i is a function of w, then j is a function of w. Therefore, the cost function j

represents a hypersurface of dimension equal to the dimension of w. Figure 3.7 illustrates that the cost function (MSE) for a single input value x changes considering a single weight w and an assumed learning rate.

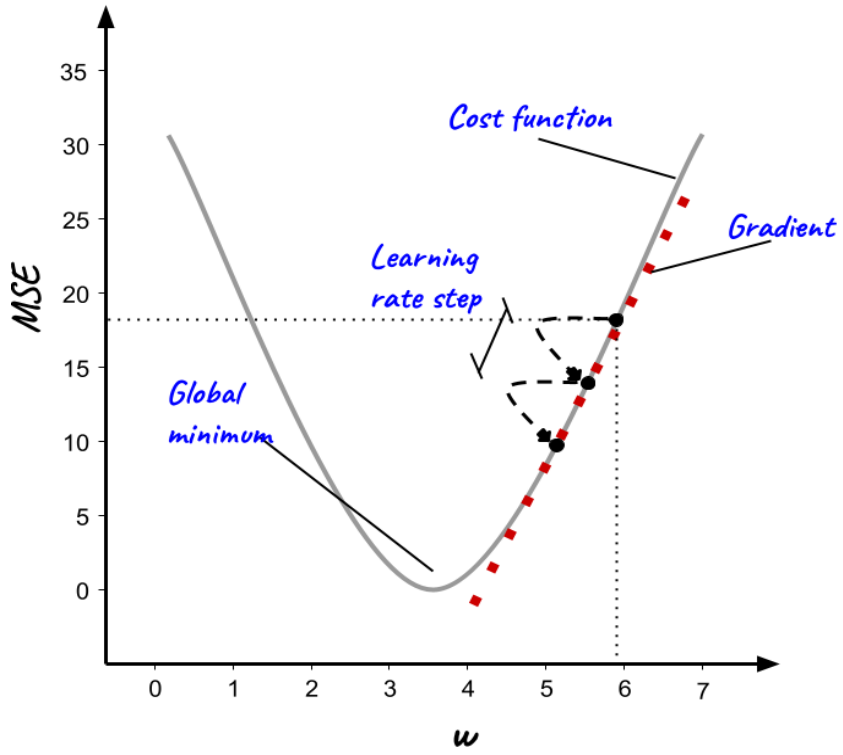

Figure 3.7: Cost function diagram for an ANN model.

Minimizing the cost function J means finding weight values w that make J reach its global minimum. Consequently, the partial derivative of J is calculated with respecting the weights w as:

$$\overrightarrow{d} = \frac{\partial J(w)}{\partial w_j} = \frac{\partial \frac{1}{n}\sum_{i=0}^{n}(a^i - \hat{y})^2}{\partial w_i} = \frac{1}{n}\sum_{i=0}^{n}\frac{\partial (a^i - \hat{y})^2}{\partial w_j} = \frac{2}{n}\sum_{i=0}^{n}\frac{\partial y^i}{\partial w_j}(a^i - \hat{y}). \tag{3.14}$$

If $a^i = x^i.w$, then $\frac{\partial y^i}{\partial w_j} = x^i_j$. Therefore, the derivative is given by:

$$\frac{\partial J(w)}{\partial w_j} = \frac{2}{n}\sum_{i=0}^{n} x^i_j(a^i - \hat{y}). \tag{3.15}$$

Then, weights are updated by following the rule for each iteration:

$$w := w - \alpha \frac{\partial(J(w))}{\partial w_j} = w - \alpha \frac{2}{n} \sum_{i=0}^{n} x_j^i (a^i - \hat{y}). \tag{3.16}$$

3.3.3 Logistic regression

Logistic regression is almost similar to linear regression, with one output difference. In logistic regression, the outputs are a special function: $\sigma(x^i.w_j)$, which squashes the value of $(x^i.w_j)$ in the interval of $(0:1)$. That means that the output values are two labels 1 or 0. The logistic algorithm is a function that works as a probability function. The closer the result is to 1, the greater the chance that the output is closer to the target and vice versa. Since the outputs are in the $(0, 1)$ range, the logistic function can be used for 2-class (binary) classification problems. It uses a logistic sigmoid as an activation function.

Supposing the logistic sigmoid function is $\sigma(a)$, where a is the neuron activation value $(x.w)$. For each sample x, the probability y $(y = \sigma(a))$ for given weights w, is donated as:

$$P(y|x, w) = \begin{cases} \sigma(a) & if \quad y = 1 \\ 1 - \sigma(a) & if \quad y = 0 \end{cases}. \tag{3.17}$$

Succinctly, the equation can be written as:

$$P(y|x, w) = \sigma(a)^y (1 - \sigma(a))^{1-y}. \tag{3.18}$$

Since the probability $\mathrm{P}(y^{(i)}|x^{(i)}, w)$ are independent for each sample $x^{(i)}$, the global probability is given by:

$$P(y|x, w) = \prod_{i}^{n} P(y^i|x^i, w) = \prod_{i}^{n} \sigma(a^i)^{y^i} (1 - \sigma(a^i))^{(1-y^i)}. \tag{3.19}$$

To turn products of the Equation 3.19 into sums, the natural *log* is employed.

$$\begin{aligned} log(P(y|x,w)) &= log(\prod_{i}^{n} \sigma(a^i)^{y^i}(1-\sigma(a^i))^{(1-y^i)}) \\ &= \sum_{i}^{n}[y^i log(\sigma(a^i)) + (1-y^i)log(1-\sigma(a^i))]\,. \end{aligned} \tag{3.20}$$

The goal is to maximize the *log* to get the highest probability of predicting the correct values. As for linear regression, the derivative of the cost function with respect to the weights can be calculated by

$$\begin{aligned} \frac{\partial log(P(y|x,w))}{\partial w_j} &= \frac{\sum_i^n [y^i log(\sigma(a^i)) + (1-y^i)log(1-\sigma(a^i))]}{\partial w_j} \\ &= \sum_{i}^{n} \frac{\partial [y^i log(\sigma(a^i)) + (1-y^i)log(1-\sigma(a^i))]}{\partial w_j} \\ &= \sum_{i}^{n} [y^i \frac{\partial log(\sigma(a^i))}{\partial w_j} + (1-y^i)\frac{\partial log(1-\sigma(a^i))}{\partial w_j}] \\ &= \sum_{i}^{n} [y^i(1-\sigma(a^i))x_j^i + (1-y^i)\sigma(a^i)x_j^i]\,. \end{aligned} \tag{3.21}$$

The last equation can be obtained by following the chain rule for derivatives. It states that if we have a function $F(x) = f(g(x))$, then the derivative of F with respect to x would be:

$$F^{'}(x) = f^{'}(g(x)g^{'}(x)), \tag{3.22}$$

or in another form

$$\frac{dF}{dx} = \frac{d}{dx}[f(g(x))] = \frac{d}{dg(x)}[f(g(x))].\frac{d}{dx}[g(x)]. \tag{3.23}$$

Applying the chain rule to the derivative of logistic regression

$$\frac{\partial \sigma(a^i)}{\partial a^i} = \sigma(a^i)(1-\sigma(a^i))$$

$$\frac{\partial \sigma(a^i)}{\partial a^j} = 0$$

$$\frac{\partial \sigma(a^i)}{\partial w^j} = \frac{\partial \sum_k^n w_k x_k^i + b}{\partial w_j} = x_j^i. \tag{3.24}$$

Therefore, according to the chain rule, the following is true:

$$\begin{aligned} \sum_i^n \frac{\partial \sigma(a^i)}{\partial w^j} &= \sum_i^n \frac{\partial log(\sigma(a^i))}{\partial a_i} . \frac{\partial a^i}{\partial w_j} = \frac{1}{\sigma(a^i)} \sigma(a^i)(1 - \sigma(a^i)) x_j^i \\ &= (1 - \sigma(a^i)) x_j^i. \end{aligned} \tag{3.25}$$

Similarly, the following applies:

$$\sum_i^n \frac{\partial log(1 - \sigma(a^i))}{\partial w_j} = \sigma(a^i) w_j^i. \tag{3.26}$$

This is similar to the update rule that was mentioned in linear regression.

3.3.4 Back-propagation

In previous sections, updating the weight values for one layer has been described. The latter concept is easily adapted for a network model with one hidden layer, where the outputs of a hidden layer are reviewed considering target outputs and, therefore, weights will be tuned. However, this is not the case in multi-layered networks with more than one hidden layer. That is because the target values for each hidden layer are not available and known. By defining w_{ij}, a weight between the i^{th} neuron of layer l and the j^{th} neuron of layer $l + 1$. In a multi-layered network, l and $l + 1$ can be any two successive layers, including inputs, hidden, and output. y is referred to values in the hidden layers. Therefore, y is the output of the activation function of layer l, and it is the input to the layer $l + 1$, see Figure 3.8.

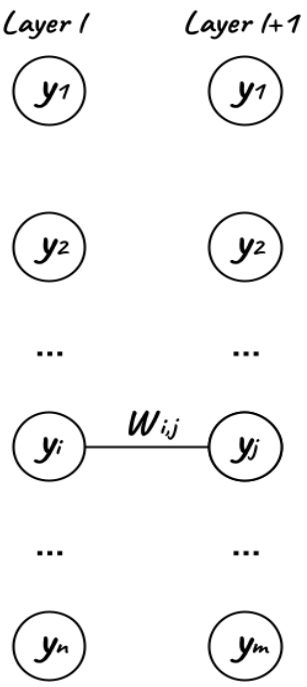

Figure 3.8: The figure represents two layers, the input (layer 1) and the output (layer 2), and $w_{i,j}$ connects the y_i activation in layer 1 to the inputs of the $j-th$ neuron of layer 2.

Using chain rule (Eq.3.23), It is possible to write the following for the last hidden layer:

$$\frac{\partial J}{\partial w_{i,j}} = \frac{\partial J}{\partial y_j}\frac{\partial y_j}{\partial a_j}\frac{\partial a_j}{\partial w_{i,j}}. \tag{3.27}$$

Since $\frac{\partial a_j}{\partial w_{i,j}} = y_i$, then:

$$\frac{\partial J}{\partial w_{i,j}} = \frac{\partial J}{\partial y_j}\frac{\partial y_j}{\partial a_j}y_i. \tag{3.28}$$

For a previous (hidden) layer, the same formula holds

$$\frac{\partial J}{\partial w_{i,j}} = \frac{\partial J}{\partial y_j}\frac{\partial y_j}{\partial a_j}\frac{\partial a_j}{\partial w_{i,j}}. \tag{3.29}$$

Since the $\frac{\partial a_j}{\partial w_{i,j}} = y_i$, and also $\frac{\partial y_j}{\partial a_j}$ is the derivative of the activation function. Therefore, what needs is to calculate the derivative of the error with respect to the activation function in the next (or output) layer. The latter can be applied by calculating all the derivatives, starting from the last layer and moving backward. By applying the chain rule to the cost

function

$$\frac{\partial J}{\partial y_i} = \sum_j^n \frac{\partial J}{\partial y_j}\frac{\partial y_j}{\partial y_i} = \sum_j^n \frac{\partial J}{\partial y_j}\frac{\partial y_j}{\partial a_j}\frac{a_j}{y_i}. \tag{3.30}$$

Note that the sum over j reflects that in the feed-forward part, the output y is fed to all neurons in the next layer(s); therefore, they all contribute to y_i when the error is propagated backward.

Once $\frac{\partial y_j}{\partial a_j}$ and $\frac{\partial a_j}{\partial y_i} = w_{i,j}$ is calculated. And $\frac{\partial J}{\partial y_j}$ is known. Then, $\frac{\partial J}{\partial y_i}$ can be calculated. In addition, when $\frac{\partial J}{\partial y_j}$ for the last layer is found, it can be moved backward and calculates $\frac{\partial J}{\partial y_i}$ for any layer. And therefore, $\frac{\partial J}{\partial w_{i,j}}$ for any layer.

For a sequence of layers, the following applies:

$$y_i \rightarrow y_j \rightarrow y_k\,.$$

Then, those two fundamental equations are given by:

$$\frac{\partial J}{\partial w_{i,j}} = \frac{\partial J}{\partial y_j}\frac{\partial y_j}{\partial a_i}\frac{\partial a_j}{\partial w_{i,j}}, \tag{3.31}$$

$$\frac{\partial J}{\partial y_j} = \sum_k^n \frac{\partial J}{\partial y_k}\frac{\partial y_k}{\partial y_j}. \tag{3.32}$$

Using the latter equations, the derivatives of the cost function considering each layer can be computed. Setting $\delta_j = \frac{\partial J}{\partial y_j}\frac{\partial y_j}{\partial a_j}$. Then δ_j represents the variation in the cost function with respect to the activation value. δ_j can be assumed as the error at neuron y_j.

The latter equations can be rewritten as follows:

$$\frac{\partial J}{\partial y_j} = \sum_j^n \frac{\partial J}{\partial y_j}\frac{\partial y_j}{\partial y_i} = \sum_j^n \frac{\partial J}{\partial y_j}\frac{\partial y_j}{\partial a_i}\frac{\partial a_j}{\partial y_i} = \sum_j^n \delta_j w_{i,j}\,. \tag{3.33}$$

This implies that $\delta_i = (\sum_j^n \delta_j w_{i,j})\frac{\partial y_i}{\partial a_i}$. These equations give an alternate view of back-propagation when there is a variation in the cost respecting activation value. Therefore, the variation for any layer can be determined once the variation for the following layer is

calculated:

$$\delta_j = \frac{\partial J}{\partial y_j}\frac{\partial y_j}{\partial a_j}$$

$$\delta_i = (\sum_j^n \delta_j w_{i,j})\frac{\partial y_i}{\partial a_i}.$$

Therefore,

$$\frac{\partial J}{\partial w_{i,j}} = \delta_j \frac{\partial a_j}{\partial w_{i,j}} = \delta_j y_i. \tag{3.34}$$

Finally, the update rule for tuning the weight values for each layer is given by the following equation:

$$w_{i,j} := w_{i,j} - \alpha \delta_j y_i. \tag{3.35}$$

3.4 Overfitting and underfitting issues

In general, the fundamental issue of artificial neural networks or machine learning is the tension between optimization and generalization [5]. Optimization refers to tuning the model to get the best performance on the training data. Whereas generalization explains how well the trained model performs on the test data that has never been seen before. The goal of training the model is to get a good generalization. However, the generalization is not controllable, and it depends on the training data.

At the beginning of the training process, optimization and generalization are well correlated (as the lower cost function value for training data also means a lower value of the test data). During the training, the model is underfitted. It means progress is still to be achieved, and the network model has not yet found the best relevant patterns for the training data. After certain iterations, generalization stops improving and starts to degrade. That means that the model is starting to overfit. Then the model starts learning patterns specific to the training data but misleading for new data.

To prevent the model from learning irrelevant patterns that could be found in the

training data. The best solution for such a problem is to get more training data. The model will generalize better when trained on more data. When this option is not possible, the second best solution is to modulate the quantity of information the model is allowed to store or to add some constraints on what types of information are allowed to be stored [5]. In other words, the optimization process will force the network model to concentrate on the most prominent patterns. This increases the probability of better generalization. The process of fighting overfitting is called regularization. It is always necessary to know that deep learning models tend to be good at fitting between training data and targets, but generalization is still a real challenge [5].

Overfitting solutions:

- Reducing the size of the network model: the simplest way to prevent the model from falling into overfitting is to reduce the size of the model. That can be done by changing the model's capacity or learnable parameters. Those parameters are the number of layers and units per layer. However, no universal formula can determine the suitable model's size. It should be evaluated from different perspectives to determine the appropriate parameters that fit the training data. The general rule is to start from a simple network with few parameters and then increase the size until obtaining a reasonable accuracy.

- Adding weight regularization: another way to prevent overfitting in a network model is adding weight regularization. It is a common way to magnitude the overfitting that puts constraints on a network by adding additional coefficients to the cost function to force the model to decrease the cost function values [5]. This process makes the distribution of weight values more regular. Weight regularization is done by adding to the cost function a penalty (term) that is given in two ways:

    1. $L1$ regularization: also called lasso regression. This regularization type adds the weight coefficients' absolute values to the cost function (Equation 3.36 in

red).

$$Cost\ function = \frac{1}{n}\sum_{i=0}^{n}(x^i * w - \hat{y})^2 + \lambda \sum_{i=0}^{n} |w|. \tag{3.36}$$

2. *L2* regularization: also called ridge regression. This type adds the square value of the weight values to the cost function. The latter is also called weight decay regularization (Equation 3.37:

$$Cost\ function = \frac{1}{n}\sum_{i=0}^{n}(x^i * w - \hat{y})^2 + \lambda \sum_{i=0}^{n} w^2. \tag{3.37}$$

– Adding dropout: it is one of the most efficient and commonly used regularization techniques. Dropout refers to dropping out hidden and visible units from the neural network model [98]. Dropping a unit out means removing it from the network, along with output features of the layer during the training process (see Figure 3.9). The choice of selecting units to be dropped is entirely random. Each unit is retained with a fixed probability p, where p can be chosen depending on the problem. The typical value of the fixed probability is p = 0.5, which is an optimal value for a wide range of tasks [99].

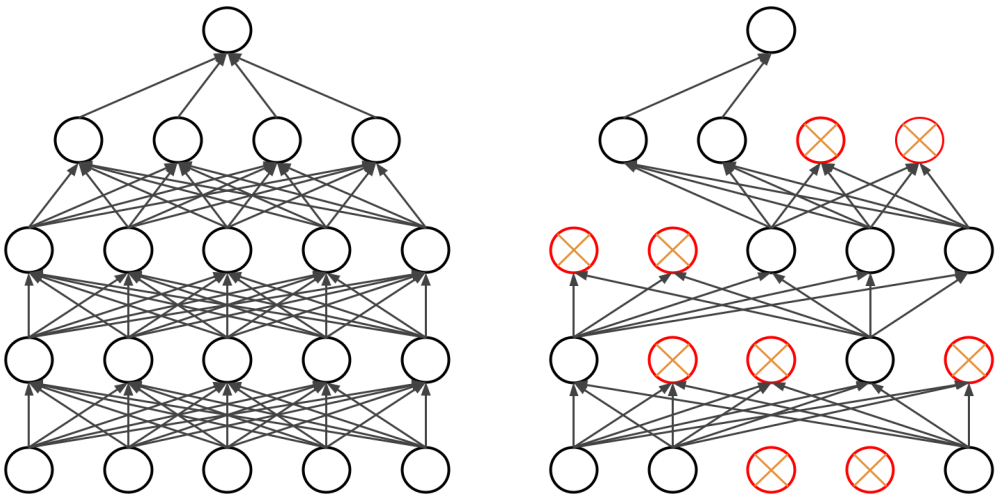

(a) *(b)*

Figure 3.9: Dropout neural network model. (a) Standard neural network. (b) Neural network after applying dropout technique.

3.5 Sensitivity analysis approach

Explaining the mechanism of complex deep learning models, such as neural networks, is quite cumbersome as they are identified as black box predictor tools [100]. To understand which features the model relies on, the problem of attributing a deep network's prediction power to input features must be identified. The attribution problem was formerly studied in several papers [101–103].

A significant challenge in attribution techniques is that they are difficult to evaluate empirically. In addition, it is hard to distinguish between errors that came from the model's misbehavior or the attribution method's misbehavior. Taking an axiomatic approach, called Integrated Gradients approach (IG) [104], can compensate for this limitation. The latter differs from the gradient descent algorithm [105], a common way to optimize ANN models.

The latter is denoted here as $IG_i(x)$ and uses a function $F : R^n \rightarrow [0, 1]$ that presents a neural network and an input $x = (x^1, ..., x^n) \in R^n$. An attribution of the prediction at the input x relative to a baseline input $z \in R^n$ is a vector $A_F(x, z) = (a^1, ..., a^n) \in R^n$, where a^i is the attribution of x^i of the prediction function $F(x)$. The integrated gradients can be defined as the integral of the gradients along the straight path from the baseline input z to the input x. The integrated gradient for the i^{th} dimension between a baseline and an input is defined by [104]:

$$IG_i(x) = (x_i - z_i) * \int_{\alpha=0}^{1} \frac{\partial F(z + \alpha * (x - z))}{\partial x_i} d\alpha \,. \tag{3.38}$$

In those graphs, the $y-$ axis represents the effect size, which quantifies the importance of each parameter on the prediction of sound insulation curves. If the y values are greater than zero, this indicates a direct relationship between the parameters and the outputs. However, values near zero suggest a weaker relationship. The integrated gradient technique focuses on the importance of each parameter in the prediction [104]. It often produces signed values, which can be challenging to interpret in specific applications [100]. Whether to take the absolute values depends on the dataset's characteristics. For

this research, taking the absolute value of the gradient can provide a better understanding of the results, as the goal is to identify the most significant parameters.

3.6 Mechanism used to develop the ANN models in the study and to extract the results

The ANN models were developed using Python language (3.7.4 version). They were used within the PyTorch framework [106] (version 1.5.0). The code was developed by the author for the three models. In addition, MySQL software [107] is used to organize the database of acoustic measurements. Figure 3.10 shows the mechanism that is used to develop the ANN models for different structures and how the results are obtained. The process starts with identifying the structural parameters for each assembly using MySQL software. The parameters contain categorical variables and metrically measured variables. Categorical variables are ways to label or identify objects [108]. An example of categorical variables is the structural materials used in assemblies (i.e., CLT panel, plasterboard). However, metrically measured variables reflect relative quantity and are appropriate for considering the amount of magnitude [108]. An example of the latter in the database is the thickness of the assemblies or the sound insulation performance values. Then the entire database is split (randomly) into three subsets: training (80%), validation (10 %), and training (10%) sets. see Figure 3.10. Each set contains inputs (structural parameters) and outputs (insulation curves) used to develop the ANN model. The ANN network starts to initiate its features (weights, biases, etc.) through several epochs or iterations using a training set. The prediction values are compared to measured ones in each epoch to minimize the cost function by tuning the weight values. In this study, measured curves are assumed as reference values to be compared with (although they would have uncertainty, as will be discussed in Chapters 5, 6, and 7). Therefore a world error represents the differences between measured and predicted values. Once the cost function reaches the minimum, weights, and biases are fixed. Then the validation and testing sets are used to evaluate the model's performance. Finally, a sensitivity analysis is

carried out on the developed model (Figure 3.10).

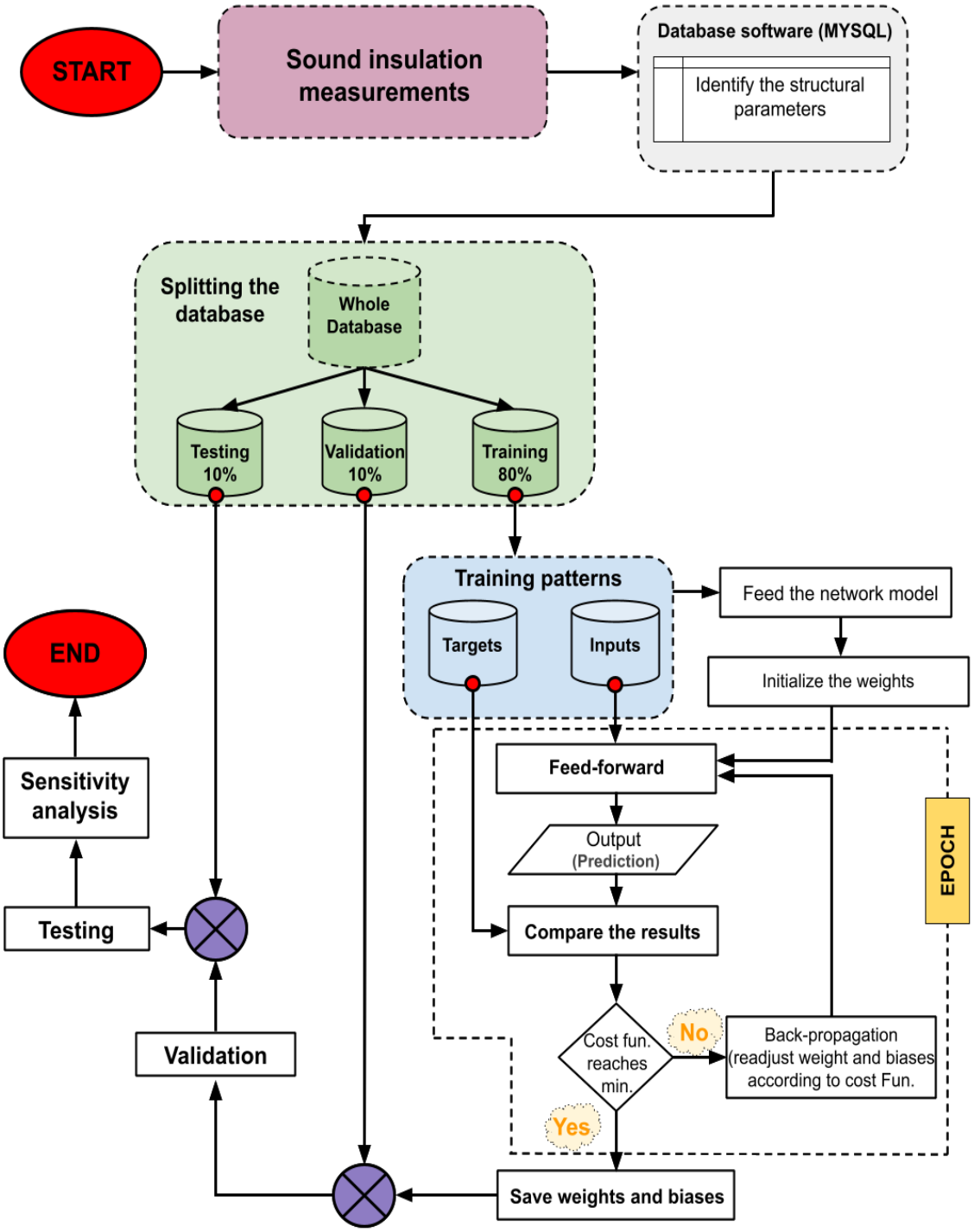

Figure 3.10: The methodology is utilized to develop network models to estimate the sound insulation performance of different wooden structures.

Chapter 4

EXPERIMENTAL SOUND INSULATION MEASUREMENTS AND DATABASE ORGANIZATION USED TO DEVELOP THE ANN MODELS

4.1 Acoustic measurements used to build the database

Developing an artificial neural network model needs diverse data to train the network model. Big data is utilized to develop acoustic prediction tools based on ANN models for different wooden configurations. Three models have been developed in this research project. ANN Model-I and Model-II (in Chapters 5 and 6) are created to predict acoustic performance based on laboratory measurements. Lab-based measurements are received from different institutes, such as Lund University in Sweden, FCBA in France, FPInnovations, and CRNC in Canada. The measurements are not necessarily implemented at the latter sources but could be from their database. However, the third model (Model-III, Chapter 7) simulates acoustic field measurements. This chapter provides details about assemblies and measurements used in this research. Alongside this, part of the measurement that the author has assisted will be highlighted in this chapter.

Measurement data based on ASTM standards were converted to comply with ISO standards descriptors, the weighted airborne sound reduction index R_w and the weighted

normalized impact sound pressure level $L_{n,w}$. The latter are described in ISO 717-1 (2013) [37] and ISO 717-2 (2013) [38] respectively. This conversion is done in order to have an agreement with the acoustic descriptors that are calculated from the airborne and impact sound insulation curves.

4.1.1 Sound insulation measurements for Model-I

The first model (Model-I) deals with the prediction of sound insulation of lightweight floor structures, 252 standardized laboratory measurements received from Lund University in Sweden, FCBA in France, FP innovations, and the National Research Council (NRC-CNRC) [109] in Canada, see Table 4.1. The measurement curves are all presented in Figures A1 and A2 in Annex A. The database contains two measurement curves: airborne sound reduction index R and normalized impact sound pressure level L_n in one-third octave frequency bands ($50 - 5000\ Hz$). The measurements concern 142 different floor structures (CLT-based and joist floors), corresponding to the data observations. Hence, for every floor structure or observation, there are the technical and materials parameters, the airborne sound reduction index data, and/or the normalized impact sound pressure levels data. There are 107 structures with airborne and impact sound insulation data, 26 with only airborne sound data, and 12 with only impact sound curves.

Each floor configuration in the database is arranged in three parts: upper, main, and ceiling part, following the order of material layers. The main part presents the dominant material for the structure's character among all floor components. The upper and ceiling parts represent materials located and clustered above and below the main part of each floor structure (Figure 4.1). The database contains two types of floor assemblies: CLT and joist floors; see Figure 4.1.

The database is organized with MySQL software [107]. Table 4.2 illustrated the structural parameters employed in the database classification. The parameters of the observations are arranged with respect to the type of materials, material layers order, thickness, density, joists type, width and depth of joist, area of test floor (S), the volume

of the receiving room (V), the ratio (S/V), total mass and total density of the structure, mass per unit area (P.U.A) of upper, main and ceiling parts, depth of the resilient metal channel, spacing between resilient channel, the slope of curves in three different frequency ranges (Low: 50 – 200 Hz, Middle: 250 – 1000 Hz and High: 1250 – 5000 Hz), and the airborne and impact sound insulation curves in dB in one-third octave bands (50 – 5000 Hz). Additionally, the classification contains two-floor solution systems: wet and dry solution systems. The wet system can be defined as a lightweight wooden floor structures with a light concrete part on top as a floating layer, whereas dry floor systems refer to wooden floors without any concrete layer on the top.

The acoustic measurements are implemented following ISO and ASTM standards. The measurements consist of airborne and impact sound insulation tests performed on 142-floor structures from 50 Hz to 5000 Hz. The airborne sound reduction index measurements were carried out according to ISO 140-3 (1995) [110] or the latest ISO 10140-2 (2010) [89] and ASTM E90-09 (2016) [32]. The impact sound pressure level data were measured following ISO 140-6 (1998) [111] or the latest ISO 10140-3 (2010) [43] and ASTM E492-09 (2016) [44].

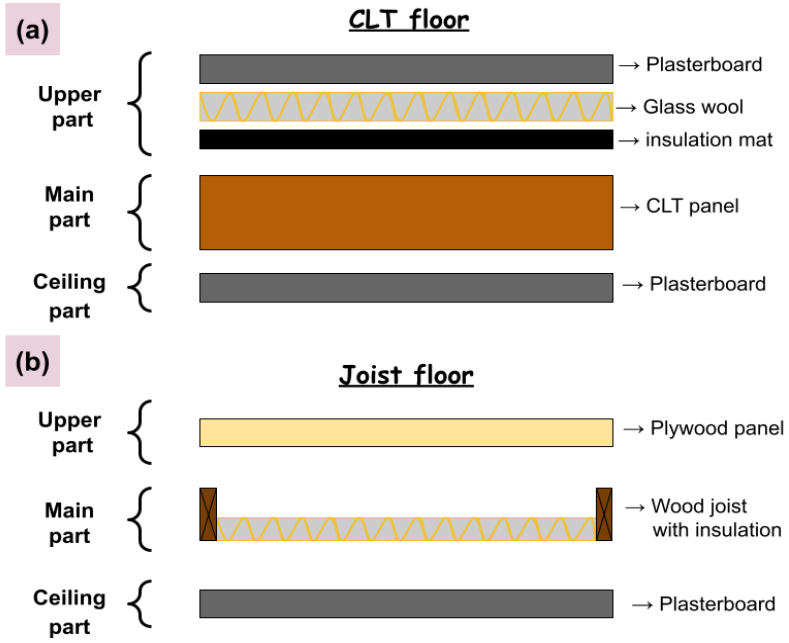

Figure 4.1: Database classification for floor assemblies. (a) An example of CLT floor assembly. (b) An example of the joist floor assembly.

4.1.2 Sound insulation measurements for Model-II

Model-II is developed using 100 standardized laboratory measurements that are implemented on different façade assemblies. The technical reports are received from Lund University and NRC-CNRC [112] in Canada. The measured data consists of airborne insulation measurements of 100 various façade walls in one-third-octave bands (50 Hz to 5000 Hz). They were performed according to ISO 10140-2 (2010) [89] and ASTM E90-09 (2016) [32]. The measurements used relate to complete wall systems without considering the presence of doors, windows, and small openings in the façades. Figure B1 in Appendix B illustrates the 100 insulation curves of façades of airborne sound reduction index $R(f)$ in the frequency range from 50 Hz to 5000 Hz. Every façade assembly in the database has technical parameters and a full-spectrum insulation curve. Table 4.2 summarizes the parameters used for each façade wall to be used as inputs for the network model.

In the database, each façade configuration is clustered in three parts: interior, main, and exterior, respecting the installation order of each façade component. The main part represents the dominant component or material. Therefore, The interior and exterior sections present components clustered and located alongside the main façade material (Figure 4.2). The database contains CLT and frame walls, as Figure 4.2 illustrates.

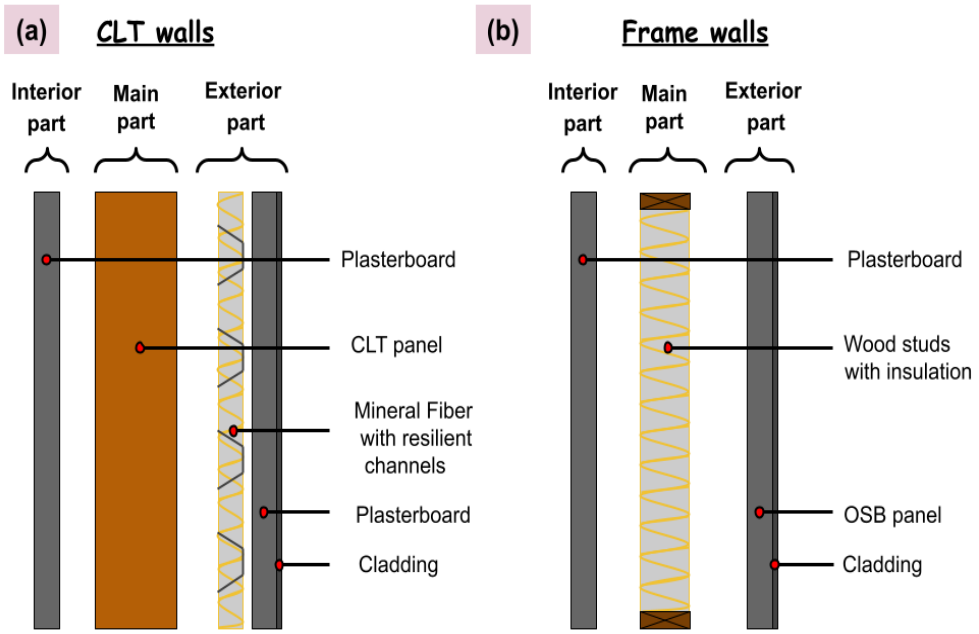

Figure 4.2: Database classification for façade assemblies. (a) An example of CLT façade assembly. (b) An example of frame façade assembly.

MySQL software is also used to organize the database using variables of structural parameters of each façade assembly (Table 4.2). Those parameters are arranged considering the type of each façade component, their installation position, thickness and density of each layer, depth of studs and spacing between them, area of a façade (S), the volume of a receiving room (V), group and total thickness and mass of a structure, resilient metal channel depth and spacing between them, and airborne sound reduction index in one-third-octave bands.

4.1.3 Sound insulation measurements for Model-III

The database collection comprises 104 acoustic field measurements implemented on multi-layered CLT-based floor systems for different buildings in Europe. The measurements include airborne and impact sound insulation in one-third-octave bands (50 Hz – 5 kHz). Fifty-one of them are airborne insulation measurements, and fifty-three are impact curves. Measurements were carried out according to ISO 16283 (Part 1 & 2) [33, 34] and ISO 717 (Part 1 & 2) [37, 38]. The floor structures contain two construction systems: wet and dry-rise solutions. A wet system can be identified as a CLT-based floor with a thin, lightweight concrete layer on the top as a floating panel.

A dry-rise solution is (in this thesis) referred to as a system without a concrete topping, with boards on top of point supports with integrated resilient interlayers. The dry-rise system separates the toppings and the CLT panel with an insulation layer in between; see Figure 4.3. The measurements are related to 19 projects related to 15 wooden buildings. Five buildings use a wet floor system, and the rest (ten) have a dry-rise system. Overall, 38 acoustic measurements are conducted on wet-floor systems (21 airborne curves and 17 impact curves). Moreover, 66 measurements are carried out on the dry-rise system (30 measurements are airborne, and 36 are impact curves).

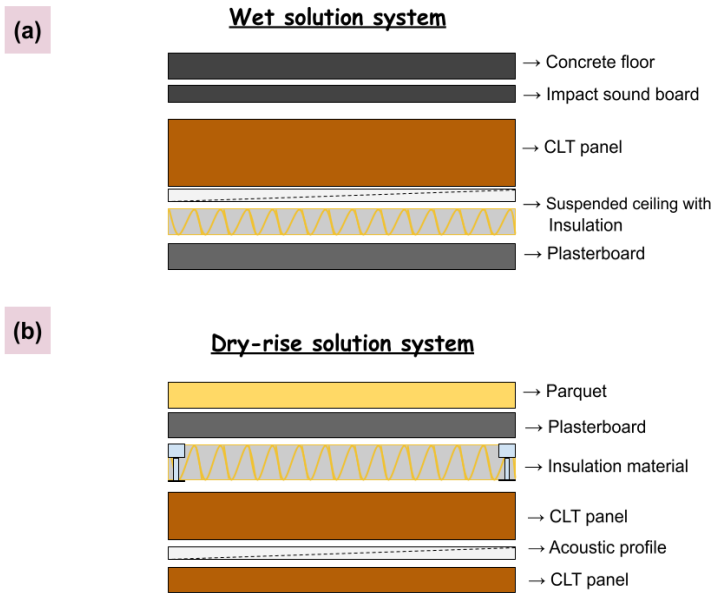

Figure 4.3: Database classification for CLT-based assemblies. (a) An example of a wet solution system. (b) An example of a dry-rise solution system.

The database includes several structural parameters of the measured floors, surrounded walls, and specific information about linked junctions. For each acoustic measurement, the structural materials of each floor and wall and their installation orders, thickness, densities, floor construction system, wall type, junction type, and visco-elastic interlayer thickness are considered in the modeling. In addition, each test floor's area and the receiving room's volume are included in the classification. However, openings in the surrounding walls are not considered during the modeling. Table 4.2 summarizes the categorical variables of the structural parameters that are considered in the modeling.

Table 4.1 shows each model's measurement number and type and the structures on

which the measurements are performed. Moreover, it summarizes the number of airborne and impact insulation curves for each network model.

Table 4.1: A division summary of the acoustic measurement numbers that are used to develop each ANN model sound insulation estimations.

ANN model	**Model-I**	**Model-II**	**Model-III**
Measurement number	252	100	104
Airborne measurements	113	100	51
Impact measurements	119	–	53
Measurements type	laboratory	laboratory	field
Test structures	floors	façades	floors

Table 4.2: Structural parameters used to classify the acoustic measurements for the ANN Models.

Input parameters	Model-I	Model-II	Model-III
– Material types	✓	✓	✓
– assembly solution system	✓	✓	✓
– Material installation order	✓	✓	✓
– Material thickness	✓	✓	✓
– Group thickness	✓	✓	—
– Total thickness of the assembly	✓	✓	—-
– Group density	✓	✓	—
– Total density of the assembly	✓	✓	—
– Structure area S	✓	✓	✓
– Volume of the receiving room V	✓	✓	✓
– Group mass	✓	✓	—
– Total mass	✓	✓	—
– Junction type	—	—	✓
– Surrounding wall type	—	—	✓
– Visco-elastic inter-layer thickness	—	—	✓
– Joist type	—	—	✓
– Joist depth	✓	—	✓
– Spacing between joists	✓	—	✓
– Studs depth	—	✓	—
– Spacing between studs	—	✓	—
– Resilient channels depth	✓	✓	✓
– Spacing between Resilient channels	✓	✓	✓
– Curve slope	✓	—	—

4.2 Acoustic laboratory measurements in Lund university

The research project started at Lund University by attending courses related to the thesis subject. In addition, the author implemented some lab-based acoustic measurements at Lund University. The measurements were for quantifying airborne and impact sound insulation for different structure components and following the latest ISO standards. The latter measurements were used in this study in order to develop artificial neural network models. Other previously implemented acoustic measurements at Lund University were added to the database to create the network models. The acoustic measurements obtained from Lund University are confidential and intended for research purposes only. Figure 4.4 shows an example of a floor assembly's airborne and impact insulation measurement. It shows a CLT panel is connected to joists, and the spacing between the latter is filled by an insulation material. Additionally, the details of the ceiling are also illustrated. However, Figure 4.4 depicts the removal of the floor structure, and the test structure is usually directly set up in the laboratory opening.

Since controlling the acoustic environment is vital in building acoustics, many solutions are being proposed to decrease the noise level in buildings. Figure 4.5 illustrates a dry-rise solution system used in Europe efficiently in the noise control aspect for floor structures. It depicts boards on top of point supports with integrated resilient interlayers. The the dry-rise system separates the toppings and the structural panel with an insulation layer in between.

Figure 4.4: A wooden floor structure is installed in the laboratory of Lund University to quantify the sound insulation measurement.

Figure 4.5: A dry-rise solution system that uses boards on top of point supports with integrated resilient interlayers.

4.3 Sound insulation measurements in a mock-up building in Luleå, north of Sweden and in the research center of FPInnovations in Quebec

During the research project, the author had opportunities to carry out additional acoustic measurements in mock-up buildings in Lule*å*, in the north of Sweden and the research center of FPInnovations in Quebec (industrial partner of the doctoral project). The measurements were meanly for different structures' reverberation time, airborne, and impact sound insulation. Some of the measurements were conducted in empty spaces and with furnished ones. Figure 4.6 shows joists fabrication and assembly using metal connectors, which are utilized to set up a floor structure in a mock-up building in Lule*å*. The joists are installed in the mock-up opening as illustrated in Figure 4.7 (a). In between the joists, an insulation material is employed to fill the gaps to improve the acoustic performance of the structural element. Figure 4.7 (b) showed an insulation matrix that is installed under the floor topping, which is efficient in acoustic improvements.

Generally, many products are used as a floor toppings, such as lightweight concrete layers, gypsum-based toppings, or parquet using different types of wood. Figure 4.8 shows the installation of the topping floor utilizing an underlying sheet and a parquet layer.

Some of the measurements that are carried out in the mock-up in Lule*å* were aimed to evaluate the low-frequency annoyance. For this purpose, the Japanese ball was utilized to evaluate the impact sound insulation performance for the test floor; see Figure 4.9 (a). However, the measurements in the mock-up building were not limited to airborne and impact sound insulation; different measurements also were included. Figure 4.9 (b) illustrates the measurement of floor deflection under a specific load to verify the floor and the joists assemblies. Moreover, the vibration of the assembled floor was also measured using accelerators in different locations of the floor structure, see Figure Figure 4.10 (a) and (b).

(a) (b)

Figure 4.6: An example illustrates the joists assemblage used in a floor composition in a mock-up building in Luleå. (a) Poisi-joists fabrication and assemblies using metal connectors. (b) Joists are ready to be used in a floor structure.

(a) (b)

Figure 4.7: An example for floor installation in a mock-up building in Luleå. (a) Insulation material filled the spaces between joists. (b) Insulation matrix used under the top flooring to improve the sound insulation.

Figure 4.8: Topping floor installation using a parquet layer and underlying sheet in Luleå.

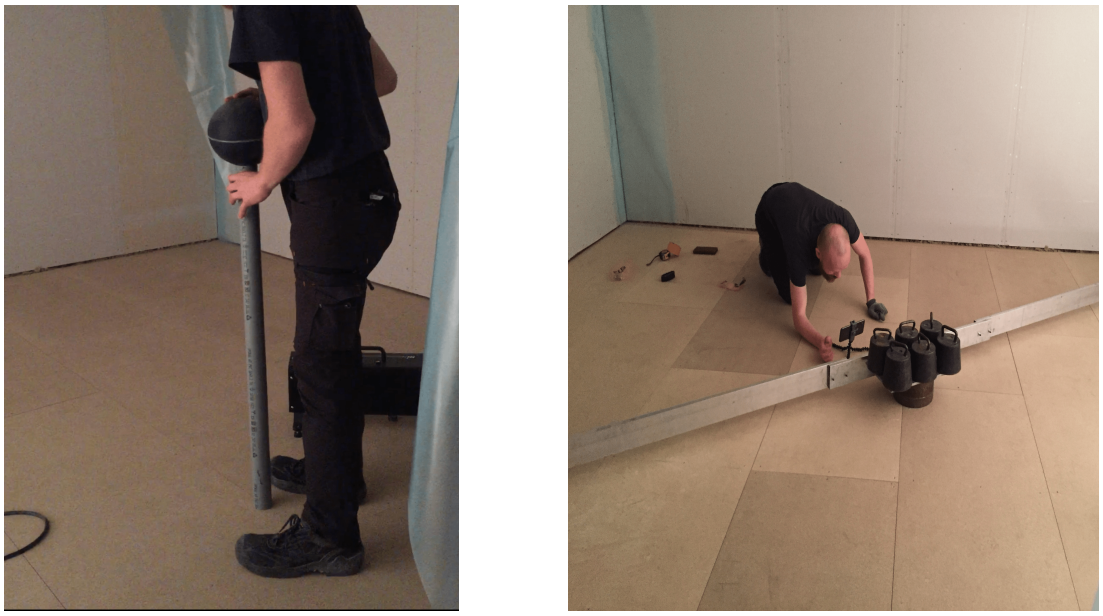

(a) *(b)*

Figure 4.9: Measurement types that are carried out at the mock-up building in Luleå. (a) Impact sound measurement using the Japanese ball. (b) Deflection measurement of a floor.

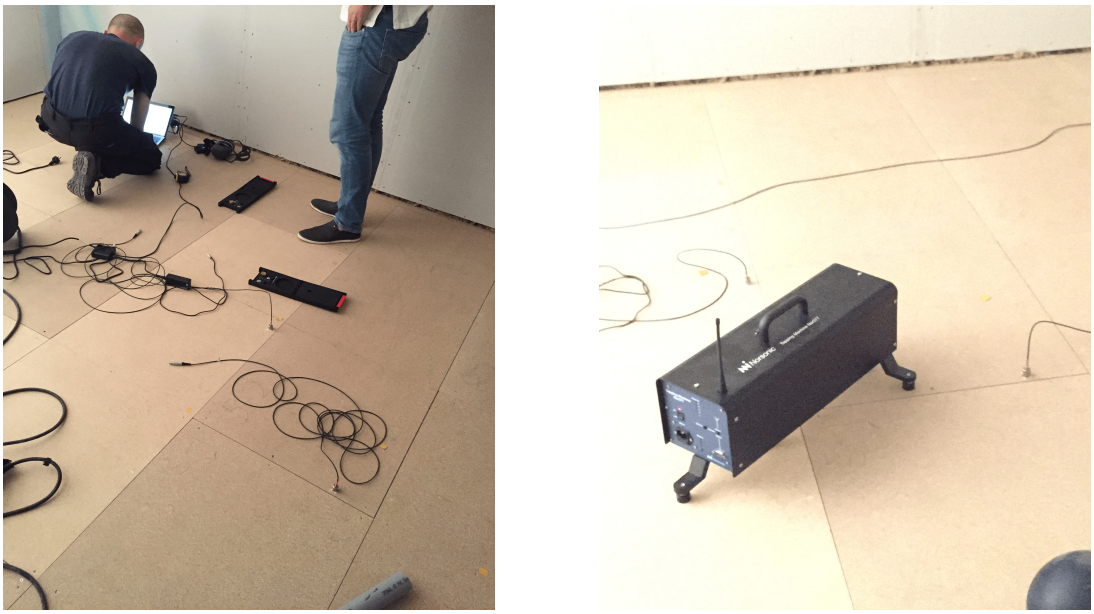

(a) *(b)*

Figure 4.10: Measurement set up for floor vibrations using accelerators on different locations in Luleå. (a) Transferring measured data. (b) Accelerators and tapping machine.

In addition, some measurements were implemented in the mock-up building in the research center of FPInnovations in Quebec. The measurements follow the ASTM standards for different partition types. The measurements in FPInnovations and in Luleå were educational and informative opportunities for the author to stay updated with the innovative industrial solutions and different measurement techniques in Europe and North America. Figure 4.11 depicts some materials used as floor components in FPInnovations. Figure 4.11 (a) illustrates parquet layers for floor topping. In addition, Figure 4.11 (b) shows an insulation matrix fabricated from recycled rubber tires and can contribute to sound insulation improvements. The relationship between sound insulation and embodied carbon emission (EC) was discussed by the author's contribution in a conference paper [113].

(a) *(b)*

Figure 4.11: Examples of materials that could be used in floor components in the mock-up building in FPInnovations in Quebec. (a) Floor topping parquet layer. (b) Insulation materials that are fabricated from recycled tires.

4.4 Field sound insulation measurements at University of Quebec in Chicoutimi

Sound insulation measurements were carried out in classrooms at the University of Quebec in Chicoutimi. Measurements were for airborne sound insulation curves for walls and floors of certain classrooms and the reverberation time measurements. In addition, vertical and horizontal impact sound insulation measurements were also implemented. Figure 4.12 shows acoustic setup equipment in a classroom using a sound source, amplifier, and sound meter. However, those measurements are not included in the database to develop the artificial neural network models. The research project aims to develop prediction tools for wooden structures, and the university building is mainly made from concrete. Then those measurements were implemented from an educational and training point of view and were out of the scope of this research.

Figure 4.12: Acoustic measurements set up in a classroom at University of Quebec in Chicoutimi.

(a) *(b)*

Figure 4.13: An experimental study to assess the noise levels induced by three coolers to be installed at the University of Quebec in Chicoutimi. (a) Generating noise similar to cooler noise. (b) measuring noise levels in the laboratory.

Furthermore, the author has had the opportunity to participate in acoustic projects

other than building acoustics for wooden structures. Figure 4.13 reveals an experimental study set-up to assess the noise levels generated by three coolers installed in different locations outside the university's main building and near two laboratories (on the first and the second floor). The noise levels of an installed cooler were measured to generate similar noise in future cooler positions. Then a sound source is installed in the future positions to generate noise, and the noise level is measured in the adjacent laboratories. The results were satisfactory, and façades of the university have good sound insulation that fulfills the acoustic requirements for students.

Chapter 5

PREDICTION OF SOUND INSULATION USING ARTIFICIAL NEURAL NETWORKS – PART I: LIGHTWEIGHT WOODEN FLOOR STRUCTURES

Résumé

L'approche des réseaux neuronaux artificiels est appliquée pour estimer les performances acoustiques des courbes d'isolation aux bruits aériens et aux bruits d'impact de différents planchers légers en bois. Le modèle de prédiction est développé sur la base de 252 courbes de mesure normalisées en laboratoire dans des bandes d'un tiers d'octave (50 Hz − 5000 Hz). Les caractéristiques physiques et géométriques de chaque structure de plancher (matériaux, épaisseur, densité, dimensions, masse, etc.) sont utilisées comme paramètres de réseau. La capacité de prédiction est satisfaisante et le modèle peut estimer les bruits aériens mieux que les bruits d'impact, en particulier dans la gamme de fréquences moyennes (250 Hz − 1000 Hz), alors que les bandes de fréquences plus élevées présentent souvent des erreurs importantes. La prévision de l'indice pondéré de réduction du bruit aérien R_w a été calculée avec une erreur maximale de 2 dB. Cependant, l'erreur a augmenté jusqu'à 5 dB dans le cas le plus défavorable de la prévision du niveau de pression acoustique d'impact normalisé pondéré $L_{n,w}$. Le modèle a montré de fortes variations près des zones de fréquence fondamentale et critique, ce qui affecte la précision. Une analyse d'attribution des caractéristiques a

exploré les paramètres essentiels de l'estimation de l'isolation acoustique. L'épaisseur des matériaux d'isolation, la densité des dalles en bois lamellé-croisé et des planchers flottants en béton, ainsi que la densité totale des structures de plancher semblent affecter le plus les prédictions. Une comparaison entre les systèmes de plancher sec et humide a montré l'importance de la partie supérieure des planchers pour l'estimation des bruits aériens et des bruits d'impact dans les basses fréquences.

Mots clés: bruit aérien, bruit d'impact, isolation, modèle de prédiction, réseaux neuronaux artificiels

Abstract

The artificial neural networks approach is applied to estimate the acoustic performance of different lightweight wooden floors' airborne and impact sound insulation curves. The prediction model is developed based on 252 standardized laboratory measurement curves in one-third octave bands (50 Hz − 5000 Hz). Physical and geometric characteristics of each floor structure, such as materials, thickness, density, dimensions, mass, etc., are utilized as network parameters. The predictive capability is satisfactory, and the model can estimate airborne sound better than impact sound cases, especially in the middle-frequency range (250 Hz − 1000 Hz), while higher frequency bands often show high errors. The weighted airborne sound reduction index estimate R_w was calculated with a maximum error of 2 dB. However, the error increased to 5 dB in the worst-case prediction of the weighted normalized impact sound pressure level $L_{n,w}$. The model showed high variations near the fundamental and critical frequency areas, affecting accuracy. A feature attribution analysis explored the essential parameters of estimation of sound insulation. The thickness of the insulation materials, the density of the cross-laminated timber slab, the concrete floating floors, and the total density of floor structures affect predictions the most. A comparison between wet and dry floor solution systems indicated the importance of the upper part of floors to estimate airborne and impact sound in low frequencies.

Keywords: airborne sound, impact sound, insulation, prediction model, artificial neural networks

5.1 Introduction

Managing the acoustic environment in buildings is a vital issue of both new and renovated structures, particularly dwellings [114]. Enhancing the acoustic comfort level of the occupants is also a key consideration in the research, design, and development of current constructions [115]. Standardized measurements are used to obtain helpful insulation data for existing building components, providing an indication or prediction of the performance of these elements in a new structure. Such measurements may be conducted in situ, or various test building elements can be set up in a laboratory, such as for testing the insulation of wall or floor partitions [3, 43, 89, 110, 111, 116, 117].

In order to ensure an adequate indoor climate, it is necessary to use prediction models and acoustic products with the expected performance. Previous works have presented several prediction tools to estimate the acoustic behaviour inside buildings [8–12, 17, 79]. However, some of these tools have shown a significant deviation from the expected outcomes [19–22]. In order to improve the accuracy of these tools, specific building parameters must be taken into consideration, such as modeling the connection between assemblies [12, 22, 30, 80].

Many problems arise for the acoustic performance prediction from that data due to: uncertainties in the measurements and the material properties, workmanship, and variations between field measurements (in a realized building) and laboratory measurements (in a controlled environment). The sound insulation curves measured for the same partition in a laboratory setup and in situ may deviate significantly due to lots of reasons, the most profound being flanking transmission, i.e., indirect propagation paths from the adjacent components in the entire mechanical system of a structure [3]. The acoustic comfort perception of residents may vary as well based on the material properties (heavyweight or lightweight structures) and the different cases of the measured sound insulation, e.g., airborne or impact sound related [30, 118, 119].

Wood has been widely used in construction engineering for its abundance in nature and ease of use [120]. North America has seen wood-frame structures as the leading housing

building system in the 20^{th} century [121]. Lightweight construction is a technique that uses materials to reduce the overall mass of a structure while maintaining its quality [122]. The term 'lightweight construction systems' often refers to wooden buildings. The study in this chapter (and thesis) focuses on this type of construction, and it could refer to joist floors, framing walls, and CLT floors and walls. A challenge in some types of lightweight construction is that the subjective sound insulation quality is perceived to be lower than that of a heavier structure with the same sound insulation data [123].

The most straightforward prediction model based on mass, stiffness, and losses is commonly used for single-wall structures but unsuitable for multi-layered and lightweight constructions [114]. Accurately estimating sound insulation for double structures has proven to be a challenge [3]. Mechanical connections between different materials, which are difficult to consider in analytical approaches [28] and the variety of construction materials make the prediction process complicated. Furthermore, the standardized methods for estimating the acoustic performance of building elements indicated in ISO 12354 Parts 1 and 2 [29, 124], which were developed based on data from heavy monolithic constructions, are not appropriate for multi-layered, complex, and lightweight structures [30].

Recently, machine learning (ML) and its applications have been employed for tackling complex problems across various domains, such as image classification, speech recognition, and building acoustic applications [17, 78, 125–131]. ML can be defined as a branch of statistics wherein a model can learn autonomously based on data without requiring explicit programming [132]. Thus, it is a tool utilized for large-scale data processing. ML techniques, and deep learning (DL) in particular, demonstrate superior performance when provided with large data sets, thus leading to enhanced predictive and analytic power, with greater accuracy and fewer errors. In other words, ML models and Deep Learning artificial neural networks (ANN) are more effective when supplied with large and varied data sets encompassing a representative sample of cases.

Artificial Neural Networks have been employed for various purposes in the field of acoustics. In audio engineering, studies have utilized ANN for optimizing the

acoustic performance of car interiors [133, 134] and for other applications such as speech recognition [135–139]. In environmental acoustics, ANN has been used to recognize the position of wind turbines using sound emission data of wind farms [140, 141]. Moreover, ANN has been used to predict the sound absorption of various materials based on their physical properties [142, 143].

In building acoustics, ANN models have been used to predict the sound insulation of sandwich partition panels and to accurately estimate the weighted airborne sound reduction index R_w and sound transmission class (STC) values with an error of ±3 dB and a confidence level higher than 95% [79]. Similar research was conducted on wooden window insulation to estimate the R_w based on technical parameters such as window typology, frame and shutters thickness, number of gaskets, R_w of glazing, and R_w of the window [80]. However, these two studies were limited to estimating a single value for the weighted index without utilizing full measurement curves in different frequency bands.

An Artificial Neural Network (ANN) was applied to predict the airborne sound insulation curves of masonry walls [17]. Thirty-four laboratory measurements of simple monolithic brick walls were studied, and their geometric and physical characteristics were used as input data for the ANN model: material, dimensions, density, mass, Poisson's module, Young's modulus, etc. Subsequently, a feature attribution analysis identified the most statistically significant parameters influencing the airborne sound insulation [17]. The parameters found to have the most significant effect on the estimation were: mass per unit area, the thickness of the wall, Young's modulus, the length, and the height of the brick. Although the predicted values agreed with the actual ones, the study was restricted to a specific type of construction.

In a previous study by the authors [144], an artificial neural networks model was used to accurately predict the acoustic spectrum of different lightweight wooden floor structures. The model was based on only 67 measurements and two parameters (thickness and installation order of the materials). Despite the model's limitations, it demonstrated acceptable accuracy in predicting R_w with 1 dB variation, suggesting that more precise estimations can be made by adding more parameters and measurement data. However,

the prediction of $L_{n,w}$ gives higher deviations of 9 dB.

This chapter seeks to develop a prediction tool based on artificial neural networks for estimating airborne and impact sound insulation for different floor structures. The data used to carry out this study are measurements from different floor configurations that have been standardized in a laboratory. A feature attribution analysis is conducted to determine the most influential parameters and their effect on sound insulation.

5.2 Materials and methods

5.2.1 Laboratory acoustic measurements

The database is constructed with data collected from 252 standardized laboratory tests conducted at Lund University in Sweden, FCBA in France, FPInnovations, and CNRC [109] in Canada. The measurements are not necessarily implemented at the latter sources but could be from their database. The tests involved 142-floor structures, measuring airborne and impact sound insulation in the frequency range of 50 Hz to 5 kHz. The airborne sound reduction index was measured following ISO 140-1 (1995) [110] or the latest ISO 10140-2 (2010) [89] and ASTM E90-09 (2016) [32]. The impact sound pressure level was assessed based on ISO 140-6 (1998) [111] or the latest ISO 10140-3 (2010) [43] and ASTM E492-09 (2016) [44].

The measurement data was adjusted to meet ASTM and ISO standards, which included the calculation of the weighted airborne sound R_w and the weighted normalized impact sound pressure level $L_{n,w}$ as described in ISO 717-1 (2013) [37] and ISO 717-2 (2013) [38] respectively. This conversion was necessary to ensure consistent acoustic descriptors derived from the airborne and impact sound insulation curves.

In this study, Figures A1 and A2 in the Annex visually represent the 252 standardized laboratory measurement curves utilized as input data for the ANN model. The database contains two types of measurement curves: airborne sound reduction index R and normalized impact sound pressure level L_n in one-third octave frequency bands (50 Hz − 5000 Hz). Table 5.1 summarizes the data observations based on 142 different floor

structures. Of these, 107 structures have airborne and impact sound insulation data, 26 have only airborne sound data, and 12 have only impact sound curves.

24 floor structures were used to validate the characteristics of the models, and another 24 was employed for testing and making predictions. Figure A3 in Annex A displays the testing data cases of floor configurations, which were randomly selected from all the data observations. These cases generally represent the typical trends of the insulation curves but also contain some significantly higher or lower cases, such as floors #1, #4, and #9 in Figure A1, or floors #2, #3 and #4 in Figure A2.

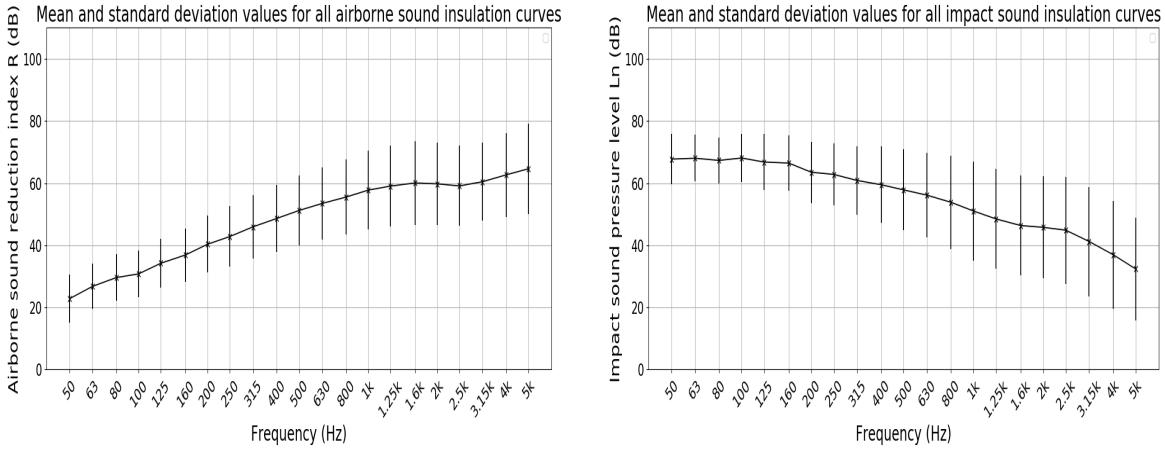

(a) *(b)*

Figure 5.1: Mean and standard variation of the standardized laboratory measurements. (a) Standardized measurements for airborne sound reduction index. (b) Standardized measurements for normalized impact sound pressure levels.

Table 5.1: A detailed description of the database number and their divided sets in the ANN model.

Database		**ANN model**		
Number of measurements	252	252		
airborne	**impact**	**training set**	**validation set**	**testing set**
133	119	204	24	24

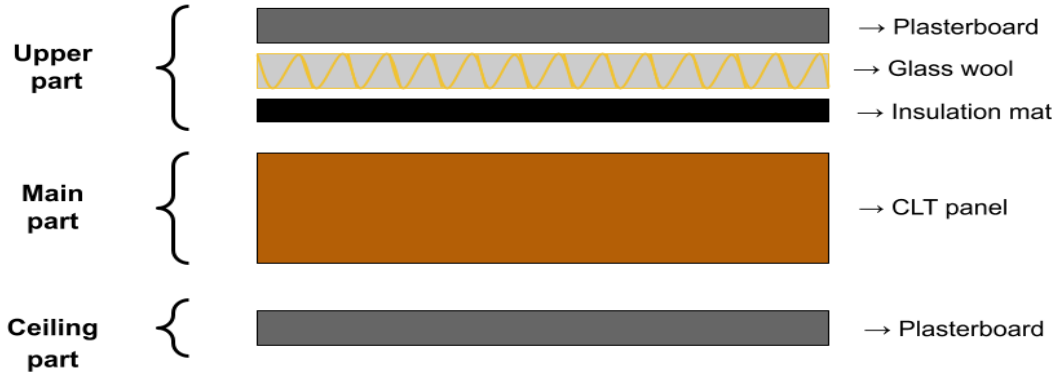

Figure 5.2: A schematic descriptive example illustrating the database organization for the floor components.

The floor structures in the database are composed of three distinct parts: upper, main, and ceiling. The main part is the most prominent material in the floor assembly. The upper and ceiling parts are collections of materials located above and below the main layer, respectively (see Figure 5.2).

Table 5.2: List of structural parameters that are used as inputs to train the ANN model.

Parameters used in the prediction model	Units	Classes
– Floor system	—	wet or dry solution
– Material types	—	i.e. concrete layer, CLT panel, insulation materials, etc.
– Material installation order	—	first/ second/...
– Material thickness	mm	—
– Group thickness	mm	upper, main and ceiling parts
– Total thickness of the floor	mm	—
– Material density	kg/m^3	—
– Group density	kg/m^3	upper, main and ceiling parts
– Total density of the floor	kg/m^3	—
– Area of the floor structure S	m^2	—
– Volume of the receiving room V	m^3	—
– Ratio S/V	—	—
– Group mass P.U.A	kg/m^2	upper, main and ceiling parts
– Total mass P.U.A	kg/m^2	—
– Joist type	—	metal/ wooden
– Joist depth	mm	—
– Spacing between joists	mm	—
– Resilient channels depth	mm	—
– Spacing between Resilient channels	mm	—
– Curve slope	—	low (50 Hz – 200 Hz), middle (250 Hz – 1000 Hz), high frequencies (1250 Hz – 5000 Hz)

The MySQL software [107] was used to organize the database in this study. A total of 23 variables were used as structural parameters (Table 5.2), which were used as inputs to train the ANN model. The model's output values were airborne and impact sound

insulation curves, with 21 values in dB in one-third octave bands for each curve. These parameters included the type of materials used, the material layers order, the thickness and density of the materials, the type of joists, the width and depth of joists, the area of the test floor (S), the volume of the receiving room (V), the ratio (S/V), the total mass and total density of the structure, the mass per unit area (P.U.A) of the upper, main and ceiling parts, the depth of the resilient metal channel, the spacing between resilient channel, the slope of the curves in three different frequency ranges (Low: 50 Hz − 200 Hz, Middle: 250 Hz − 1000 Hz and High: 1250 Hz − 5000 Hz), and the airborne and impact sound insulation curves in dB in one-third-octave bands.

5.2.2 The configuration of artificial neural networks model

The ANN model is built on a multilayer perceptron algorithm consisting of two hidden layers with 40 and 30 neurons each. Cross-validation was adopted to design and validate the model, as well as to address overfitting [96, 145]. The LeakyReLU (Leaky Rectified Linear Unit) function [97, 147, 148] was used as the activation function for both layers. This type of ReLU-based activation function has a slight slope for negative values. The Adam optimizer [149], which is a gradient descent-based optimization algorithm [105] used to optimize neural networks [150], was utilized for training the network and overcoming the vanishing gradient issues that are faced with normal activation functions such as sigmoid and tan functions by giving negative gradients instead of zeros [151].

The measurements are randomly split into three subsets: training, validation, and test set. The training set, which is 80% of the total, is used to initiate the ANN features. The validation set, which is 10% of the total, is employed to optimize the model's architecture. Finally, the test set, the remaining 10%, is used to estimate the predictive capabilities of the chosen model.

The Root-Mean-Squared Error (RMSE) is a cost function used to evaluate a model's performance when making predictions with continuous values, such as when predicting an acoustic curve.

$$RMSE = \sqrt{\frac{1}{n}\sum_{i=1}^{n}(\hat{y}_i - y_i)^2}, \tag{5.1}$$

where n is the total number of acoustic measurements that are used as a training set, $\hat{y}_i$ and y_i are the predicted and measured values, respectively. The overall prediction accuracy of the model (using the test set) is equal to 3.97 dB. For better evaluation in different frequency ranges, each predicted curve is evaluated individually against the measured one using RMSE function.

5.3 Results and discussion

5.3.1 Prediction of airborne sound insulation

After training and validating the ANN model with 202 and 24 laboratory measurements, respectively, another 24 sound insulation curves are randomly selected to test the model's accuracy (12 for airborne reduction index and 12 for impact sound pressure levels). The acoustic performance (in dB) in one-third octave bands (50 Hz − 5 kHz) is the set of dependent variables the model is used to be estimated. Figure A3 in Annex A displays the testing data cases of floor configurations.

The comparison between the measured and predicted curves of different floor configurations for airborne sound insulation, as shown in Figure 5.3, reveals that the predicted curves are very close to the measured ones, particularly in the low-frequency ranges. However, there are some discrepancies in the high-frequency bands. Floor #1 has the smallest deviation, with a RMSE of 1.65 dB, while floor #9 has the most significant deviation at 7.63 dB. Floor #9 comprises a simple configuration of 160 mm CLT and two light layers on top, and floor #1 is only slightly more complex.

It is often observed that significant variance in sound radiation is present at high frequencies (1.25 kHz − 3 kHz), which is typically the critical frequency for lightweight floors. This is due to resonance, which makes the sound radiation more efficient at this frequency [152]. It is possible to observe that the predicted curves tend to be smoother near the critical frequency, which is indicative of the limitations of the model when it comes to understanding these phenomena. This behavior is typical for plate-type structures, that is, components where the third dimension is negligible compared to

length and width, such as a gypsum plate [3].

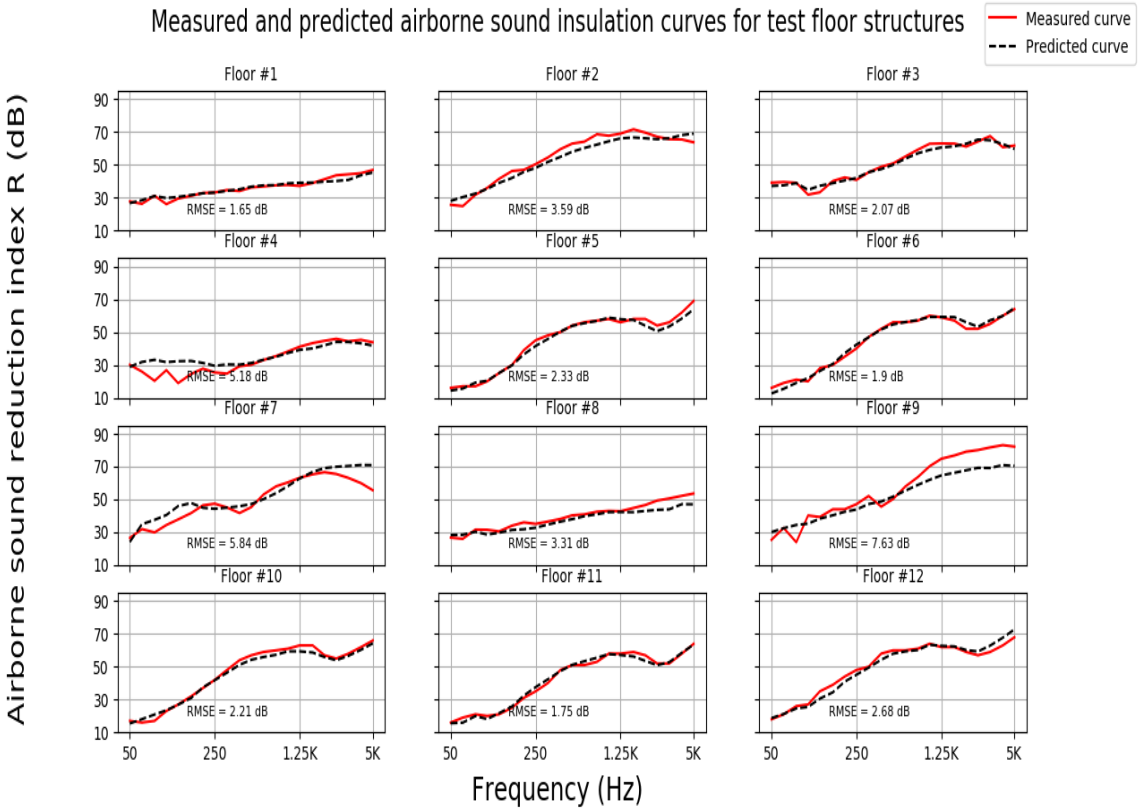

Figure 5.3: Comparison between measured and predicted acoustic curves for the tested floor structures for airborne sound reduction index.

Table 5.3: Comparison between measured and predicted sound reduction indexes for airborne sound insulation in test floor structures.

Floor no.	**RMSE (dB)**	R_w **(dB)**	$C_{100-3150}$	$C_{50-5000}$	R_{wPred} **(dB)**	$C_{Pred\ 100-3150}$	$C_{Pred\ 50-5000}$
1	1.65	38	0	1	39	-1	0
2	3.59	61	-2	-4	59	-2	-2
3	2.07	54	-2	-1	54	-2	-1
4	5.18	35	0	0	37	-1	0
5	2.33	49	-4	-5	49	-4	-5
6	1.9	48	-3	-3	50	-4	-5
7	5.84	54	-2	-2	54	-1	0
8	3.31	43	0	0	41	-1	0
9	7.63	57	-1	-3	56	-2	-1
10	2.21	50	-3	-5	51	-4	-5
11	1.75	44	-2	-2	46	-4	-4
12	2.68	55	-3	-4	54	-4	-5

However, this behaviour at the critical frequency may not be as apparent when dealing

with thicker floor slabs or multilayered floor configurations. The sound radiation is dependent on the overall vibration response of the system after excitation, as well as the material's properties included [152]. As such, every plate structure is excited below the critical frequency and radiates sound at low levels. However, significant sound radiation is observed in the mechanical system at the critical frequency. Above this, the whole plate structure can synchronize and radiate sound.

In certain cases, deviations can be seen at low frequencies below 150 Hz, where the fundamental resonances (first eigenfrequencies) are more evident [3], for example, floors #4 and #9. At these low frequencies, the airborne sound reduction performance is challenging to estimate accurately by the network model.

Table 5.3 demonstrates the total root-mean-square error between measured and predicted airborne sound curves for each tested floor configuration in one-third octave bands. The table also reveals the measured and predicted single-number quantities, R_w and $R_{wPredicted}$ respectively, for each test floor. The differences between the weighted reduction indices range from zero deviation (floors #3, #5, and #7) to a maximum deviation of 2 dB (floors #2, #4, #8, and #11). The calculated and predicted correction terms $C_{100-3150}$ and $C_{50-5000}$ in Table 5.3 demonstrate similar levels of deviation that do not exceed the deviations from the weighted reduction index comparison.

Figures 5.4 and 5.5 illustrate the differences between the measured and predicted sound insulation curves regarding dB and normalized errors, respectively. The most significant errors are seen in the high frequencies, while in the low frequencies, the model shows acceptable accuracy except for floors #4 and #7 (Figure 5.4). For the normalized errors, the frequencies are scattered randomly in the interval $[-1, 1]$ with a higher density in the low and high frequencies (Figure 5.5).

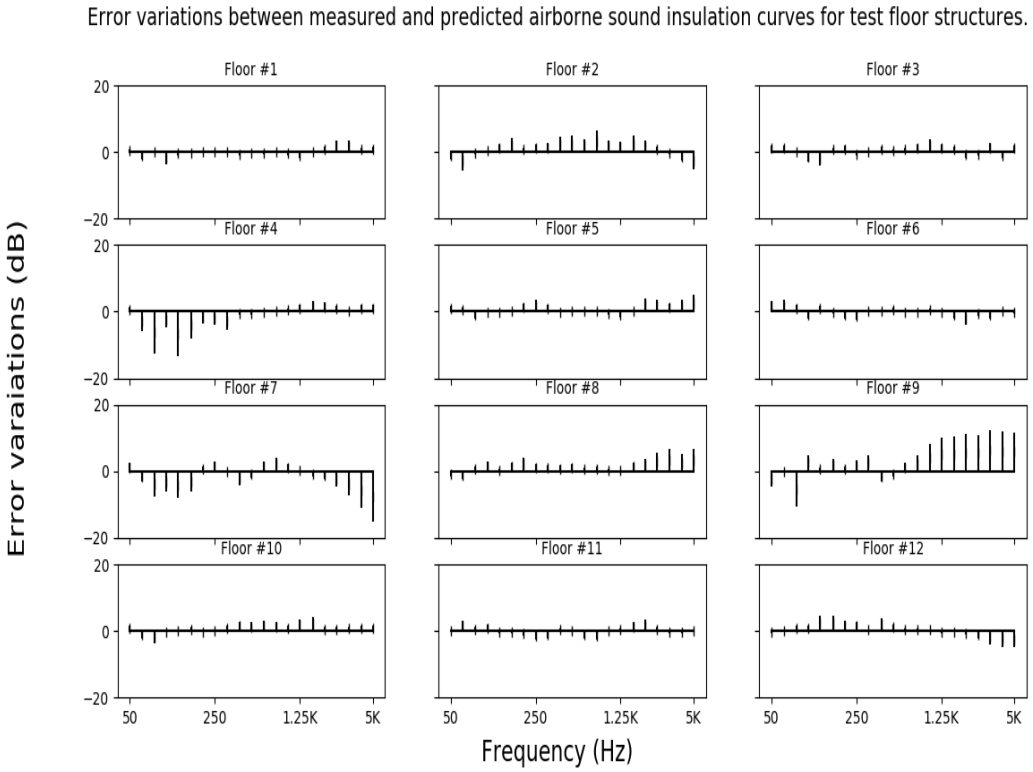

Figure 5.4: Error variations between measured and predicted airborne sound reduction index curves ($R(f)$-$R(f)_{Predicted}$) for test floor structures.

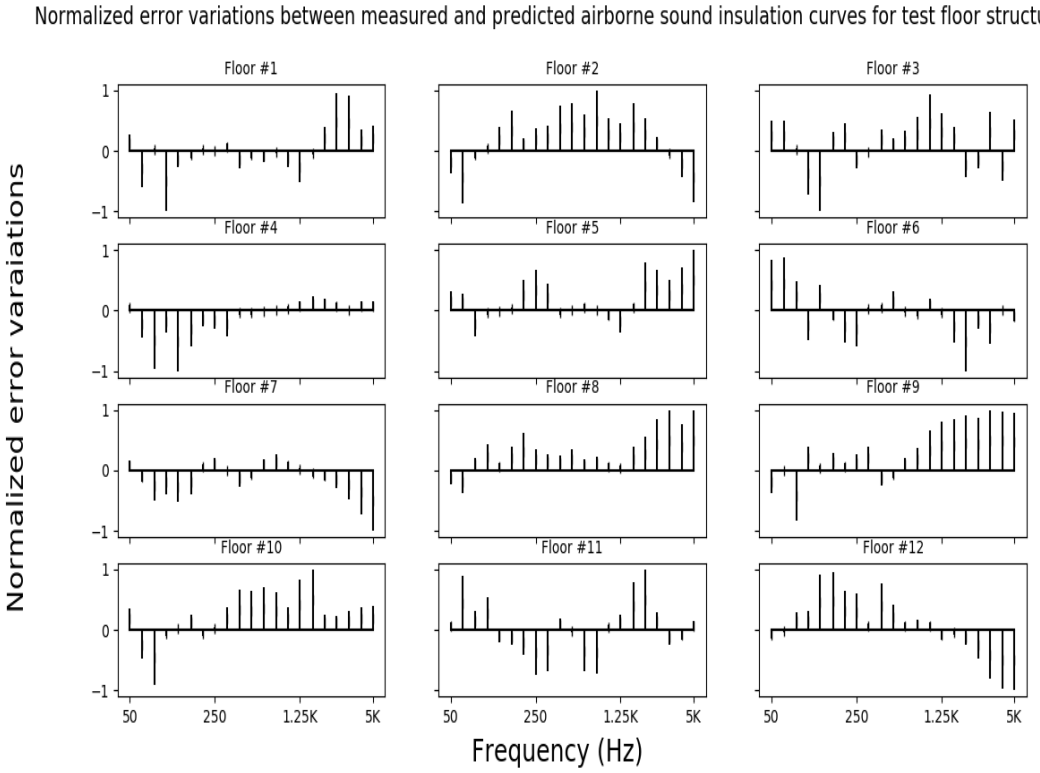

Figure 5.5: Normalized error variations (interval of $[-1, 1]$) between measured and predicted airborne sound reduction index curves for test floor structures.

5.3.2 Prediction of impact sound insulation

The model was tested on 12 randomly chosen test floors to evaluate its performance in predicting the normalized impact sound pressure level curves from 50 Hz to 5 kHz (Figure 5.6). The results showed that the model generally had a good agreement between the measured and predicted curves, particularly in middle frequencies. The greatest accuracy was found for floor configuration #12, with a deviation of only 2.28 dB (RMSE). Floor #7 had the greatest difference of 7.07 dB.

At frequencies close to 1.25 kHz, the critical frequency effect is again responsible for discrepancies between the measured and predicted curves, which can be seen in floors #3, #4, and #10. In addition, similar disagreements between the two curves appear near fundamental natural frequencies (first eigenfrequencies) of the floor below 200 Hz, for example, for floors #2, #3, #4, #7 and #9 (Figure 5.6).

The weighted normalized impact sound pressure level indices ($L_{n,w}$ and $L_{n,wPredicted}$) are presented in Table 5.4. The largest error deviation is up to 5 dB (RMSE) for floors #2 and #3, while for floors #1 and #11, the estimated weighted index is equal to the measured one. Additionally, the correction terms, $C_{I,100-2500}$ and $C_{I,50-5000}$, show errors between $0-3$ dB, which are within the range of deviations for the weighted indices.

Figures 5.7 and 5.8 show the prediction error and normalized error deviations for the impact sound pressure levels of the floor samples. The predicted dB values for impact sound pressure levels in the low-frequency bands are more accurate than high frequencies, except Floors #7 and #8. This is important as the lower frequencies are typically more influential in building acoustics for lightweight wood assemblies [153–155].

It is also known that impact sound curves have significantly low-frequency content with potentially more significant measurement uncertainty due to laboratory receiving room effects [156, 157]. These effects depend on the location of the Schroeder frequency, which is the point above which the diffuse field assumptions hold. Below this frequency, there can be unpredictable influence from the room's sound field during measurements.

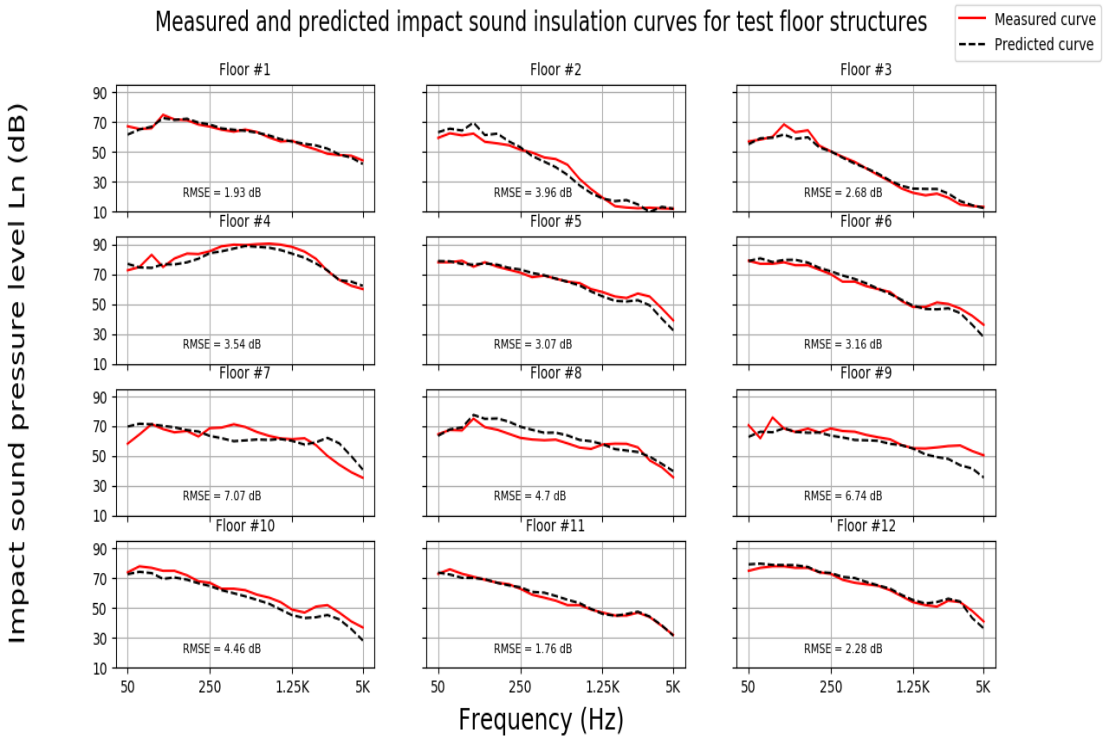

Figure 5.6: Comparison between measured and predicted values for the test floor structures for impact sound pressure level.

Table 5.4: Comparison between measured and the predicted weighted normalized impact sound pressure level for impact sound insulation in tested floor structures.

Floor no.	**RMSE (dB)**	$L_{n,w}$ **(dB)**	$C_{I,100-2500}$	$C_{I,50-5000}$	$L_{n,wPred}$ **(dB)**	$C_{Pred\ I,100-2500}$	$C_{Pred\ I,50-5000}$
1	1.93	64	1	1	64	0	0
2	3.96	48	2	6	53	4	6
3	2.68	53	3	4	48	2	4
4	3.54	88	-4	-4	85	-4	-4
5	3.07	68	0	3	67	1	4
6	3.16	66	1	4	68	2	4
7	7.07	64	-2	-1	66	-5	-2
8	4.7	64	-1	0	66	1	1
9	6.74	64	-2	1	60	0	1
10	4.46	63	1	5	60	1	5
11	1.76	60	1	6	60	0	5
12	2.28	68	0	2	70	0	3

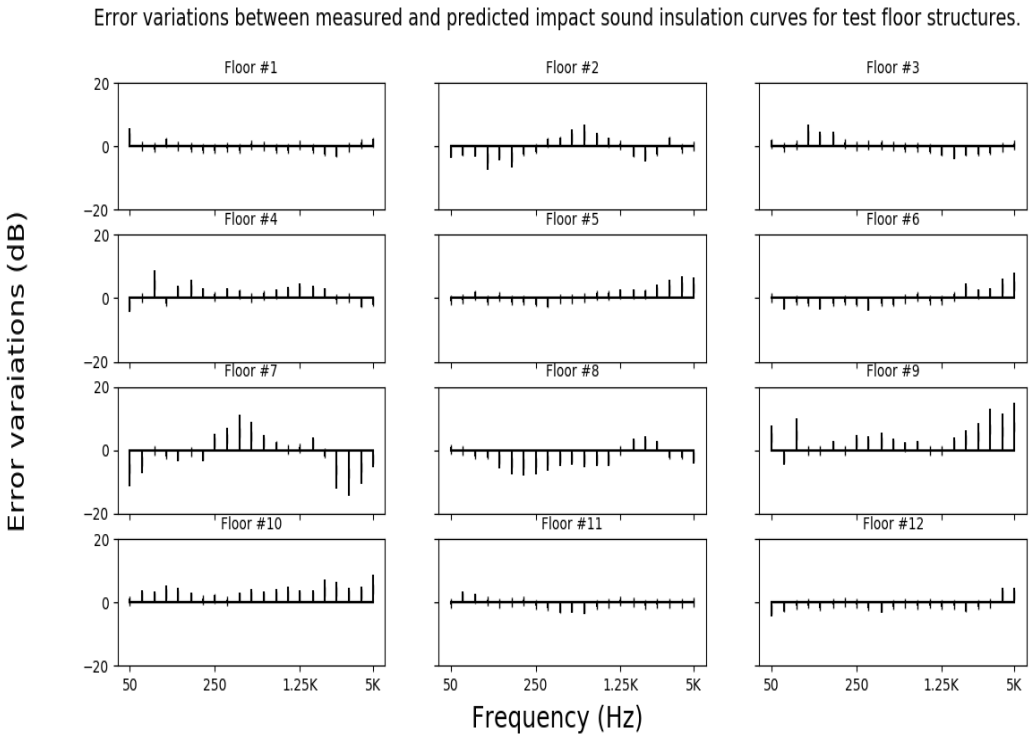

Figure 5.7: Error variations between measured and predicted impact sound pressure levels curves ($L_n(f)$-$L_n(f)_{Predicted}$*) for test floor structures.*

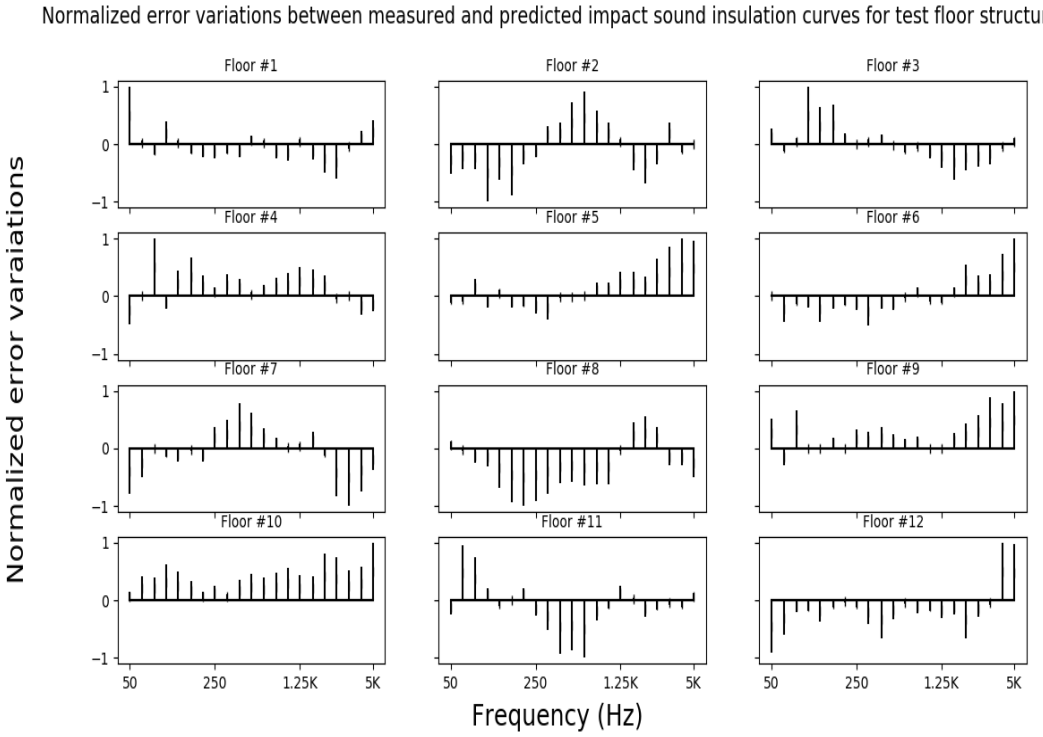

Figure 5.8: Normalized error variations (interval of $[-1, 1]$*) between measured and predicted impact sound pressure curves for test floor structures.*

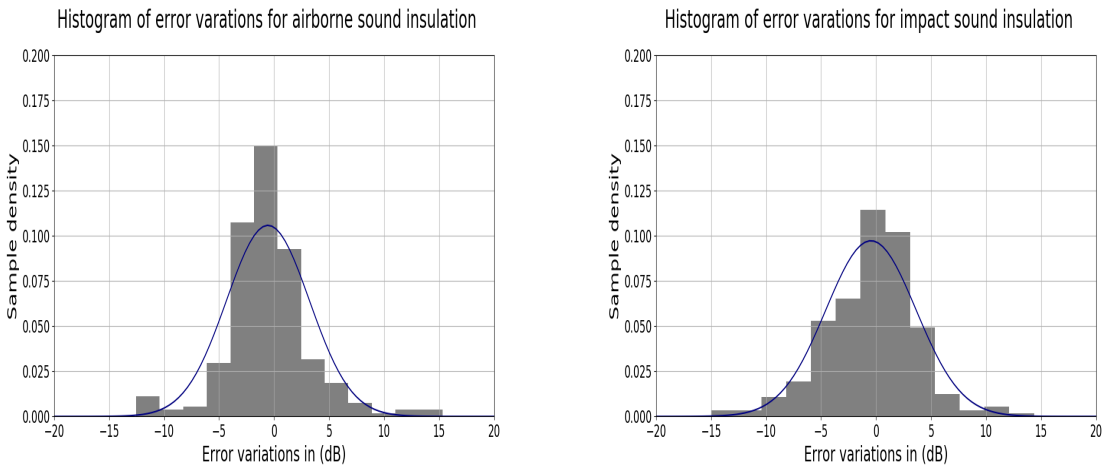

(a) *(b)*

Figure 5.9: Histograms of error variations in the prediction model for airborne sound reduction index and impact sound pressure levels for test floor structures in the frequency range (50 Hz − 5000 Hz) in one-third octave bands. (a) Airborne sound reduction index. (b) Normalized impact sound pressure levels.

The results of the normalized error distribution across frequency bands appear to be equally random and consistent for both low, middle, and high-frequency bands. Figure 5.9 illustrates the histograms of error variations in predicting airborne sound and impact sound insulation curves for test floor structures in the frequency bands (50 Hz − 5000 Hz). It can be seen that the errors are concentrated in the range of (-5, 5) dB for both airborne and impact sound estimations. Additionally, Figure 5.9 (a) and Figure 5.9 (b) demonstrate that the histograms are not symmetrical, with a higher peak for airborne sound reduction index and a lower peak for impact sound pressure levels. This indicates a higher accuracy of forecasting airborne sound insulation curves than impact sound insulation curves, which is also reflected in the calculation of single number quantities (R_w and $L_{n,w}$).

5.3.3 Sensitivity analysis results

A feature attribution analysis is conducted to investigate the connections between parameters and how they affect sound insulation estimations. This analysis is critical for this kind of modeling to evaluate the relevance of each dataset parameter on the prediction. It assesses the significance of different parameters and gives a comprehensive view of the

influence in each frequency band.

Certain materials were selected to investigate their contribution to sound insulation estimation based on their most common presence in acoustic measurements. Physical parameters such as the area of the floor being tested, the volume of the receiving room, the thickness and density of the upper, main, and ceiling parts of the floor, as well as other parameters, were taken into account to explore the effect they have on the modeling.

A further division is made on the measurements to assess the effect of dry and wet floor systems' upper, main, and ceiling elements on estimating acoustic insulation curves. A wet floor solution is described as a lightweight wooden floor structure with a thin concrete layer on top as a floating layer, while a dry floor system is a wood floor without any concrete layer on the top.

Feature attributions for airborne sound estimations

Figure 5.10 illustrates the correlation between the thickness and density of specific materials and their contribution to airborne sound insulation. It shows that, in the low frequencies, the densities of the concrete and CLT (cross-laminated timber) layers significantly impact the prediction. In the middle and high-frequency bands, the sensitivity of the density of the concrete layer and CLT panel remain essential, though diminished. Furthermore, the density of OSB (oriented strand board), chipboard, and plasterboard layers also have notable attributions across all frequency bands.

The thickness of some insulation materials (e.g., fiber glass, rock fiber, cellulose fiber) is usually a major factor that affects the prediction of insulation curves. This is not true for glass wool and rock wool in the presented ANN model. Contradicting the results of a previous study [161], there are no differences in sound reduction index in frequencies above 1.25 kHz for different densities of the rock wool. However, the ANN model shows that the effectiveness of rock wool in the middle frequencies is significant, which is also concluded in [161]. In addition, other floor components, such as rock wool, cellulose fiber sprayed on, and air gap, are more influential than their thicknesses or densities regarding the material effect.

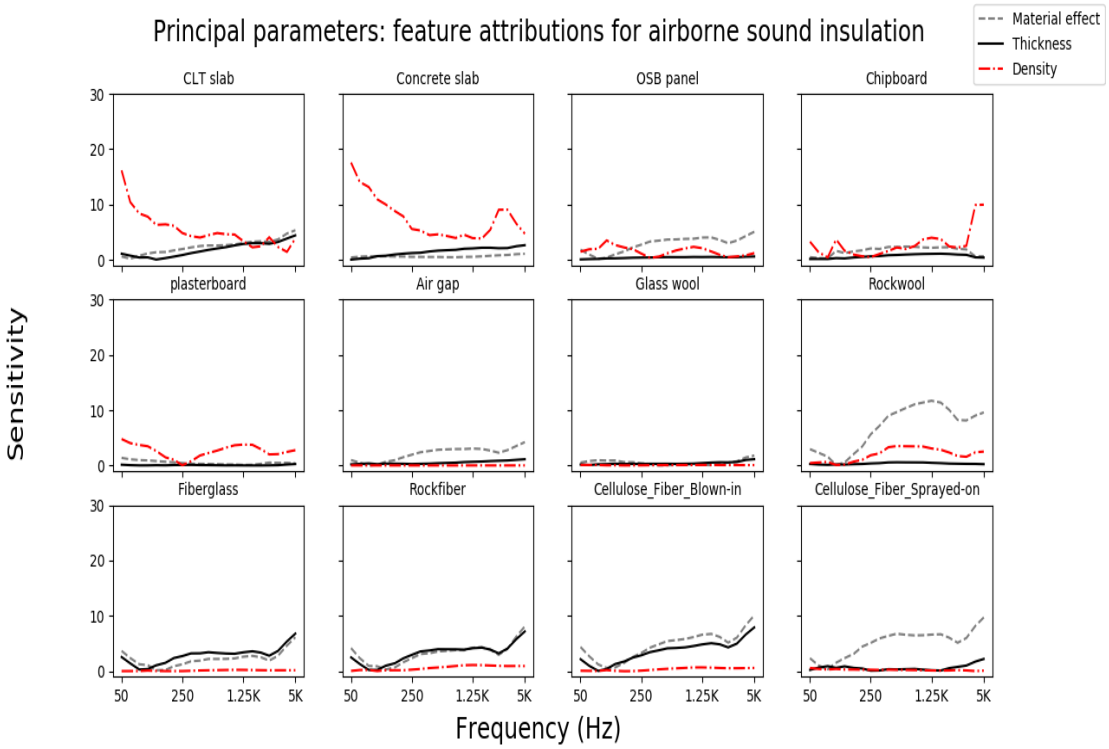

Figure 5.10: Feature attributions of structure layers and material types for airborne sound prediction.

The results of Figure 5.11 indicate that the volume of the receiving room V affects low-frequency sound. However, the area of the test floor S influences high frequencies, which agrees with another study that highlighted the importance of S in the predictions [162]. The ratio S/V does not have any notable effect. This contrasts the findings of a different study [162], which reported that S/V had a significant impact.

The total thickness parameter and thickness of the main part have an obvious correlation with higher frequency bands. The spacing (central distance) between joists impacts the estimation of airborne sound insulation in the middle and high frequencies. It is also observed that the spacing between the resilient metal channels (in suspended ceilings) affects the prediction of airborne sound insulation in the middle frequencies. However, parameters such as the slope of the acoustic spectrum (in low, middle, and high frequencies), depth of the joist and resilient channels, and type of the joist appear to have only minor influences.

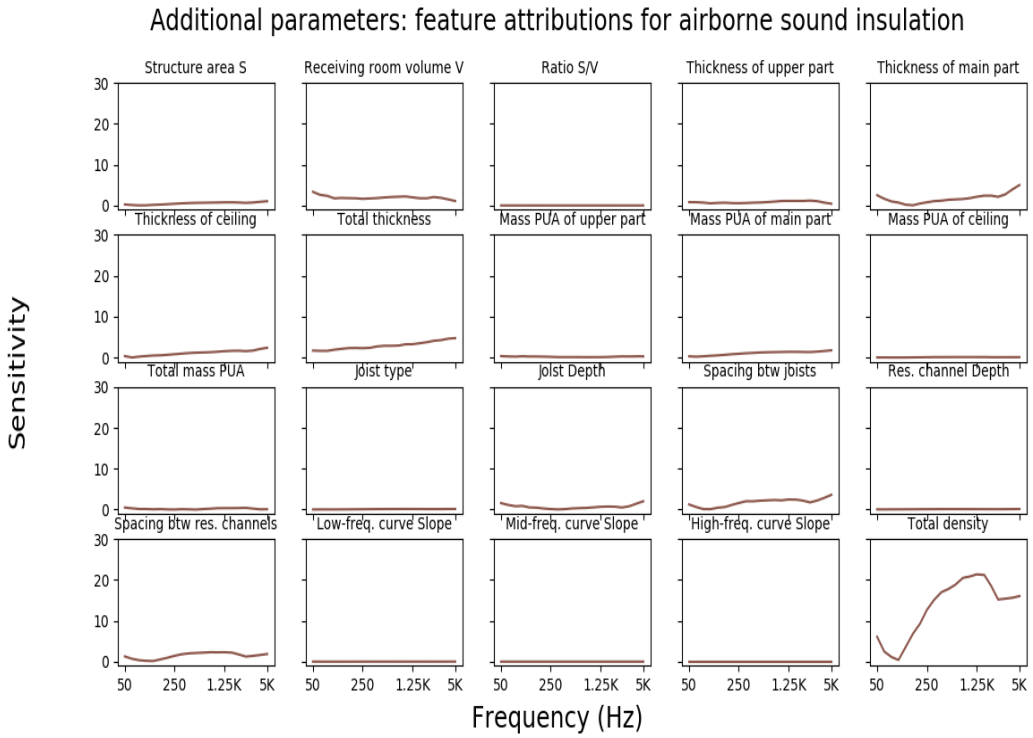

Figure 5.11: Feature attributions of additional parameters for airborne sound prediction.

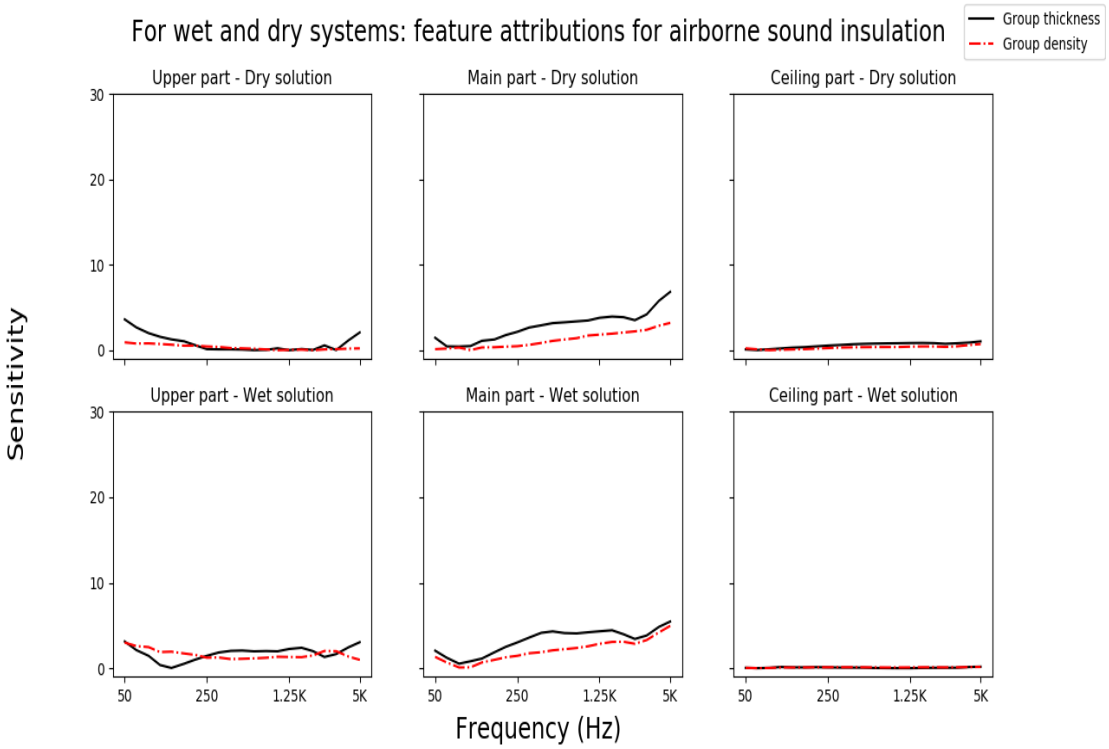

Figure 5.12: Feature attribution of dry and wet floor solutions' upper, main, and ceiling parts for airborne sound prediction.

The results of Figure 5.12 suggest that the thickness and density of the upper, main,

and ceiling parts of dry and wet floor solutions influence the airborne sound insulation. Surprisingly, the ceiling part's effect appears insignificant for all floor solutions. For dry floor systems, the thickness of the upper part has a noticeable effect only for frequencies in the low and high ranges. In middle and high frequencies, however, the thickness and density of the main part have a significant impact.

The density of the wet floor systems' upper part (containing a concrete layer) affects the prediction of airborne sound at all frequencies. This is shown in Figure 5.10, which demonstrates the impact of the density of a concrete layer. For dry solutions, the thickness of the main part plays a significant role in the middle and high frequencies.

Feature attributions for impact sound estimations

Figure 5.13 shows the effect of different materials on the prediction of normalized impact sound pressure levels. The thickness of the CLT panel has a similar effect size for all frequencies (as seen in Figure 5.10). However, the thickness of the concrete layer has a minor impact on the prediction. The density of the CLT slab has a significant attribution in low and high frequencies and decreases in the middle frequencies. The density of the concrete layer has the highest sensitivity for frequencies between 50 Hz and 250 Hz.

The thickness of insulation materials is essential in higher frequency ranges, particularly for fiberglass, rock fiber, and cellulose fiber, but not for glass wool in the ANN model. Additionally, it is generally accepted and assumed that no significant noise reduction is achievable in low-frequency bands, as stated by the force transmissibility theory, which states that the injected force is transmitted directly to the structure without any attenuation at low frequencies [158, 159].

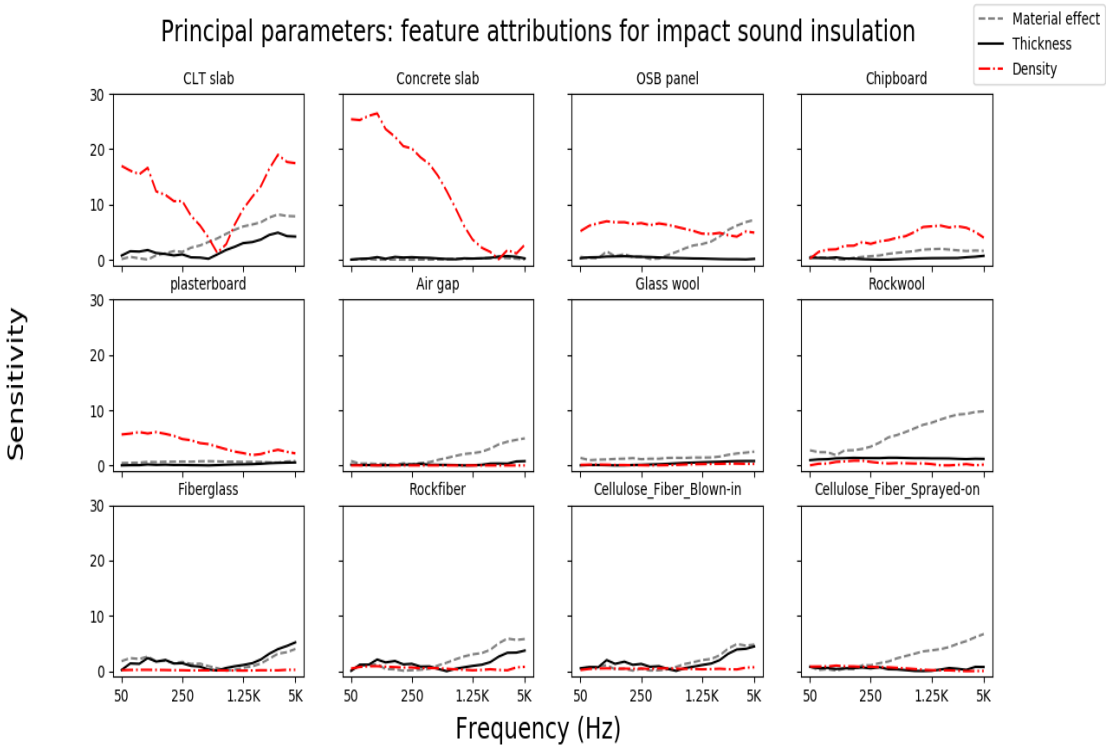

Figure 5.13: Feature attributions of structure layers and material types for impact sound prediction.

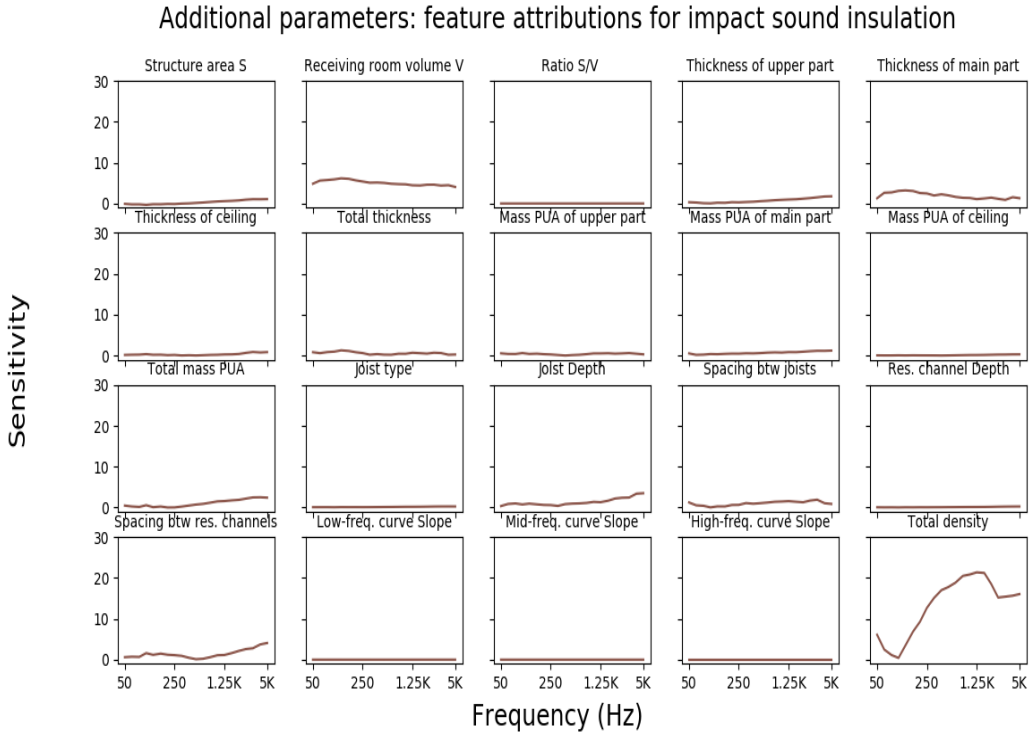

Figure 5.14: Feature attributions of additional parameters for impact sound prediction.

Figure 5.14 shows that the spacing between joists and the spacing between resilient

channels affect the estimation of impact sound insulation only in high frequencies. Additionally, the volume of the receiving room V has a more significant effect on the prediction of sound insulation in low-frequency bands, compared to the findings of [156], which concluded that the effect of the volume is not frequency dependent. The slope of the measurement curves, the floor area, the ratio S/V, and the joist type have a minimal impact on the prediction of impact sound insulation.

Figure 5.15 results suggest that the thickness of the upper part has the most significant influence on the impact of sound insulation predictions for dry floor systems in low and middle frequencies. For wet floor systems, the thickness of the upper part appears to affect the predictions more than the density in low and high frequencies, while the main part has a lesser effect on the predictions in the middle and high frequencies. The ceiling part has little impact on the dry and wet floor solutions in middle and high frequencies. The effect of concrete toppings in wet systems is also highlighted in an experimental study of different concrete topping thicknesses [160].

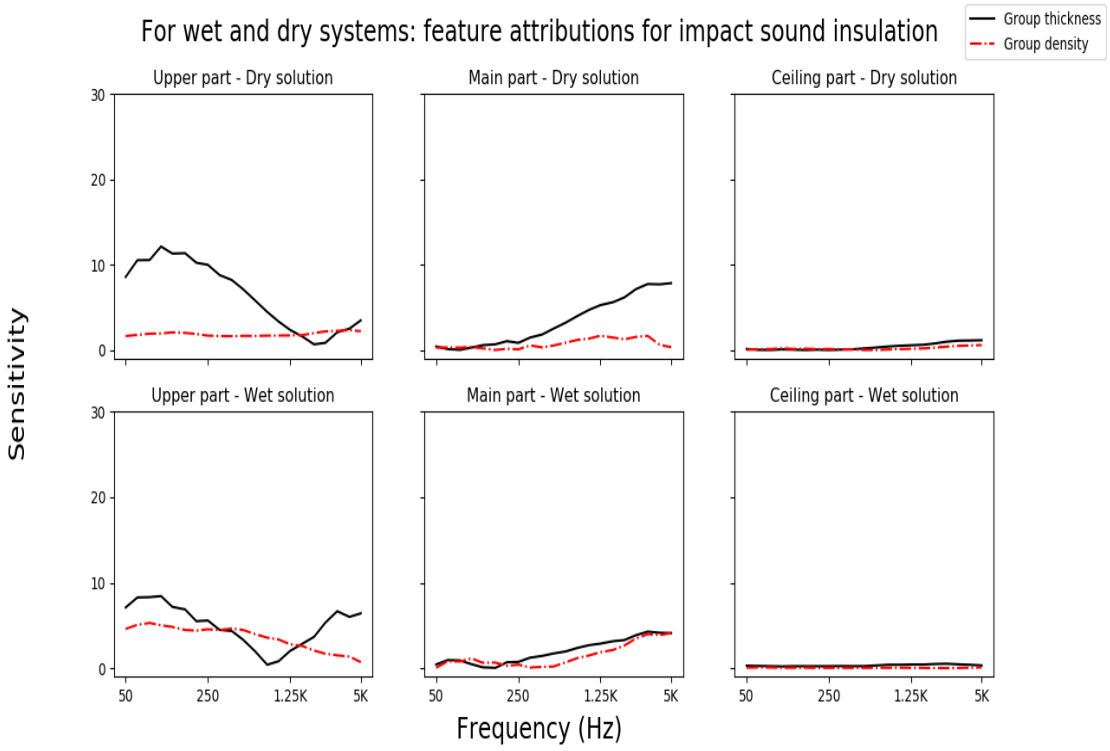

Figure 5.15: Feature attribution of dry and wet floor solutions' upper, main, and ceiling parts for impact sound prediction.

The data in Figure 5.15 is consistent with the classic mass-spring-damping system

approach [3], indicating that below the first eigenfrequency (the stiffness-controlled region) thickness is the main parameter in predicting impact sound insulation. Additionally, the results confirm the previously established conclusion that density and thickness have a more significant contribution in the middle and high-frequency bands (the mass-controlled and coincidence-controlled regions, separated by the critical frequency). The latter findings were also highlighted in [114].

Common observations in prediction of for airborne and impact insulation

It appears that the most significant discrepancies between the measured and predicted values in the results of the ANN model (for both airborne and impact sound insulation) are found for the simplest floor configurations, such as floor #4 in Figure 5.3 and floor #9 in Figure 5.6. This is likely due to the lack of measurements taken on simple structures in the database, which could affect the accuracy of the estimation. The results indicate significant difficulties in estimating airborne and impact sound insulation curves at high frequencies. This is probably because of the critical frequency locations for the test floors at high frequencies, as well as the increasing standard deviation of the sound insulation curves above 1 kHz (Figure 5.1). This limitation in the ANN model was previously noted by [17]. Similar problems appear with the estimations in the low-frequency band at the fundamental frequencies.

The ANN model is not able to accurately predict all fluctuations of the measured curves, leading to smoother forecast curves compared to the measured curves, as seen in Floors #4, #7, #8, #9, and #10 in Figures 5.3 and 5.6. This is due to the statistical nature of neural networks, which rely on the measurements in the database to form an estimation that follows an average trend. The more similar measurements to the test floors in the training set, the higher the likelihood of accurately estimating the test floor curves.

Table 5.5 provides a comparison between the measured and the predicted airborne and impact sound insulation curves split into three different zones: low (50 Hz – 200 Hz), middle (250 Hz – 1000 Hz) and high frequencies (1250 Hz – 5000 Hz). The error variations are assessed using the root-mean-square error (RMSE) function. The

RMSE value in low frequencies for airborne sound estimations is similar to that of the impact insulation cases. However, the model's predictive capability for airborne sound in the middle-frequency range is better than impact insulation's. In high frequencies, the accuracy is lower than the other zones for airborne and impact sound forecasts due to critical frequency. Overall, Table 5.5 demonstrates that the prediction of airborne sound reduction curves is more accurate than impact sound insulation curves, particularly in the middle-frequency range.

The results of Figures 5.11 and 5.14 demonstrate that the floor structures' total density significantly impacts the prediction of airborne and impact sound insulation in all frequencies. Additionally, the volume of the receiving room V has a minor effect on predictions of airborne and impact sound at lower frequencies.

The sensitivity analysis results suggest that the material composition of the concrete layers and CLT panels significantly impacts sound estimation, particularly at lower frequencies. The effects of CLT, concrete layers, and rock wool can be seen in airborne and impact sound prediction. Moreover, similar trends are observed for the thickness parameters of certain insulation materials (fiberglass, rock fiber, cellulose fiber), although the sensitivity is higher in higher frequencies. This is reasonable, as fiber insulation materials have better noise absorption capabilities in the middle and high-frequency ranges.

A similarity between wet and dry floor solutions regarding sound sensitivity is that the main part influences sound (particularly in higher frequencies). In contrast, the ceiling part has a minimal influence on both kinds of insulation (airborne or impact).

Table 5.5: Comparison between measured and predicted airborne sound reduction index R and normalized impact sound pressure levels L_n *clustered in low, middle, and high frequencies using the RMSE function for test floor structures.*

	Root-Mean-Square Errors in dB		
Frequency range	**Low**	**Middle**	**High**
	50 Hz – 200 Hz	**250 Hz – 1000 Hz**	**1250 Hz – 5000 Hz**
R (airborne sound)	3.76	2.55	4.79
L_n (impact sound)	3.79	3.48	4.97

5.4 Conclusions

This chapter presents a model based on artificial neural networks to predict the airborne sound reduction index R and normalized impact sound pressure levels L_n for various lightweight floor structures. This model is validated with 252 standardized laboratory measurements and has good accuracy with a root-mean-square error (RMSE) of 1.67 – 7.63 for the frequency bands 50 Hz – 5000 Hz. Furthermore, when considering the single-number quantities, the weighted airborne sound reduction index R_w and the weighted normalized impact sound pressure levels $L_{n,w}$, the accuracy improves with an RMSE of 0 – 2 dB and 0 – 5 dB, respectively.

The model demonstrated a better accuracy for airborne sound prediction, particularly in the mid-frequency range of 250 Hz – 1000 Hz. However, its predictions around the fundamental and the critical frequencies were often inaccurate, emphasizing the importance of coupling effects in developing a reliable prediction tool.

A sensitivity analysis was conducted to determine which material had the most significant impact on the prediction of sound insulation. The thickness of the insulating materials is crucial in the middle and high frequencies. Additionally, the density of the CLT panels and concrete floating floors on top of lightweight floors also affects the prediction of airborne and impact sound insulation. Furthermore, the total density of the floor structure is an essential factor in forecasting these insulation curves.

When comparing wet and dry solution systems, the thickness of the main part of the floor structure has the most influence on the prediction sensitivity across all frequencies. No effects were seen on the prediction sensitivity for the ceiling part of the floor structure. However, the structure's upper part significantly impacts the prediction sensitivity of low-frequency impact sound in wet and dry cases.

Chapter 6

PREDICTION OF SOUND INSULATION USING ARTIFICIAL NEURAL NETWORKS – PART II: LIGHTWEIGHT WOODEN FAÇADE STRUCTURES

Résumé

Un modèle de prédiction basé sur des réseaux neuronaux artificiels est adapté pour prévoir les performances acoustiques de l'isolation contre les bruits aériens de divers murs de façade en bois léger. 100 courbes d'isolation ont été utilisées pour développer le modèle de prévision. Les données sont des mesures en laboratoire de murs de façade dans des bandes de tiers d'octave (50 Hz − 5 kHz). Pour chaque mur de façade, les informations géométriques et physiques (type de matériau, dimensions, épaisseurs, densités, etc.) sont utilisées comme paramètres d'entrée. Le modèle montre une capacité de prédiction satisfaisante pour la réduction des bruits aériens. Une plus grande précision est obtenue aux fréquences moyennes (250 Hz − 1 kHz), tandis que les gammes de fréquences inférieures et supérieures présentent souvent des écarts plus importants. L'indice pondéré de réduction du bruit aérien (R_w) des façades peut être estimé avec une différence maximale de 3 dB. Parfois, le modèle présente de fortes variations dans les fréquences fondamentales et critiques qui influencent la précision de la prédiction. Une analyse de sensibilité est mise en œuvre pour étudier l'importance des paramètres dans les estimations d'isolation. La densité des matériaux (panneaux de bois lamellé-croisé,

plaques de plâtre), l'épaisseur des matériaux d'isolation, l'épaisseur et l'espacement entre les montants intérieurs et la densité totale des façades sont des facteurs qui ont un impact significatif sur les prédictions. Les résultats soulignent également l'importance de l'épaisseur des façades et de la densité totale des couches extérieures groupées.
Mots clés: bruit aérien, façade, modèle de prédiction, réseaux neuronaux artificiels

Abstract

A prediction model based on artificial neural networks is adapted to forecast the acoustic performance of airborne sound insulation of various lightweight wooden façade walls. One hundred insulation curves were used to develop the prediction model. The data are laboratory measurements of façade walls in one-third-octave bands (50 Hz − 5 kHz). For each façade wall, geometric and physical information (material type, dimensions, thicknesses, densities, and more) is used as input parameters. The model shows a good predictive capability for airborne sound reduction. Better accuracy is obtained at middle frequencies (250 Hz − 1 kHz), while lower and higher frequency ranges often show deviations in the results. The weighted airborne sound reduction index (R_w) of façades can be estimated with a maximum difference of 3 dB. Often, the model shows high variations within fundamental and critical frequencies that influence the predictive precision. A sensitivity analysis is implemented to investigate the significance of parameters in insulation estimations. The material density (i.e., cross-laminated timber panel, gypsum board), thickness of the insulation materials, thickness and spacing between interior studs, and the total density of façades are factors of significant weight on predictions. The results also emphasize the importance of façades thickness and the total density of the clustered exterior layers.

Keywords: airborne sound insulation, façade, prediction model, artificial neural networks

6.1 Introduction

Timber is a favorable choice in construction engineering due to its availability in nature and ease of handling [120]. Additionally, it has a lower carbon footprint than concrete and offers excellent thermal performance [163, 164]. This has led to wooden buildings becoming increasingly popular in places such as Scandinavia and Australia [165,166]. In North America, wood-frame structures have been the most common form of building construction in the 20^{th} century [121]. Recently, cross-laminated timber (CLT) has become an innovative product for the North American construction market, and its serviceability as a sustainable material has gained much attention from researchers and the wood industry [167].

Lightweight wooden structures can reduce construction time and cost; however, they do not provide the same sound insulation as concrete or heavier structures [123]. This applies to construction components such as floors, roofs, internal walls, and façades. The quality of sound insulation in these constructions is considered lower than traditional concrete constructions [123].

The importance of sound insulation of building façades is evident, and the acoustic environmental needs to be controlled. Poorly designed façade walls can decrease the acoustic comfort for occupants in a building. To ensure adequate levels of acoustic comfort, controlling the acoustic environment of new and renovated buildings is necessary [114].

Although certain façades are designed primarily for thermal insulation and fire safety; acoustic aspects are often neglected or misunderstood [168]. Standardized measurements, such as those outlined by ISO and ASTM [3, 32–34, 89, 116, 169], can be used to characterize the acoustic performance of façade structures, but they are costly and time-consuming [170]. Furthermore, results obtained from such measurements are specific to certain specimens and cannot be generalized to different structures.

It is essential to use accurate prediction tools to forecast structural elements' acoustic behavior to ensure good indoor acoustic quality. Various approaches have been developed

to predict sound transmission through multiple elements, including theoretical approaches [8–11], numerical tools [12, 13], and machine learning applications [17, 79]. However, some of these tools have revealed significant deviations due to different reasons, such as material uncertainties or modeling limitations [13, 19–22]. It is necessary to take into account specific construction details during the modeling process to improve their accuracy, such as mechanical connections between assemblies [12, 22, 30, 80].

A direct prediction tool based on theory-based analytical expressions, including stiffness, mass, and damping, may be suitable for single-leaf elements. However, it is much more challenging to forecast the sound insulation performance of multi-layer structures accurately [3]. As such, structural connections between elements and diversity in building materials cannot be adequately considered in analytical approaches [28].

Machine learning algorithms have enabled breakthroughs in different areas that were previously difficult to tackle, such as image recognition, speech recognition, language translation, and acoustics [17, 126, 129, 171]. It is a science that allows algorithms to learn and make predictions based on data [132]. The more data fed into these models, particularly artificial neural networks (ANN), the better their predictive power will be. ANN has been commonly used for different acoustic applications, such as audio engineering, the vehicle industry, acoustic material, and environmental acoustics [133, 139, 140, 142].

In building acoustics, a convolutional neural networks model was used to classify inter-floor noise in a household by recording different noise sources for 24 hours [78]. Moreover, an ANN model was applied on sandwich partition panels for the estimation of sound insulation, weighted airborne sound reduction indices R_w and sound transmission class STC values, and the results were within ±3 dB differences [79]. Another research was conducted to predict R_w using measurements related to wooden windows utilizing technical parameters [80]. However, these researches only dealt with single-number quantities (SNQ) without estimating full-spectrum insulation curves.

By taking the predictions of ANN one step further, the authors of [17] conducted detailed predictions of airborne insulation in 1/3-octave bands for masonry walls using

laboratory measurements on thirty-four brick walls. While the estimated values agreed with the measured ones, the study was limited to a monolithic structure. To expand the scope, the authors of [144] used ANN to estimate the sound insulation behavior of different lightweight wooden floors in frequency bands (50 Hz − 5 kHz), using 67 insulation measurements and two variables (material thickness and their installation order). The model provided reasonable results regarding SNQ with a maximum difference of 1 dB in the estimation of R_w. However, the accuracy decreased with deviations up to 9 dB in the prediction of $L_{n,w}$ (normalized weighted impact sound pressure level). Despite the sample size limitation, the study showed good potential for predicting sound insulation data.

A comprehensive study was carried out by [83] in which 252 standardized laboratory measurements were conducted on lightweight wooden floors with varying construction parameters such as material type, material thickness and density, and area of the floor structure. The results found that when more data and detail were included, a better accuracy in predicting $L_{n,w}$ could be achieved, with a variance of no more than 5 dB. However, the variance in forecasting R_w increased to a maximum of 2 dB yet still yielded good results. An attribution analysis was conducted to determine the most critical parameters in forecasting sound insulation curves.

This chapter aims to create an Artificial Neural Network (ANN) model to predict the airborne sound insulation of lightweight wooden façade walls. The data consists of laboratory measurements of complete external wall systems, not including doors, windows, or other openings. A sensitivity analysis will be conducted to determine how parameters impact the prediction of sound insulation.

6.2 Materials and methods

6.2.1 Acoustic experimental tests for façade structures

The database developed includes 100 standardized laboratory measurements obtained from Lund University in Sweden and The National Research Council (NRC-CNRC)

[112] in Canada. The measurements consist of airborne insulation measurements of 100 different façade walls in one-third-octave bands ranging from 50 Hz to 5 kHz. These measurements were conducted according to ISO 10140-2 (2010) [89] and ASTM E90-09 (2016) [32]. The measurements performed in compliance with ASTM standards have been converted to the ISO 717-1 (2013) [37] descriptor (the weighted airborne sound R_w) in order to have a consistent agreement between insulation data. This conversion is necessary to standardize the acoustic descriptors in the measurements.

Figure 6.1 shows the mean and standard deviations of the insulation data of façade structures. The total insulation curves are presented in the Annex in Figure B1. The database includes curves of airborne sound reduction index R(f) in the 50 Hz to 5 kHz frequency range. Therefore, every façade structure has technical parameters and a full-spectrum insulation curve.

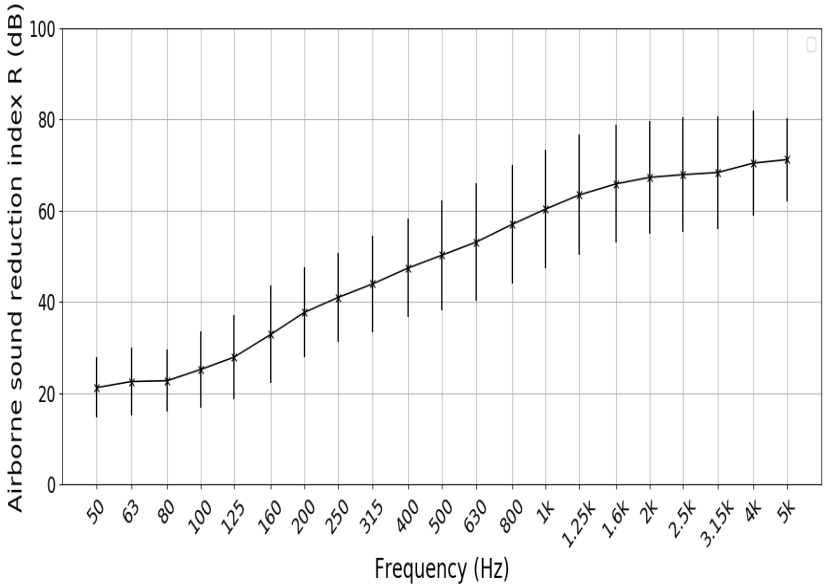

Figure 6.1: Mean and standard variation of airborne sound insulation curves of façade walls.

Ten measurements of different façade walls were used to create the features of the ANN model. Additionally, a separate set of ten curves (selected randomly) were chosen to assess the accuracy of the model (see Figure B2 in Annex B for a detailed view of the assemblies). These testing curves represent the insulation curves' average tendency and extreme values at all frequencies, as seen in façades #4, #9, and #1 in Figure B1. In the

database, each façade configuration is divided into three parts: interior, main, and exterior, corresponding to the order in which each façade component is installed. The main part of the façade holds the dominant material or component. The interior and exterior sections each consist of components that are located alongside the main façade material (see Figure 6.2).

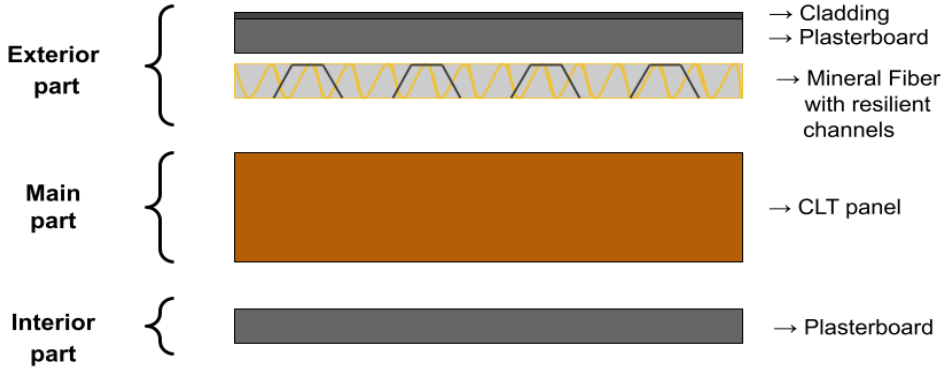

Figure 6.2: A schematic presenting the division of each façade component in the database using an example of the test façade #6.

The MySQL software [107] is used to organize the database, which contains 10 variables of structural parameters of each façade wall (Table 6.1). These parameters are used to train the network model. They are chosen based on the type of façade component, their installation position, thickness and density of each layer, depth of studs and spacing between them, area of a façade (S), the volume of a receiving room (V), group and total thickness and mass of a structure, resilient metal channel depth and spacing between them. The output/target of the ANN model is the value of the airborne sound reduction index in one-third-octave bands. Despite the significant effect of specific elastic properties on sound transmissions, such as dynamic stiffeners and the modulus of elasticity of each material, they are not considered in the input parameters due to the lack of information in acoustic measurement reports.

Table 6.1: Structural variables are utilized to organize the database and employed as inputs for the network model.

Parameter	Unit	Class
– type of material	—	i.e., CLT panel, insulation materials, etc.
– Material installation order	—	first/ second/...
– Material thickness	mm	—
– Group thickness	mm	interior, main and exterior parts
– Total thickness of a façade	mm	—
– Material density	kg/m^3	—
– Group density	kg/m^3	interior, main and exterior parts
– Total density of a façade	kg/m^3	—
– Façade area S	m^2	—
– Volume of the receiving room V	m^3	—
– Studs depth	mm	—
– Spacing between studs	mm	—
– Resilient channels depth	mm	—
– Spacing between Resilient channels	mm	—

6.2.2 ANN network configuration

This model uses a multilayer perceptron class of ANN with two hidden layers, each containing 40 and 30 artificial neurons, respectively. The network model in this Chapter has the same number of hidden layers as the used model in Chapter 5. However, it differs with the number of neurons in the input layer and the measurement types. Cross-validation technique is employed to validate the network model and prevent overfitting issues [96, 145]. LeakyReLU is chosen as the activation function for the hidden layers to avoid the vanishing gradient problem that could face other activation functions, such as tan or sigmoid [151]. For training, the Adam optimizer is used to minimize the errors of the prediction model [105, 149, 150].

80% of the total measurements are allocated to the training set, 10% to the validation set, and 10% to the testing set (Table 6.2). The training set develops the network parameters, such as bias and weights. The validation set optimizes the model's hyperparameters, such as the number of hidden layers and neurons. Since the predictions are continuous values (insulation curves), the root-mean-square error (RMSE) function

can be used as a cost function,

$$RMSE = \sqrt{\frac{1}{n}\sum_{i=1}^{n}(\hat{y}_i - y_i)^2}, \tag{6.1}$$

where n presents the number of observations (measurements) used in the training phase. Output (predicted) and input (measured) values are donated by $\hat{y}_i$ and y_i, respectively. The developed model in this study achieved an overall prediction accuracy of 4.44 dB for all the predicted and measured curves. Each estimated insulation curve is compared to the measured one using the RMSE function in each one-third-octave band from 50 Hz to 5 kHz to evaluate the results more accurately.

Table 6.2: A description summary of measurement numbers used by the prediction model.

Measurements		**ANN Model**		
Measurement number	100		100	
	airborne	training set	validation set	testing set
	100	80	10	10

6.3 Results and discussion

6.3.1 Airborne sound insulation estimations

The ANN model is trained and validated using 80 and 10 standardized laboratory measurements, respectively. Additionally, ten measurements are used to test the accuracy of predictions of airborne sound reduction curves. The acoustic behavior of each wall (as measured in decibels) in 1/3-octave frequencies (ranging from 50 Hz to 5 kHz) is utilized as the dependent variable for the predictions.

Figure 6.3 demonstrates the predicted and measured airborne curves of test façades. Figure B2 in Annex B illustrates each test wall's assemblies. The predicted and measured insulation curves are similar, with some variations in certain cases. The discrepancies between predicted and measured curves are more significant in some low and/or high-frequency band samples. The slightest deviation is observed in façade #3 with a RMSE

of 2.19 dB, while the most significant discrepancy is 5.73 dB in façade #10, which has a slightly complex structure.

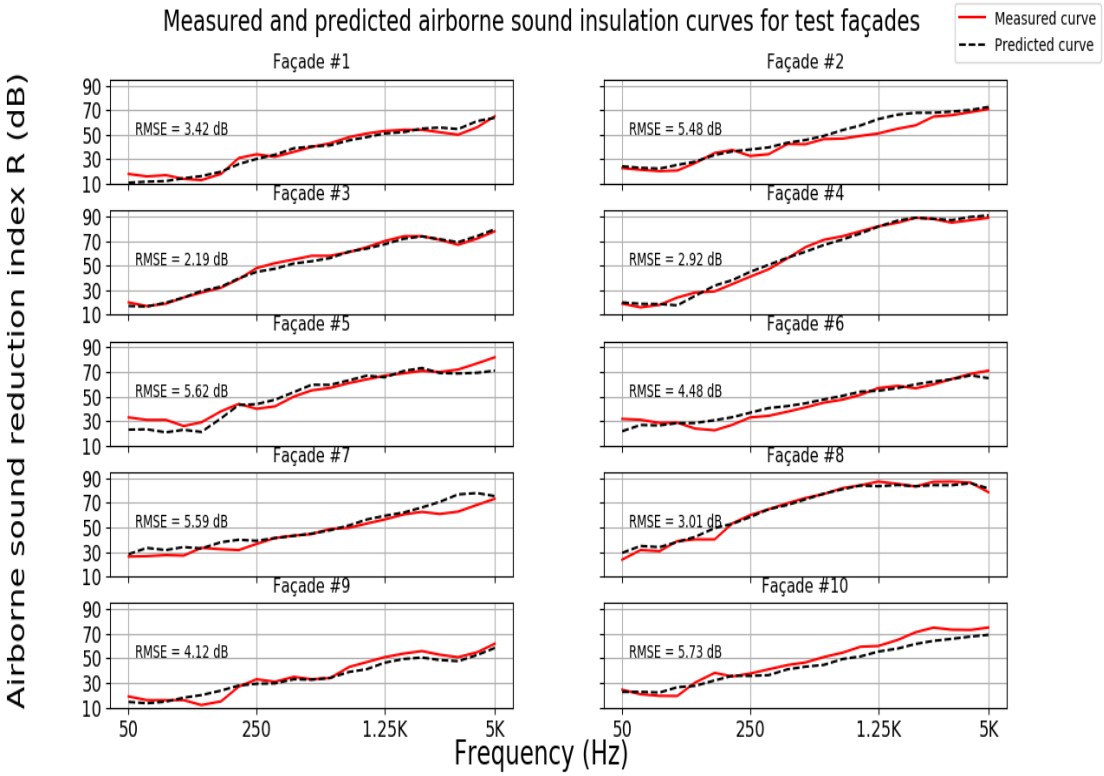

Figure 6.3: Predicted and measured airborne insulation curves for test façade walls.

A noticeable difference in the results can be seen at high frequencies (1.25 kHz – 3 kHz). This frequency range usually includes the critical frequency of lightweight constructions, also known as the coincidence frequency. At this frequency, the wavelength of the bending wave in the plate matches up with the incident acoustic wavelength projected onto the plate [3]. This indicates that the structure will be able to effectively radiate sound at and above this frequency [152].

Table 6.3: Predicted and measured weighted sound reduction indices of test façades.

Façade no.	**RMSE (dB)**	R_w **(dB)**	$C_{100-3150}$	$C_{50-5000}$	R_{wPred} **(dB)**	$C_{Pred\ 100-3150}$	$C_{Pred\ 50-5000}$
1	3.42	39	-4	-3	40	-3	-3
2	5.48	46	-2	-2	48	-1	-1
3	2.19	53	-4	-6	53	-4	-6
4	2.92	50	-3	-4	51	-6	-6
5	5.62	52	-2	-2	51	-6	-6
6	4.48	55	-4	-4	55	-5	-5
7	5.59	48	-1	-1	51	-2	1
8	3.01	65	-5	-7	67	-4	-5
9	4.12	37	-4	-3	38	-1	-1
10	5.73	49	-3	-3	47	-2	-1

Similar variations can be seen at frequencies lower than 200 Hz in façades #1, #8, and #9. This can be attributed to the effect of first eigenfrequencies or fundamental natural frequencies [3]. Additionally, it is observed that the estimated curves become smoother near low fundamental and/or critical frequencies. This indicates that the main challenge of estimating sound reduction values occurs in those bands. Similar issues with ANN models have been reported in other research [17, 83].

Table 6.3 illustrates the root-mean-square errors (RMSEs) in the prediction of airborne sound reduction curves, as well as the single-number quantities (SNQs) R_w and $R_{wPredicted}$ that correspond to each curve. The largest error is up to 3 dB (façade #7), while the model can accurately predict the same weighted values for façade #3 and #6. Additionally, the correlation terms $C_{100-3150}$ and $C_{50-5000}$ show a maximum difference of 4 dB in façade #5.

In Figure 6.4, the normalized error deviation values are displayed within the range of [-1, 1]. It can be seen that the most significant variations in error occur in the high-frequency range (1.25 kHz − 5 kHz) for façade #2, #7, and #10. Additionally, the model seems to struggle at the lower frequencies (50 Hz − 200 Hz), with notable discrepancies between measured and predicted curves for façade #5 and #9. Furthermore, it can be observed that the errors are distributed similarly in both low and high frequencies, while a better prediction is noticed in the mid-frequency region (250 Hz − 1 kHz).

The graph in Figure 6.5 demonstrates the probability distribution of errors in estimating airborne sound insulation curves across all frequencies. The highest density of errors is

in the (-5,5) dB range, with a peak close to 0 dB, indicating the model's accuracy in producing satisfactory results.

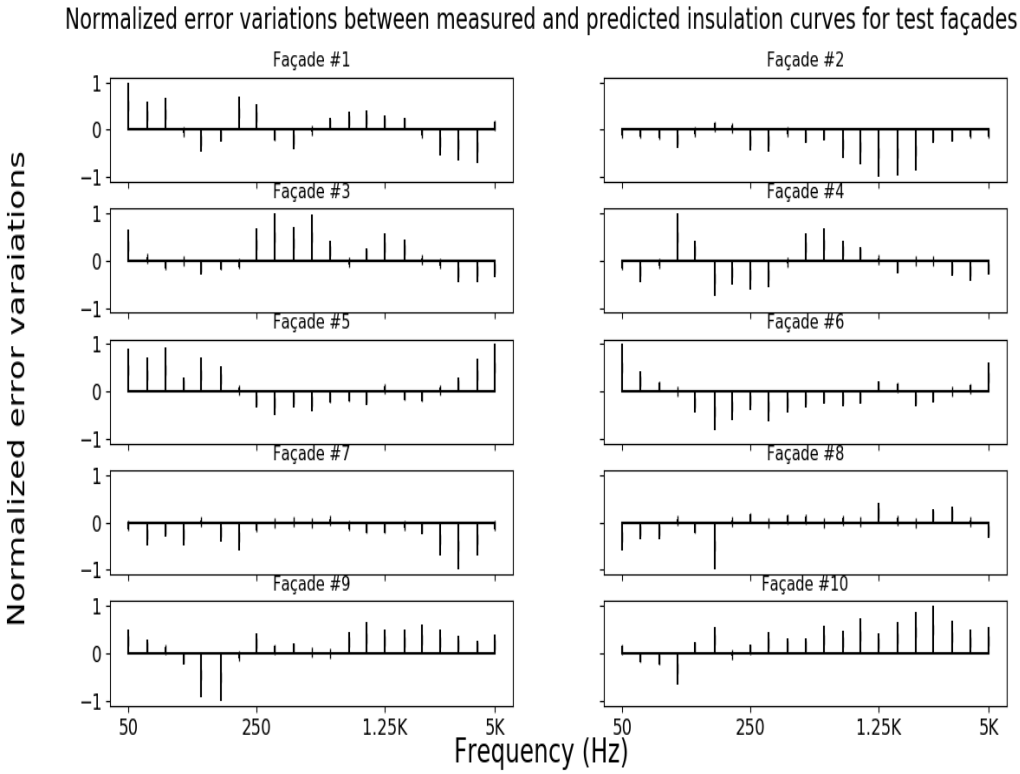

Figure 6.4: Normalized error distributions for the estimated airborne insulation curves for tested walls.

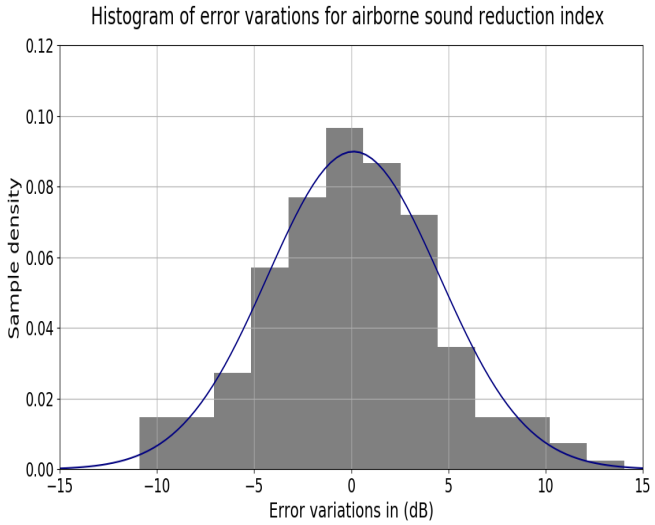

Figure 6.5: The probability density function of error distribution for the sound insulation curves from 50 Hz to 5 kHz.

6.3.2 Feature attribution of structural parameters

A sensitivity analysis is performed to examine the effect of each structural parameter on the predicted sound insulation. This analysis also provides insights into the contribution of different input variables at each frequency band. Furthermore, commonly used building materials in façade components are selected to evaluate their impact on the network model (Figure 6.6). Additionally, physical parameters of the façade, such as tested area, the volume of the receiving room, and thickness and density of the interior, main, and exterior parts of the façade (Figures 6.7 and 6.8), are incorporated in the attribution analysis. Furthermore, another categorization is carried out on the dataset to explore the impact of the thickness and density of the exterior, main, and interior parts of the façade structure on the predicted airborne sound insulation curves.

Figure 6.6 demonstrates the influence of the thickness and density of various building materials on sound insulation prediction. At low frequencies, the density of materials such as cross-laminated timber (CLT) panels, oriented strand board (OSB), and lightweight concrete panels has a significant effect. However, the sensitivity of lightweight concrete and CLT panel increase at middle and high frequencies, except for the OSB panel. Furthermore, the density of the gypsum board has a more prominent effect at higher frequency bands. The density of gypsum fiberboard has a more significant effect on sound insulation than typical gypsum board, particularly at lower frequencies. This is because the stiffer material of gypsum fiberboard is more dominant at lower frequencies (stiffness-controlled region). While the density of insulation materials impacts sound insulation at all frequencies, it is more pronounced for wood fiber insulation at higher frequencies. A previous study [161] found that rockwool density plays a vital role in improving sound insulation below 1.25 kHz, which is supported by the results in Figure 6.6. Additionally, the density of the coating material (mineral plaster) is critical for sound insulation in both low and high frequencies.

It is observed that the thickness of CLT panels is significant at all frequencies, as is the thickness of insulation materials, air gaps, and coating materials. However, the thickness of certain materials, such as OSB panels and gypsum boards, is more important in middle

and high frequencies when the mass control region dominates [3]. In addition, specific building components (e.g., air gaps and glass fiber) have a more significant effect on airborne sound insulation than the densities or thicknesses of the materials.

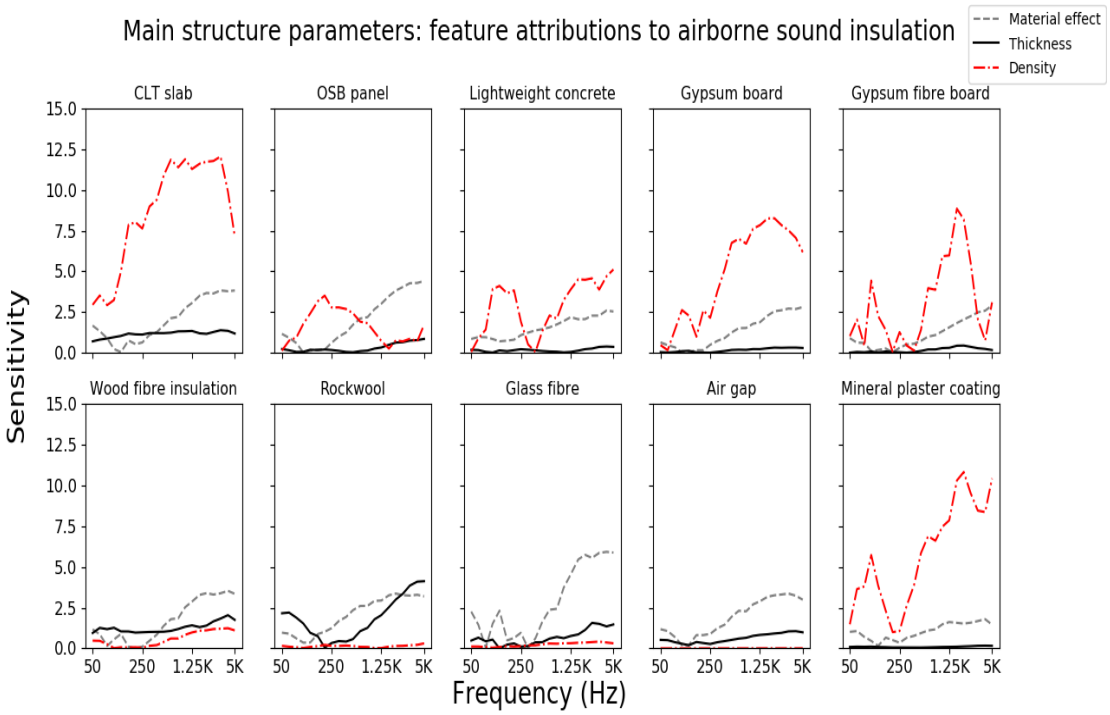

Figure 6.6: Sensitivity analysis of façade structural components on predicting airborne insulation curves.

Figure 6.7 illustrates the influence of various parameters on the estimation of airborne sound. It is evident that, for very low and high frequencies, the surface area S of the façade structure has a small impact. The importance of the structure area for predicting airborne sound in the low-frequency range is also reported in [162]. In contrast, the volume of the receiving room V is significantly significant at all frequencies, particularly in higher ranges, where the energy of short sound waves can be easily dampened due to relaxation phenomena, which is more evident at high frequencies and/or in larger rooms. This agrees with [83] and in contrast to [162], which showed the unimportance of V in the low-frequency range. The thickness of the interior studs has a more significant influence on prediction across all frequencies, while the spacing between the interior studs affects the predictions at low and middle frequencies.

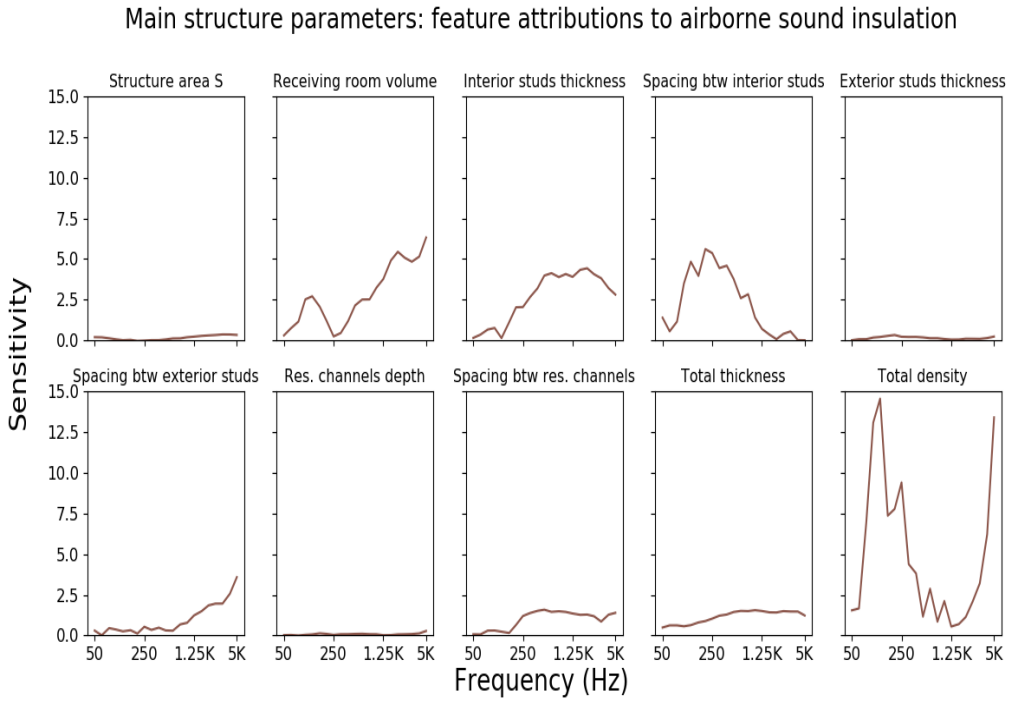

Figure 6.7: Attributions analysis of various parameters to the prediction of airborne insulation curves.

The importance of the spacing between the exterior studs is only revealed at high frequencies, which emphasizes the role of mechanical connections, also known as sound bridges, in creating transmission paths and thus reducing insulation improvements [3, 172]. No extraordinary effects have been identified for the sound insulation of resilient channels, except at extremely high frequencies. However, the distance between resilient channels has a recognizable impact in middle and high-frequency ranges. The total thickness of a façade affects the predictions at all frequencies, which is affirmed in [162]. Furthermore, the total density has the most influence across all frequencies, as indicated in [83]. The attribution spectrum of the total density of a façade reveals a peak near 150 Hz and a dip near 1.25 kHz, likely due to the effects of fundamental and critical frequencies, respectively. This is probably caused by the coupling of resonant façade components, allowing energy to be exchanged between elements [152]. This happens when the elements are physically connected and have sufficiently close natural or critical frequencies. This intensifies the radiations from components, negatively affecting the insulation [3].

The plots in Figure 6.8 show how the thickness and density of the interior, main, and exterior parts of the façade wall affect the insulation curves. The density and thickness significantly impact the estimations across all frequencies. The same trends are seen for the total density of the façade (Figure 6.7), as well as for the total density of the exterior part. The effects of the fundamental and critical frequencies are also noteworthy for the total density of the interior and main parts but with a lower scale.

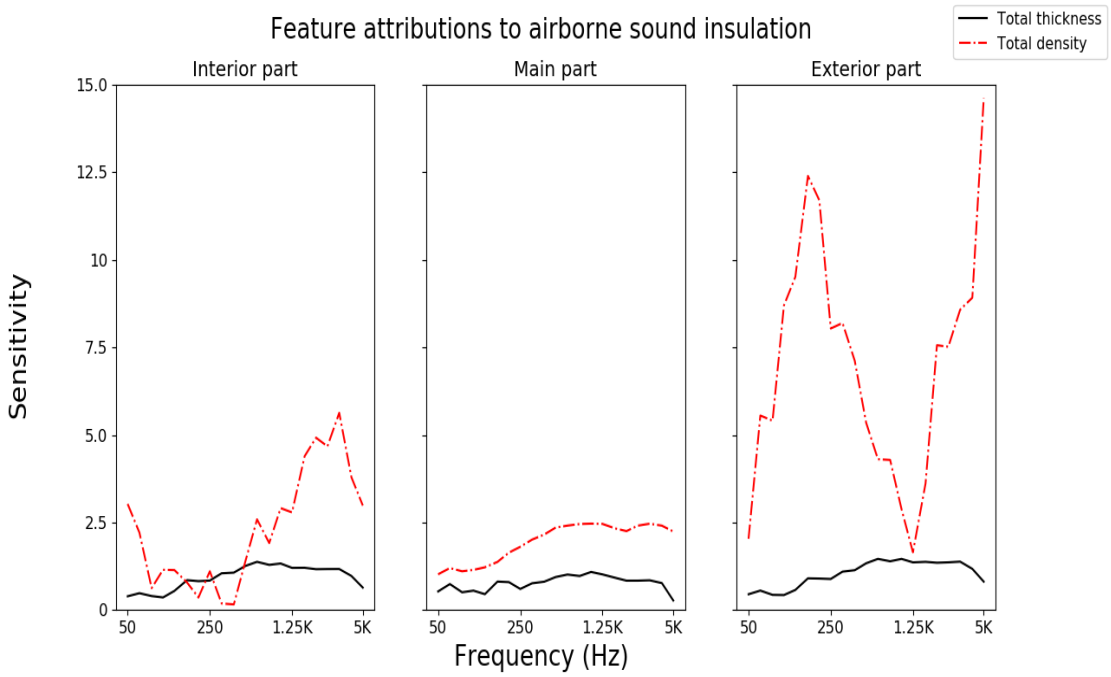

Figure 6.8: Feature attributions of interior, main, and exterior parts façade walls to insulation predictions.

Table 6.4 presents the error distribution of the predicted airborne insulation curves in three frequency ranges: low (50 Hz – 200 Hz), middle (250 Hz – 1 kHz), and high frequency (1.25 Hz – 5 kHz) by using the (RMSE) function. The results show that the best accuracy is obtained in the middle frequencies, with an error of 3.52 dB. However, the errors become more significant at low and high frequencies, yielding RMSE values of 4.67 and 4.99 dB, respectively. These higher deviations can be attributed to fundamental and critical frequencies.

Another reason that can affect the accuracy is that the ANN model does not consider uncertainties (that could be presented in acoustic measurements). This is reflected in the results of research of a European project that conducted acoustic measurements

for lightweight partitions using 19 different European laboratories [173]. The authors highlighted that the measured acoustic performance of structures could differ from one laboratory to another based on factors such as the installation details of the partitions, the laboratory design, the number of diffuses, etc. [173]. Additionally, the accuracy of acoustic measurements can be affected by the person performing them, depending on their knowledge and experience [174]. These factors are not considered when developing an ANN and thus may influence its predictive capability.

Table 6.4: Error distributions in the airborne sound reduction index R prediction considering three frequency regions.

	Root-mean-square errors in dB		
Frequency bands	**Low**	**Middle**	**High**
	50 Hz – 200 Hz	**250 Hz – 1000 Hz**	**1250 Hz - 5000 Hz**
R (airborne sound)	4.67	3.52	4.99

6.4 Conclusion

This Chapter explores the potential of a prediction model using artificial neural networks to forecast airborne insulation curves based on 100 laboratory measurements of different lightweight façades. The model depicts reliable results with a root-mean-square error (RMSE) of 2.19-5.73 dB for estimating the sound insulation curves of various façades in the frequency bands 50 Hz – 5 kHz. When the comparison considers the single-number quantity, the weighted sound reduction index R_w, prediction accuracy is further improved with 0-3 dB errors.

The model showed more accurate mid-frequency predictions (250 Hz - 1 kHz). However, the estimation of R(f) at fundamental and critical frequencies for some tested façades revealed inconsistencies, indicating the influence of resonance on the sound insulation performance of façades and the inadequacy of the model to forecast in those frequency ranges.

A sensitivity analysis is conducted to evaluate the influence of building parameters on the estimated airborne insulation curves. It is shown that the density of CLT panels

is significant in all frequency bands. Additionally, the thickness and density of the insulation material, as well as the total thickness and density of interior, main, and exterior parts of façades, all have a significant effect on the prediction in all frequencies, with higher contribution from the exterior part's total density. The interaction between the various façade components - resulting from each component's fundamental and critical frequencies - significantly affects the prediction.

The present model offers a valuable tool for engineering work on sound insulation in buildings as it can predict R_w with a maximum error of 3 dB; this is a significant improvement, as differences of 1 to 2 dB are barely noticeable in terms of noise levels. Furthermore, this predictive model could save time and cost associated with acoustic measurements for various partitions.

Chapter 7

MODELING FIELD MEASUREMENTS OF SOUND INSULATION PERFORMANCE FOR MULTI-LAYERED CLT-BASED FLOOR SYSTEMS: A MEANS OF A PREDICTION MODEL USING ARTIFICIAL NEURAL NETWORKS

Résumé

Un outil de prédiction basé sur l'approche des réseaux neuronaux artificiels est développé pour prédire les différences de niveau normalisées et le niveau de pression acoustique d'impact normalisé pour les systèmes de planchers multicouches à base de CLT. Les données collectées sont 104 mesures d'isolation acoustique sur le site dans des bandes de tiers d'octave allant de 50 Hz à 5 kHz. Les mesures acoustiques ont été effectuées dans 15 bâtiments différents en Europe et dans des chambres de fonctions et de dimensions différentes. Pour développer le modèle de réseau, divers paramètres structurels ont été organisés, tels que les composants du plancher, les types de murs environnants et leurs composants, les types de jonction et leur couche viscoélastique intermédiaire, le volume de la pièce réceptrice, la surface de séparation, etc. Le réseau développé donne des résultats satisfaisants dans la prédiction des courbes normalisées d'isolation aux bruits aériens et aux bruits d'impact sur le terrain, pour

toutes les fréquences. La différence de niveau normalisée pondérée D_{nTw} est estimée avec une variation de 1 dB, tandis qu'elle atteint 2 dB pour le niveau de pression acoustique d'impact normalisé L'_{nTw}. Une bonne corrélation est mise en évidence pour les estimations des bruits aériens dans les fréquences moyennes (200 Hz – 1000 Hz), alors que les fréquences plus élevées révèlent souvent quelques écarts. Cependant, les estimations de l'isolation par impact ont montré une meilleure précision dans la gamme des hautes fréquences (1,25 kHz – 5 kHz). Une étude de sensibilité est réalisée pour comprendre les paramètres sur lesquels le modèle s'appuie. Dans les deux types d'estimations, le trajet direct du son à travers le sol est dominant. Ensuite, les trajets latéraux affectent les estimations au deuxième ordre. En outre, le volume de la pièce réceptrice joue un rôle important dans les basses fréquences pour les estimations d'impact. Les résultats ont également mis en évidence l'importance de la couche viscoélastique intermédiaire entre les jonctions pour les prédictions aériennes dans toutes les gammes de fréquences.

Mots clés: acoustique des bâtiments, mesures sur site, isolation acoustique, modèle de prédiction, réseaux neuronaux artificiels

Abstract

A means prediction tool based on an artificial neural network approach is developed to predict standardized level differences and impact sound pressure levels for multi-layered CLT-based floor systems. The collected data are 104 field sound insulation measurements in one-third-octave bands from 50 Hz to 5 kHz. The acoustic measurements were carried out in 15 different buildings in Europe and for different room functions and sizes. Various parameters were categorized to develop the network model, such as floor components, surrounding wall types and their components, junction types and their visco-elastic interlayer, receiving room volume, and surface separating area. The developed network demonstrates satisfactory results in predicting airborne and impact sound insulation curves (considering field conditions) across all frequencies. The weighted standardized level differences D_{nTw} is estimated with 1 dB variation, while it is up to 2 dB for standardized impact sound pressure level $L^{'}_{nTw}$. A good correlation is highlighted for airborne estimations in the middle frequencies (200 Hz − 1000 Hz), while higher frequencies often reveal deviations. However, impact insulation estimations showed higher accuracy in the high-frequency range (1.25 kHz − 5 kHz). A sensitivity study is carried out to understand which parameters the model relies on. In both estimations, the direct path of the sound through the floor is the dominant, followed by the flanking paths. Additionally, the volume of the receiving room plays a significant role at low frequencies for sound impact predictions. The results also highlighted the importance of the visco-elastic interlayer between the junctions for airborne predictions in all frequency ranges.

Keywords: building acoustics, field measurements, sound insulation, prediction model, artificial neural networks

7.1 Introduction

Recently, the rise of environmental awareness has been the critical factor in driving the use of more sustainable materials, such as wood, in building construction [175, 176]. Of the many renewable materials available, engineered wood products (EWPs) are some of the most sustainable in the sector [177]. Their utilization leads to a significant decrease in carbon emissions [178], as well as offering advantages such as thermal insulation [164] and easy installation [179]. Cross-laminated timber (CLT) was first developed in Europe in the 1990s and has recently gained recognition in the North American building market [167,180]. CLT panels are known for their good mechanical properties and can be directly used on roofs, walls, and floors.

Wood has many advantages as a construction material, but its relatively low stiffness and mass lead to lower subjective sound insulation quality compared to heavier materials like concrete [123]. It is necessary to use additional elements to supplement CLT panels to fulfill the sound insulation requirements [181]. Diverse materials are developed as complemented elements to improve the sound insulation performance of CLT-based assemblies. Testing is necessary to determine the acoustic performance of assemblies, which can be costly and time-consuming. The ISO standard 12354 Part 1 [29] provides an estimation tool, but it is based on a heavy monolithic element and unsuitable for lightweight multi-layered structures. Furthermore, the variety of construction materials makes the process challenging. Additionally, the acoustic performance of tested structures may differ between laboratory and on-site measurements [26]. Laboratories measure direct sound transmission paths, while in real buildings, sound can also be transmitted through walls, ceilings, or common junctions [27]. This is called sound flanking transmission, which can significantly lower construction acoustic performance.

Creating an accurate prediction tool is a challenging endeavour, especially when it comes to simulating field sound insulation measurements. Variations and discrepancies in sound insulation measurements are usually attributed to the construction system, craftsmanship, and testing implementation. This can be a significant concern for

building contractors, who ensure a large safety margin when project decisions are taken to meet the sound insulation requirements. Qian has studied the uncertainties generated by material properties such as Young's and shear modulus and their effect on FEM modeling [15]. These uncertainties affect the development of a reliable prediction tool. Various prediction tools have been developed to assess sound insulation performance, such as theoretical models [8–11], numerical approaches [12–14], or artificial intelligence applications [17, 18]. Nevertheless, several deficiencies remain in some of these models [13, 19–22]

Recently, artificial intelligence algorithms have enabled a range of technological advancements in fields that were previously challenging, such as language translation [171, 182], image and speech recognition [183, 184], and building acoustics [17, 18]. This approach involves creating methods that can learn from samples to improve the accuracy of a set of tasks. By providing a large and varied set of data, the predictive capabilities of these algorithms can be greatly increased. This is especially true for artificial neural network models (ANN), which have seen a wide range of applications, such as estimating acoustic properties of materials [185], evaluating interior vehicle noise [134], and modeling environmental noise [186].

A limited number of studies have been conducted in the literature concerning building acoustics using artificial neural networks. For example, a convolutional neural network model was developed to classify inter-noise floors between apartment houses by recording noise for 24 hours [78]. Another study used ANN to predict weighted sound reduction index (R_w) and sound transmission class (STC) for sandwich partition panels [79]. The results showed good accuracy, with errors in the estimations within ±3 dB. A further investigation used ANN to predict R_w for wooden windows using limited technical parameters and a number of measurements [80]. Nevertheless, these models were only able to predict single-number-quantities (SNQ), and full-spectrum insulation curves were beyond their scope.

Using ANN estimations to predict 1/3-octave-band curves, a model was developed for monolithic brick walls based on 34 sound insulation measurements [17]. Similarly,

49 types of aramid honeycomb sandwich panels were studied in the 100 - 6300 Hz [81]. It is essential to extend the evaluation of the acoustic performance of lightweight wooden structures (floors and façades) down to lower frequency ranges (50 Hz - 5 kHz) since the most noise annoyance in these structures comes from low-frequency ranges. The authors published two studies using lab-based measurements to bridge the gap of limitation in broader frequency evaluation and data number [82–84]. The models developed from 252 and 100 lab-based acoustic measurements for floors and façades, respectively, demonstrated good results with maximum differences of 1 and 3 dB in the estimation of R_w. However, the deviation was up to 5 dB in the prediction of $L_{n,w}$ (weighted normalized impact sound pressure level). Although lab-based measurements have been used to develop ANN models for the acoustic performance of lightweight wooden structures where the direct sound transmission paths control the insulation, no research has attempted to simulate the field sound insulation for such structures using ANN.

This chapter aims to create a prediction model using an artificial neural network (ANN) approach to estimate the field sound insulation of multi-layered cross-laminated timber (CLT) floor systems. 104 field sound insulation curves are used that are on-site measurements of airborne and impact sound insulation in different real buildings located in Europe. The data is collected in one-third octave bands ranging from 50 Hz to 5 kHz. A sensitivity analysis is conducted to explore the correlations between the simulated parameters and sound insulation estimations.

7.2 Materials and methods

7.2.1 On-site acoustic measurements

This database collection consists of 104 acoustic field measurements of airborne and impact sound insulation in one-third-octave bands (50 Hz − 5 kHz) for various multi-layered CLT-based floor systems in different buildings in Europe, as depicted in Figure 7.1. These measurements were conducted according to ISO 16283 (Part 1 & 2) [33, 34] and ISO 717 (Part 1 & 2) [37, 38]. Of the 104 measurements, 51 are airborne, and 53

are impact sound insulation. The 15 wooden buildings' floor structures consist of two different construction systems: wet and dry-rise solutions. A wet system is characterized by a CLT-based floor with a continuous floating concrete topping (see components of test floor #1 in Figure C3 in Annex C). The dry-rise system does not have a concrete topping and instead features boards on top of point supports with integrated resilient interlayers that separate the toppings and the CLT panel with an insulation layer in between (Figure C3). Out of the 15 buildings, five utilize wet floor systems, and the remaining ten are equipped with dry-rise systems (Figure 7.1). Altogether, 38 acoustic measurements were taken on wet-floor systems (21 airborne and 17 impact curves), and 66 measurements were carried out on dry-rise systems (30 airborne and 36 impact curves). Figures C1 and C2 in the Annex represent the field sound insulation measurements that are used to develop the network model.

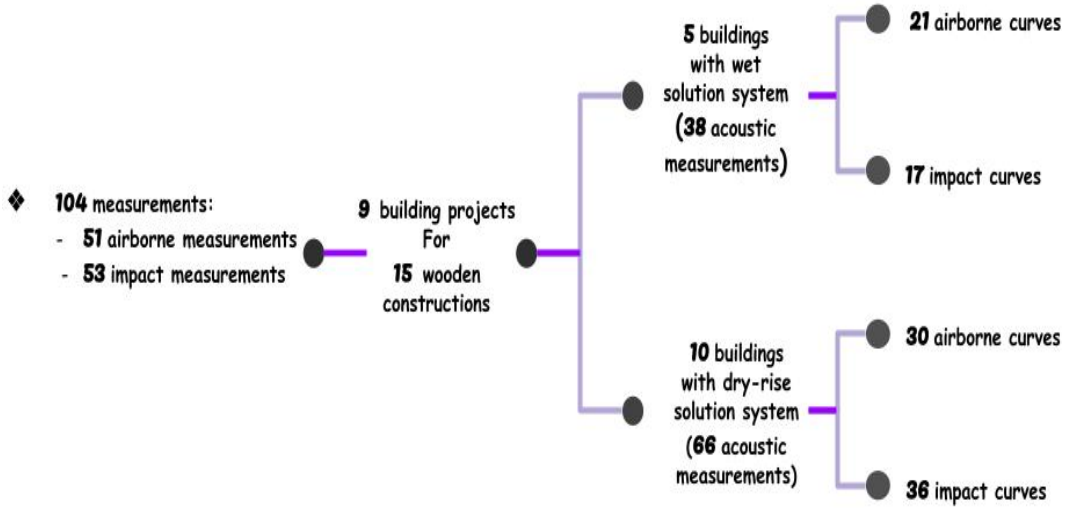

Figure 7.1: A detailed description of acoustic measurement number, constructional solution system types, and measurement types.

The database includes several parameters of the measured floors, walls, and junctions between them. These parameters include the materials of each floor and wall, their installation orders, thicknesses, densities, floor construction systems, wall types, junction types, and thickness of visco-elastic interlayer. Additionally, the area of each test floor and the volume of the receiving room are also included in the classification. However, openings in the linked walls are not considered in the modeling. Table 7.1 provides a

detailed list of the categorical variables that are considered in the modeling. Figure 7.2 shows a T-junction and an X-junction configuration, along with their construction and the locations of visco-elastic interlayers. Despite the importance of certain elastic material properties in the calculation of sound insulation, some structural properties, such as elastic modulus and dynamic stiffness, are not taken into account in the simulation due to lack of information in the acoustic reports.

Table 7.1: Structural variables utilized in the database served as inputs for the network model.

Structural parameter	**Unit**	**Class**
– floor system	—	wet, dry-rise solution system
– junction type	—	T-junction, X-junction
– surrounding wall type	—	façade, load-bearing, non-load bearing wall
– building material for floor and wall components	—	i.e., CLT panel, gypsum board, etc.
– material installation order	—	1^{st}, 2^{nd}, ...
– material thickness	mm	—
– material density	kg/m^3	—
– visco-elastic inter-layer thickness	mm	—
– floor separating area S	m^2	—
– volume of the receiving room V	m^3	—

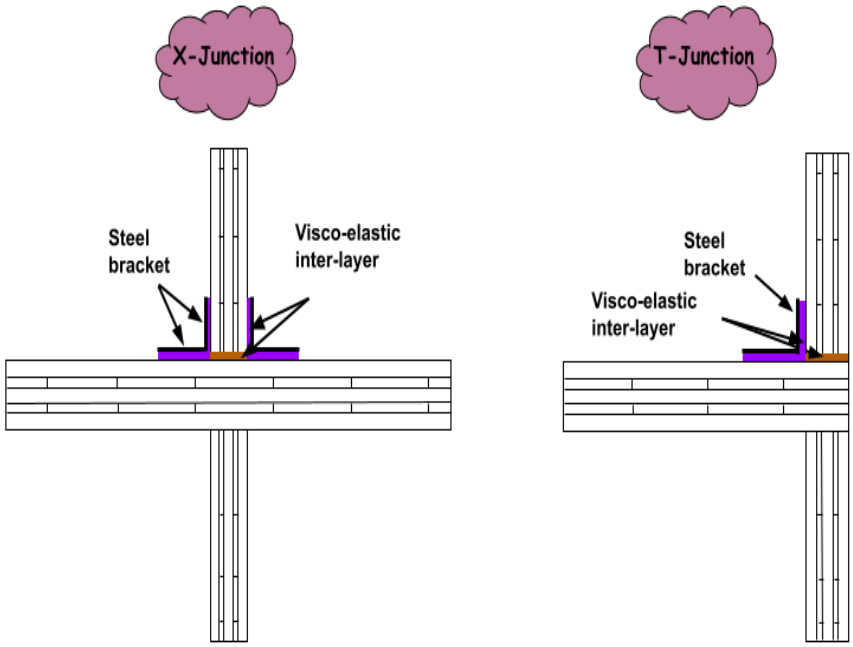

Figure 7.2: Junction types and the visco-elastic interlayer that are modeled in the network model.

7.2.2 Artificial neural networks modeling

A multi-layer perceptron (MLP) ANN model with three hidden layers (consisting of 100, 75, and 50 neurons, respectively) is developed for this study. To prevent overfitting and validate the network model, cross-validation and dropout techniques are employed [145, 146]. The LeakyReLU activation function is used for the hidden layers. The Adam optimizer algorithm [149] is employed for training the network. Figure 7.3 demonstrates how the structural parameters are transformed into a single matrix that serves as the input of the ANN model (for training, validation, and testing of the network). Each measurement is represented by a row that includes all the input parameters and acoustic spectrum.

The total number of measurements is split into three subsets: 80%, 10%, and 10% of the data are allocated to the training, validation, and testing sets, respectively. The training set is used to set up the parameters of the model (bias, weights, etc.), the validation set is used to optimize the hyper-parameters of the model (number of neurons and hidden layers), and the testing set is used to evaluate the predictive ability of the model. Table 7.2 summarizes the number and type of measurements used in each set. The root-mean-square error (RMSE) is used as the cost function to assess the accuracy of the model's predictions.

$$RMSE = \sqrt{\frac{1}{n}\sum_{i=1}^{n}(\hat{y}_i - y_i)^2}, \tag{7.1}$$

where the number of observations is represented by n. The measured and predicted values, respectively, are denoted by $\hat{y}_i$ and y_i. A cost function is used to evaluate the model's accuracy to provide a single error number for all test samples. To analyze the results in greater detail, however, the RMSE function is used to measure the deviation between each measured and predicted curve from 50 Hz to 5 kHz rather than just one error indicator. This assists in comprehending the strengths and shortcomings of the model in predicting different floor configurations.

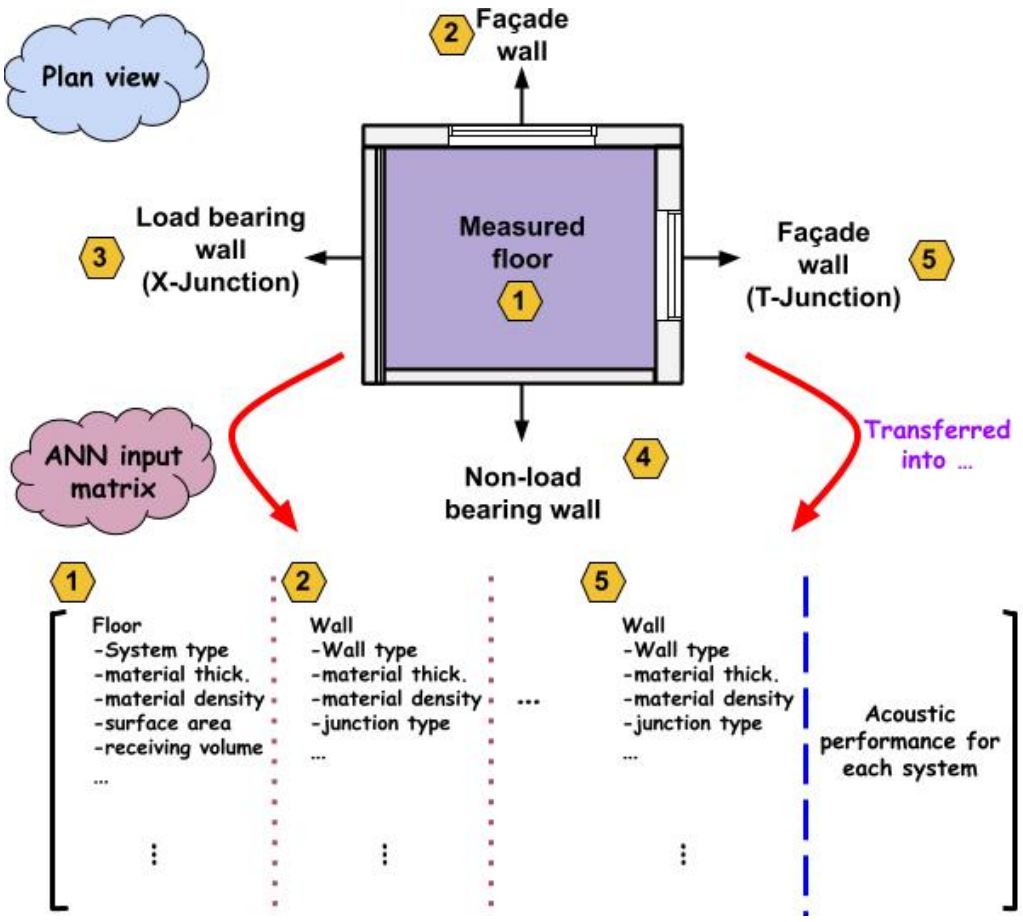

Figure 7.3: A schematic illustrates how the structural variables are organized and classified into an ANN input matrix for each acoustic measurement.

An ANN model that uses the two types of measurements (airborne and impact) yields unreliable results due to the limited number of measurements, making it difficult to differentiate between insulation curve types. The same model is used to predict the acoustic performance of floors using each measurement type separately, as shown in Table 7.2.

Table 7.2: A division summary of the acoustic measurement numbers used to develop the ANN model for airborne and impact estimations.

Measurement type	**Airborne**			**Impact**		
Total number	51			53		
ANN set type	training	validation	testing	training	validation	testing
Set numbers	41	5	5	43	5	5

7.3 Results and discussion

7.3.1 Sound insulation estimations

The ANN model was developed to separately predict the acoustic performance of based-CLT floors using airborne and impact measurements. The model was trained and validated on 80% and 10% of the total measurement number for airborne insulation (41 and 5 measurements, respectively) and impact sound (43 and 5 curves, respectively; see Table 7.2). Five floors from different buildings are chosen as a test set for airborne and impact. These included two bedrooms, two living rooms, and one studio (see Figure C3 in the Annex for a plan view of each test floor, space function, and the constructional materials of each structure). The model's overall Root Mean Squared Error (RMSE) for the test data is 3.24 dB for airborne estimations and 3.77 dB for impact cases across all frequencies. To better understand the network's behavior, each measured curve's error against its prediction in each 1/3-octave band will be analyzed.

Figure 7.4 illustrates five test floor systems' measured and predicted insulation curves. The gray area in the background of each sub-figure indicates the mean and standard deviation values of the curves used to train the network model. Test floor #1 is a wet-solution structure, while the four test floors have different dry-rise systems. The model offers reliable estimations for airborne and impact cases, with minor deviations at certain frequencies. The most significant variation is 3.54 dB in test floor #2 for airborne estimations and 4.58 dB for test floor #1 for impact cases in the entire frequency range (50 Hz – 5 kHz). Moreover, the network model did not predict outliers across all frequencies, even when the measured curves were outside the mean and standard deviation values utilized to develop the model (gray areas in Figure 7.4). This demonstrates the model's capacity to recognize general trends in sound insulation predictions.

For the wet solution system (test floor #1), the estimations are close to measured values for airborne and impact noise, with better accuracy for airborne predictions. The model also shows good predictive capabilities for the dry-rise system and both estimation types. Good correlations in the results are found at low frequencies (below 200 Hz),

where the first eigenfrequencies (fundamental natural frequencies) occur, as well as in high-frequency ranges (1.25 kHz − 3 kHz), where the critical frequencies of lightweight structures usually exist. This is also known as the coincidence frequency, at which the wavelength of the bending wave in the plate matches the incident acoustic wavelength projected onto the plate [152]. A coupling or matching enables the plate to radiate sound efficiently. Compared to other studies [17, 83, 84], estimations near the fundamental and critical frequencies agree. However, deviations between the predicted and measured curves are noticed at mid and very-high frequencies in certain cases. This may be attributed to sound flanking transmission paths, which usually exist in those ranges in field measurements. Additionally, some variations are found at high frequencies for particular dry-rise test floors (#2 and #5) with a suspended ceiling for airborne predictions (see the configurations in Figure C3). This indicates the limitations of the network in predicting accurate values at those ranges with the presence of the ceiling.

Tables 7.3 and 7.4 show the SNQs, spectrum adaption terms, and RMSE values for each acoustic curve. The maximum difference in predicting weighted standardized level differences (with or without correction terms) is 1 dB (test floor #4). For the weighted standardized impact sound pressure level, the maximum difference is 2 dB (test floor #1 and #3), and this increases to 4 dB when adaption terms are included (test floor #3).

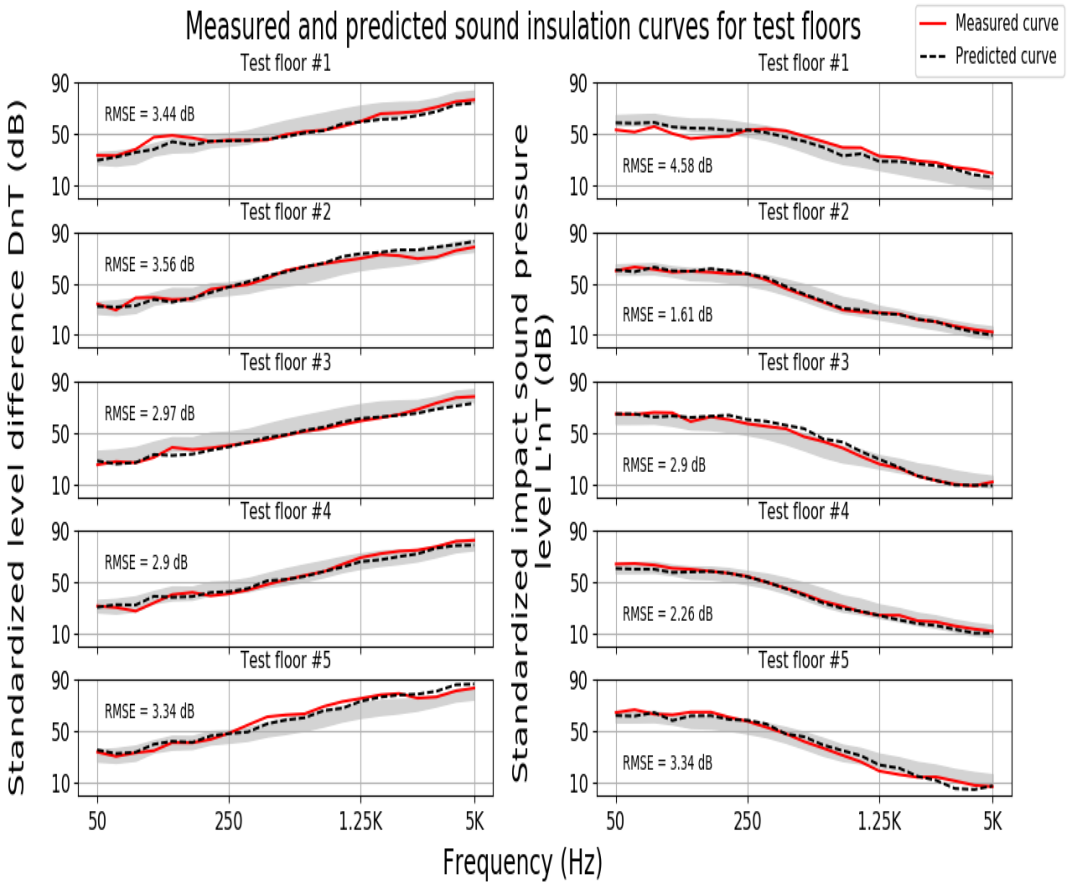

Figure 7.4: A graphical representation of the differences between the predicted and measured airborne and impact sound insulation curves for five test floors is shown with the mean and standard deviation values of the trained data indicated by the gray area in the background.

Table 7.3: Predicted and measured weighted standardized level differences of test floors and their spectrum adaption terms (in dB).

Floor no.	RMSE	D_{nTw}	C	$C_{50–3150}$	$D_{nT,wPred}$	C_{Pred}	$C_{50–3150\ Pred}$
1	3.44	54	0	0	54	−1	−1
2	3.56	58	−2	−2	58	−2	−3
3	2.97	51	−1	−1	51	−2	−2
4	2.90	54	−1	−2	55	−1	−2
5	3.34	60	−2	−3	60	−2	−3

Table 7.4: Predicted and measured weighted standardized impact sound pressure level of test floors and their spectrum adaption terms (in dB).

Floor no.	RMSE	L'_{nTw}	C_I	$C_{I,50-2500}$	$L'_{nT,wPred}$	C_{IPred}	$C_{I,50-2500\ Pred}$
1	4.58	45	0	3	47	2	4
2	1.61	51	0	3	52	1	3
3	2.90	53	1	4	55	1	2
4	2.26	50	1	5	49	0	5
5	3.34	54	1	4	53	2	3

Table 7.5 shows the distribution of errors when predicting airborne and impact insulation curves in three different frequency ranges (low (50 Hz − 200 Hz), middle (250 Hz − 1 kHz), high (1.25 kHz − 5 kHz), and the whole frequency range (50 Hz − 5 kHz)) to provide an in-depth evaluation. For airborne sound predictions, the highest deviations are in the high-frequency range, which is likely due to the involvement of flanking transmission paths. The ANN model is unable to predict sound transmission around these bands accurately. In comparison, the most remarkable errors for impact predictions are in the low-frequency range. Since there are fewer impact sound transmission paths than airborne sound, the model's inaccuracy, in this case, can be attributed to inadequate structural parameters that are involved in the modeling. Moreover, low-frequency bands tend to have more significant measurement uncertainties due to the influence of receiving room effects. These effects depend on the Schröder frequency, where the diffuse sound field is present above that frequency [156, 157]. To more accurately simulate the sound transmission phenomena, it is essential to consider complementary structural parameters such as dynamic stiffness, elastic modulus, and vibration reduction index of the junctions. Previous studies have also reported the effect of insufficient parameters on the results [83, 84]. Furthermore, field measurements are more likely to have flanking paths than laboratory measurements, so additional information must be considered.

Table 7.5: A comparison of the measured and predicted sound insulation curves (standardized level differences D_{nT} and standardized impact sound pressure level L'_{nT}) divided into three frequency ranges: low, medium, and high.

Root-Mean-Square Errors in dB				
Frequency (Hz)	**Low** (50 – 200)	**Middle** (250 – 1000)	**High** (1250 – 5000)	**Full range** (50 – 5000)
D_{nT}	3.43	2.27	3.85	3.24
L'_{nT}	3.54	3.07	2.65	3.77

Fig. 7.5 shows the probability density function of errors for both airborne and impact sound estimations across all frequency bands (50 Hz − 5 kHz). The errors are mostly found in the range of -5 to 5 dB. Additionally, the peak of the error density is higher for airborne insulation curves than impact cases, which suggests that the network predicts airborne insulation curves more accurately than impact cases. This is also reflected in the rating values in Tables 7.3 and 7.4.

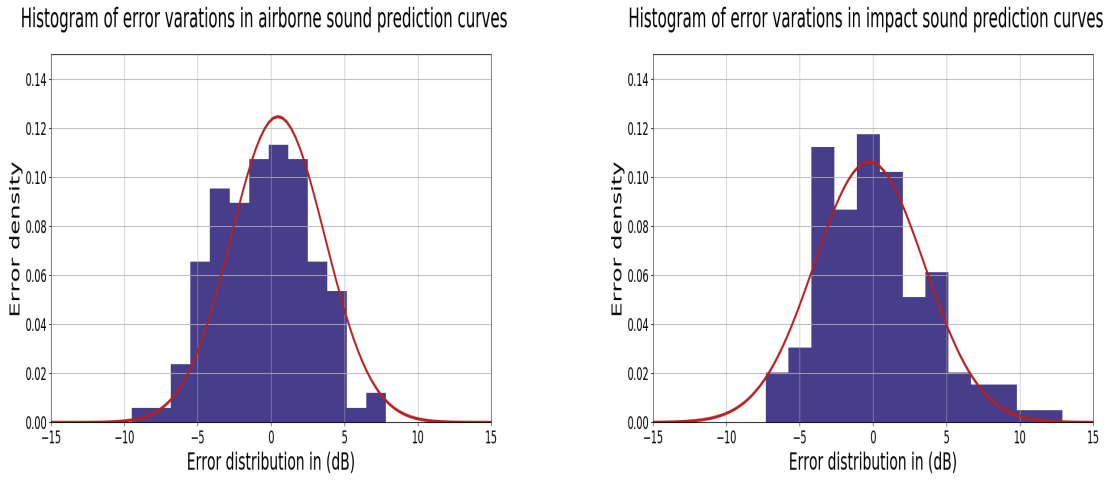

(a) *(b)*

Figure 7.5: Histograms show the error distribution in predicting sound insulation curves across all frequencies. (a) standardized level differences D_{nT}. (b) Standardized impact sound pressure level L'_{nT}.

7.3.2 Sensitivity analysis of the structural parameters on the sound insulation estimations

A feature attribution analysis is employed to assess the contribution of the structural parameters listed in Table 7.1 to the ANN model's ability to estimate acoustic sound insulation curves. This type of analysis is necessary to evaluate the model's performance and guarantee its predictive accuracy. Furthermore, sensitivity analysis is essential to investigate the connections between the parameters and their effect on the predictions. The advantage of this approach is that it offers insight into the influence of the parameters on each frequency band.

The feature attribution analysis of the model focused on the field measurements will consider certain parameters that are considered to have a higher value of importance in this type of simulation. Figure 7.6 shows the size effect of the floor and its surface area, along with the effect of surrounded walls, visco-elastic interlayer thickness, and the volume of the receiving room. The effects of thicknesses, densities, and the installation order of the materials are grouped for each structure (floor or surrounded walls) to determine their total effect on the estimations. Therefore, when discussing the effect of façade, load-bearing, and non-load-bearing walls, it is meant that all of the material components of that kind of wall are taken into account, and their effects are evaluated as a whole.

The results of Figure 7.6 (a) demonstrate that the direct path (which encompasses the effects of thickness and density) is dominant at all frequencies and tends to increase at higher frequencies. This can be attributed to mass and coincidence-control regions, where the masses and thicknesses of the structural components take control of sound insulation at those frequencies [3]. Additionally, the effects of flanking transmission paths (façade and load-bearing walls) become more evident at higher frequencies, which could explain the large deviations in airborne insulation predictions at higher frequencies. This highlights the importance of including more parameters to make the prediction of sound insulation more accurate with the ANN model. No notable differences were observed for non-load bearing or internal separating walls since these walls are typically installed in the room without junctions between them and the connected floor, thus reducing the

chance for the sound to travel through. Furthermore, a minor effect was noted for floor-separating areas, as has been reported in prior studies [83, 84, 162]. The volume of the receiving room affects sound attenuation at all frequencies, particularly in higher ranges. This is because the energy exchanged between the particles of air and the sound wave can be released after a delay, leading to a decrease in sound energy [3]. This phenomenon is more likely to occur in larger rooms or/and higher frequency ranges. This finding was also highlighted in a previous study by the authors [84]. At lower frequencies, the visco-elastic interlayer between junctions has a minimal effect on sound transmission loss. However, the predicted standardized level differences become frequency-dependent and increase with frequency [152]. This is because the transmission loss is frequency-independent and similar to a rigid connection. The study did not consider the relationship between visco-elastic interlayers and the applied load. It has been observed that the vibration reduction index of a junction decreases globally with increasing load [187]. This can be attributed to the increase in stiffness of the interlayer when the applied load is reset. The latter was also investigated in a study that linked the building height and the applied load on the airborne sound insulation [188].

Figure 7.6 (b) shows the sensitivity analysis of floor structural parameters in predicting standardized impact sound pressure level. It can be observed that the direct path is the primary factor in all frequencies, particularly at low frequencies. This agrees with the mass-spring-damping system approach, which states that impact sound transmission is mainly determined by the stiffness at low frequencies [3]. The influence of the flanking paths follows the same trend as the direct path but with a lower attribution. Non-load-bearing internal walls have no significant impact on the estimations. The receiving room volume is crucial in low-frequency predictions due to the high uncertainties in this range, which could significantly impact the estimations. This was highlighted by [189] and reported in previous studies [83, 84]. The same trend is also noted for the visco-elastic interlayer at the junctions. However, the area of the separating surface of the floor has little effect on the estimations.

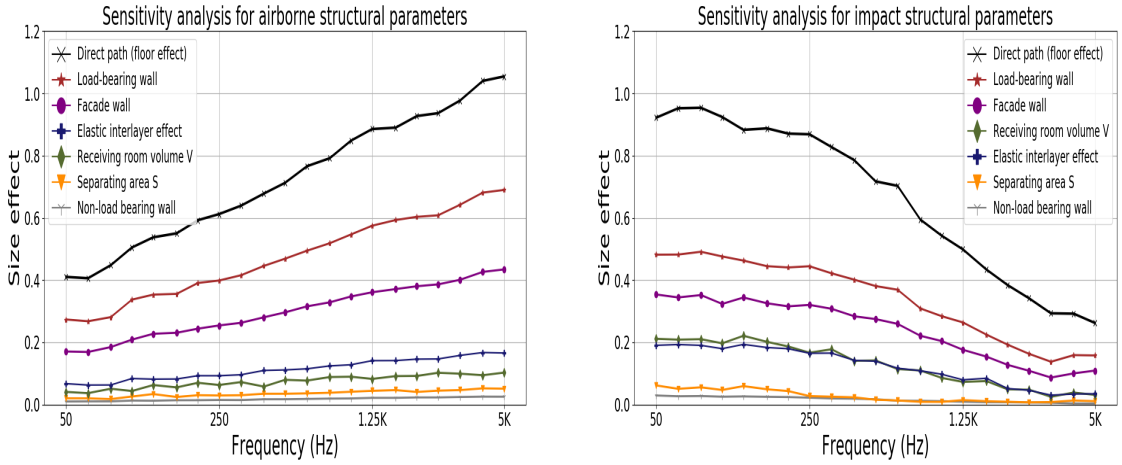

(a) *(b)*

Figure 7.6: Feature attribution analysis illustrates the importance of floor structural parameters in developing the ANN model. (a) attributions on standardized level differences. (b) attributions on standardized impact sound pressure level.

7.4 Conclusions

In this chapter, a neural network approach is presented to predict on-site acoustic insulation curves (standardized level differences D_{nT} and standardized impact sound pressure level L'_{nT}) for CLT-based floor systems. The network model is developed using various structural parameters from 104 field acoustic insulation curves. The ANN model proved effective in estimating field sound insulation performance, with a maximum RMSE of 3.56 dB for airborne curve predictions and 4.58 dB for impact estimations across all frequencies (50 Hz – 5 kHz). For single-number-quantities, the highest deviation is 1 dB in estimating weighted standardized level differences D_{nTw}. In comparison, it is 2 dB for weighted standardized impact pressure level L'_{nTw}. These results suggest acoustic designers may be able to use the network model for practical engineering works, as differences up to 2 dB are deemed unnoticeable to humans for noise levels. Furthermore, the model can be used to save the cost and time of acoustic measurements.

The predictive accuracy of the network model was better in estimating the standardized level differences except at higher frequencies (1.25 kHz – 5 kHz), where the flanking transmission paths are more common. There were higher deviations in the low frequency

(50 Hz – 200 Hz) range for the standardized impact sound pressure level predictions where more significant measurement uncertainties are present. Additional parameters should be incorporated into the modeling. This could include more detailed information about the junctions, vibration reduction indices, elastic material properties, connection type between structure material components, and an increased number of measurements to ensure the reliability of the network model.

A sensitivity analysis was conducted to examine structural parameters' impact on the insulation curves' prediction. The results showed that the direct transmission path (floor structure) effect was the most significant, followed by the effects of flanking paths. Additionally, the receiving room volume, the area of the separating surface of the floor, and the visco-elastic interlayer in the junctions also had considerable effects on the forecast.

Chapter 8

CONCLUSION AND FUTURE PROSPECTS

8.1 Conclusion

The presented thesis reveals the potential to develop prediction models using artificial neural networks to forecast sound insulation curves based on laboratory and field measurements of lightweight wooden structures. Three models have been developed to predict the insulation performance of lightweight wooden structures, particularly floor, and façade constructions. Two models (in Chapters 5 and 6) were developed based on laboratory measurements to predict the insulation curves of floors and façades. However, the third model (in Chapter 7) was used to simulate the acoustic performance of CLT-based floors considering field conditions. The ANN models were utilized to predict the acoustic spectra for the frequency bands 50 Hz − 5000 Hz, and the single number quantities were also calculated and compared to real values to estimate the predictive capability of the models. Physical and geometric characteristics of each structure (materials, thickness, density, dimensions, mass, and more) are utilized as input parameters in the developed model.

The first model (Chapter 5) has been developed to estimate acoustic performance for lightweight wooden floors' airborne and impact sound insulation curves. The model is based on 252 standardized laboratory measurement curves in one-third octave bands (50 Hz − 5000 Hz), which utilize physical and geometric characteristics of each floor structure (materials, thickness, density, dimensions, mass, etc.) as network

parameters. The model can predict the airborne sound more accurately than the impact sound, especially in the middle-frequency range (250 Hz − 1000 Hz). The model's prediction of the weighted airborne sound reduction index R_w had a maximum error of 2 dB. In contrast, the error increased to 5 dB in the worst-case prediction of the weighted normalized impact sound pressure level $L_{n,w}$. The model had high variations near fundamental and critical frequency areas, which affected its accuracy. A feature attribution analysis was conducted to identify the significant parameters in estimating sound insulation. The thickness of insulation materials, the density of cross-laminated timber slabs and concrete floating floors, and the total density of floor structures were found to have the most influence on the predictions. A comparison between wet and dry floor solution systems highlighted the importance of the upper part of floors for estimating airborne and impact sound in low frequencies.

The second artificial neural network-based prediction model (Chapter 6) was created to calculate the acoustic performance of lightweight wooden façade walls concerning airborne sound insulation. One hundred measurements of insulation curves were used for the model's development, and laboratory data gathered in one-third-octave bands (50 Hz − 5 kHz) from each façade wall were used as input parameters. The model exhibited a good capacity of accurately predicting airborne sound reduction, with an overall maximum difference of 3 dB in the weighted airborne sound reduction index (R_w). The model showed the most precision in middle frequencies (250 Hz − 1 kHz), while higher and lower frequency ranges showed more significant variance. The sensitivity analysis study found that the material density, insulation material thickness, thickness, spacing between interior studs, and total density of façades all had a considerable impact on predictions. Additionally, the thickness of the façades and the total density of the exterior layers were highlighted as essential factors in the model's precision.

The third neural network-based prediction tool (Chapter 7) was developed to predict the standardized level differences and impact sound pressure levels of multi-layered CLT-based floor systems. The data used for the model was 104 acoustic measurements from 15 different buildings in Europe, measured in one-third-octave bands from 50 Hz to 5

kHz. The structural parameters of the buildings, such as floor components, surrounding wall types, junction types, and their visco-elastic interlayers, receiving room volume, and surface separating area, were considered for the network model. The model showed satisfactory results in predicting the standardized airborne and impact sound insulation curves across all frequencies, with a variation of 1 dB for the weighted standardized level differences D_{nTw} and up to 2 dB for the weighted standardized impact sound pressure level L'_{nTw}. The best correlation was highlighted in the middle frequencies (200 Hz – 1 kHz) for airborne estimations and at high frequencies (1.25 kHz – 5 kHz) for impact estimations. The sensitivity study showed that the direct sound path through the floor is the most influential, followed by the flanking paths. The volume of the receiving room was found to be a critical factor for impact estimations at low frequencies. Additionally, the visco-elastic interlayer between the junctions was found to be essential for airborne predictions across all frequency ranges.

8.2 Future work

The presented research has demonstrated using an artificial neural network approach in predicting sound insulation curves for lightweight wooden structures. Despite the three ANN models' good performance, some discrepancies were observed in the prediction results. The latter discrepancies could be addressed due to insufficient parameters in developing the ANN models. Regardless of the fundamental role of specific elastic properties on sound transmissions, such as dynamic stiffeners and the modulus of elasticity of each material, they are not considered in the input parameters due to the lack of information in acoustic measurement reports. Moreover, sound insulation measurements are implemented in different places, such as laboratories (lab-based measurements) and buildings (on-site acoustic tests). In addition, uncertainties could also be present in the measurements due to the construction system, workmanship, and measurement implementations. It is worthy to mention that the artificial neural networks approach does not take into account the uncertainties present in acoustic measurements, which may have an effect on the accuracy of the model's predictions. To overcome such

limitations, controlling the quality of sound insulation measurements is vital.

Further investigation could be interesting by adding complementary parameters in the modeling to overcome such prediction limitations. The studied parameters could be complemented by the inclusion of detailed information about the junctions, vibration reduction indices, elastic material properties, connection type between structure material components, a bigger measurement number, and the measurements should be carried out in one place and by the same person in order to increase the reliability of the network model.

It is necessary to conduct an optimization study for this type of modeling to get the best results and highlight the most important parameters. In order to successfully implement this study, it is essential to have sufficient parameters to simulate the sound insulation phenomenon accurately. The optimization study would provide informative and reliable results if the additional parameter adequate parameters are included.

REFERENCES

[1] Kuttruff H. Acoustics: an introduction. *CRC Press*, 2007 Jan 24.

[2] World Health Organization. Environmental noise guidelines for the European region. *World Health Organization. Regional Office for Europe*; 2018.

[3] Vigran T.E. *Building Acoustics*. CRC Press: Boca Raton, FL, USA, 2014. doi: https://doi.org/10.1201/9781482266016.

[4] Svozil D, Kvasnicka V, Pospichal J. Introduction to multi-layer feed-forward neural networks. *Chemom. Intell. Lab. Syst.* 1997, 39, 43–62. doi: https://doi.org/10.1016/S0169-7439(97)00061-0.

[5] Ketkar N, Santana E. Deep learning with Python. *Berkeley, CA: Apress; 2017 Apr*.

[6] Svozil, D.; Kvasnicka, V.; Pospichal, J. Introduction to multi-layer feed-forward neural networks. *Chemom. Intell. Lab. Syst.* 1997, *39*, 43–62. doi: https://doi.org/10.1016/S0169-7439(97)00061-0.

[7] Deep learning. Adaptive computation and machine learning. *An MIT Press Book. 2017*.

[8] Davy J.L. The improvement of a simple theoretical model for the prediction of the sound insulation of double leaf walls. *J. Acoust. Soc. Am.* 2010, 127, 841–849. doi: https://doi.org/10.1121/1.3273889.

[9] Beranek L.L, Work G.A. Sound transmission through multiple structures containing flexible blankets. *J. Acoust. Soc. Am.* 1949, 21, 419–428. doi: https://doi.org/10.1121/1.1906530.

[10] Mulholland K., Price A, Parbrook H. Transmission loss of multiple panels in a random incidence field. *J. Acoust. Soc. Am.* 1968, 43, 1432–1435. doi: https://doi.org/10.1121/1.1911003.

[11] Kang H.J, Ih J.G, Kim J.S, Kim H.S. Prediction of sound transmission loss through multilayered panels by using Gaussian distribution of directional incident energy. *J. Acoust. Soc. Am.* 2000, 107, 1413–1420. doi: https://doi.org/10.1121/1.428428.

[12] Van den Wyngaert JC, Schevenels M, Reynders EP. Predicting the sound insulation of finite double-leaf walls with a flexible frame. *Appl. Acoust.* 2018, 141, 93–105. doi: https://doi.org/10.1016/j.apacoust.2018.06.020.

[13] Caniato M. Sound insulation of complex façades: A complete study combining different numerical approaches. *Appl. Acoust.* 2020, 169, 107484. doi: https://doi.org/10.1016/j.apacoust.2020.107484.

[14] Clasen D, Langer S. Finite element approach for flanking transmission in building acoustics. *Building Acoustics.* 2007 Jan;14(1):1-4. doi: https://doi.org/10.1260/135101007780661428.

[15] Qian C, Ménard S, Bard D, Negreira J. Development of a vibroacoustic stochastic finite element prediction tool for a CLT floor. *Applied Sciences.* 2019 Mar 15;9(6):1106. doi: https://doi.org/10.3390/app9061106.

[16] Qian C, Ménard S, Bard-Hagberg D, Kouyoumji JL, Negreira J. Calibration of the ISO tapping machine for finite-element prediction tool on a wooden-base floor. *Building Acoustics.* 2019 Sep;26(3):157-67. doi: https://doi.org/10.3390/app9061106.

[17] Serpilli F, Di Nicola G, Pierantozzi M. Airborne sound insulation prediction of masonry walls using artificial neural networks. *Build. Acoust.* 2021, 28, 391–409. doi: https://doi.org/10.1177/1351010X21994462.

[18] Drass M, Kraus MA, Riedel H, Stelzer I. SoundLab AI-Machine learning for sound insulation value predictions of various glass assemblies. *Glass Structures & Engineering.* 2020 Apr.7(1):101-18. doi: https://doi.org/10.1007/s40940-022-00167-z.

[19] Craik R, Smith R. Sound transmission through double leaf lightweight partitions part I: airborne sound. *Appl. Acoust.* 2000, 61, 223–245. doi: https://doi.org/10.1016/S0003-682X(99)00070-5.

[20] Hongisto V. *Airborne Sound Insulation of Wall Structures: Measurement and Prediction Methods*. Helsinki University of Technology: Espoo, Finland, 2000.

[21] Legault J, Atalla N. Sound transmission through a double panel structure periodically coupled with vibration insulators. *J. Sound Vib.* 2010, 329, 3082–3100. doi: https://doi.org/10.1016/j.jsv.2010.02.013.

[22] Santoni A, Davy J.L, Fausti P, Bonfiglio P. A review of the different approaches to predict the sound transmission loss of building partitions. *Build. Acoust.* 2020, 27, 253–279. doi: https://doi.org/10.1177/1351010X20911599.

[23] Zimmermann A. Acoustical performance of wooden lightweight industrialized buildings : airborne sound transmission loss evaluation for single and double walls using analytical models and the transfer matrix method. *Mémoire de maîtrise*, Université du Québec à Chicoutimi. 2021.

[24] Nilsson E, Vardaxis N-G, Ménard S, Bard Hagberg D. Sound Reduction of Ventilation Ducts through Walls: Experimental Results and Updated Models. *Acoustics.* 2021; 3(4):695-716. doi: https://doi.org/10.3390/acoustics3040044.

[25] Nilsson E, Ménard S, Bard Hagberg D, Vardaxis N-G. Acoustical Treatments on Ventilation Ducts through Walls: Experimental Results and Novel Models. *Acoustics.* 2022; 4(1):276-296. doi: https://doi.org/10.3390/acoustics4010017.

A review of the different approaches to predict the sound transmission loss of building partitions. *Build. Acoust.* 2020, 27, 253–279. doi: https://doi.org/10.1177/1351010X20911599.

[26] Patrício J. Case Study: Laboratory and Field Measurements for Evaluating the Weighted Reduction in Impact Noise Associated with Floor Coverings. *Building Acoustics* 2002 Jun. 9(2):151-62. doi: https://doi.org/10.1260/135101002760164580.

[27] Asselineau M. *Building Acoustics.* CRC press. 2015 Mar 18.

[28] Vorländer, M. Building acoustics: From prediction models to auralization. In Proceedings of the ACOUSTICS 2006, Christchurch, New Zealand, 20–22 November 2006.

[29] *ISO.12354-1*; Building Acoustics–Estimation of Acoustic Performance of Buildings from the Performance of Elements—Part 1: Airborne Sound Insulation between Rooms. International Organization for Standardization: Geneva, Switzerland, 2017.

[30] Guigou-Carter, C.; Villot, M.; Wetta, R. Prediction method adapted to wood frame lightweight constructions. *Build. Acoust.* 2018, 13, 173–188. doi: https://doi.org/10.1260/135101006778605424.

[31] ISO.10140-2 Acoustics – Laboratory measurement of sound insulation of building elements – Part 2: Measurement of airborne sound insulation. *International Organization for Standardization*, 2010.

[32] *ASTM.E90-09*; Standard Test Method for Laboratory Measurement of Airborne Sound Transmission Loss of Building Partitions and Elements. ASTM International: West Conshohocken, PA, USA, 2016.

[33] *ISO.16283-1*; Acoustics–Field measurement of sound insulation in buildings and of building elements—-Part 1: Airborne sound insulation. International Organization for Standardization: Geneva, Switzerland, 2014.

[34] *ISO.16283-2*; Acoustics–Field measurement of sound insulation in buildings and of building elements—Part 2: Impact sound insulation. International Organization for Standardization: Geneva, Switzerland, 2015.

[35] *ASTM.E336-20*; Standard Test Method for Measurement of Airborne Sound Attenuation between Rooms in Buildings. ASTM International: West Conshohocken, PA, USA, 2016.

[36] *ASTM.E1007-21*; Standard Test Method for Field Measurement of Tapping Machine Impact Sound Transmission Through Floor-Ceiling Assemblies and Associated Support Structures. ASTM International: West Conshohocken, PA, USA, 2016.

[37] *ISO.717-1*; Acoustics–Rating of Sound Insulation in Buildings and of Buildings Elements—Part 1: Airborne Sound Insulation. International Organization for Standardization: Geneva, Switzerland, 2013.

[38] *ISO.717-2*; Acoustics–Rating of sound insulation in buildings and of building elements—Part 2: Impact sound insulation International Organization for Standardization: Geneva, Switzerland, 2013.

[39] *ASTM.E413-16*; Classification for Rating Sound Insulation. ASTM International: West Conshohocken, PA, USA, 2022.

[40] Buratti C, Moretti E, Vergoni M. Sound insulation performances of windows: Evaluation of the influence of different traffic noise spectra in laboratory and field measurement. *In Proceedings of 17th International Congress on Sound and Vibration*, Cairo 2010 Jul.

[41] Möser M. E ngineering acoustics. *Nova York (Estados Unidos): Springer Publishing.* 2009.

[42] Beranek. Leo L Noise and vibration control *Principles and applications.* 1971.

[43] ISO.140-3 Acoustics – Laboratory measurement of sound insulation of building elements – Part 3: Measurement of impact sound insulation. *International Organization for Standardization*, 2010.

[44] *ASTM.E492-09*; Standard Test Method for Laboratory Measurement of Impact Sound Transmission through Floor-ceiling Assemblies using the Tapping Machine. ASTM International: West Conshohocken, PA, USA, 2016.

[45] 10140-5 Acoustics-Laboratory measurement of sound insulation of building elements-Part 5: Requirements for test facilities and equipment. *International Organization for Standardization*, 2010.

[46] Warnock AC. Low-frequency impact sound transmission through floor systems. *In proceedings of Inter-noise 2000* Aug 27 (Vol. 2000).

[47] JIS A 1419-1 Measurement of floor impact sound insulation of buildings - Part 1: Method using standard light impact source. Tokyo 2000.

[48] JIS A 1419-2 Acoustics—Rating of sound insulation in buildings and of building elements—Part 2: Floor impact sound. Tokyo 2000.

[49] Heckl M. The tenth Sir Richard Fairey memorial lecture: Sound transmission in buildings. *Journal of Sound and Vibration.* 1981 Jul 22;77(2):165-89.

[50] Pellicier A, Trompette N. A review of analytical methods, based on the wave approach, to compute partitions transmission loss. *Applied Acoustics.* 2007 Oct 1;68(10):1192-212.

[51] Cremer L. Theorie der Schalldämmung dünner Wände bei schrägem Einfall. *Akustische Zeitschrift.* 1942 May;7(3):81-104.

[52] Cremer L, Heckl M, Petersson BA, Cremer L, Heckl M, Petersson BA. A Little Dynamics. *Structure-Borne Sound: Structural Vibrations and Sound Radiation at Audio Frequencies.* 2005:4-26.

[53] Davy JL. Predicting the sound insulation of single leaf walls: Extension of Cremer's model. *The Journal of the Acoustical Society of America.* 2009 Oct;126(4):1871-7.

[54] Fahy FJ, Gardonio P. Sound and structural vibration: radiation, transmission and response. *Elsevier.* 2007 Jan 12.

[55] Junger MC, Feit D. Sound, structures, and their interaction. *MA: MIT press Cambridge.* 1986. vol. 225.

[56] Fagy F. Sound and structural vibration: Radiation, transmission and response((Book)) *London and Orlando, FL, Academic Press.* 1985, 325.

[57] Sewell EC. Transmission of reverberant sound through a single-leaf partition surrounded by an infinite rigid baffle. *Journal of Sound and Vibration.* 1970 May 1;12(1):21-32.

[58] Ballagh KO. Accuracy of prediction methods for sound transmission loss. *In INTER-NOISE and NOISE-CON congress and conference* proceedings 2004 Aug 22 (Vol. 2004, No. 4, pp. 3095-3102). Institute of Noise Control Engineering.

[59] Rindel, JH Sound radiation from building structures and acoustical properties of thick plates *COMETTSAVOIR Course, Noise Control in Buildings* 1995.

[60] Sharp BH. Prediction methods for the sound transmission of building elements. 1978.

[61] Tadeu A, Pereira A, Godinho L, Antonio J. Prediction of airborne sound and impact sound insulation provided by single and multilayer systems using analytical expressions. *Applied Acoustics.* 2007 Jan 1;68(1):17-42. doi: https://doi.org/10.1016/j.apacoust.2006.05.012.

[62] Cremer L, Heckl M, Ungar EE. Structure-borne sound. *Journal of Applied Mechanics.* 1974 Sep;41(3):839.

[63] Ver IL. Calculation of the Impact Noise Isolation of Composite Floors. *The Journal of the Acoustical Society of America.* 1970 Jul;48(1A):73-73.

[64] Brunskog J, Hammer P. Prediction model for the impact sound level of lightweight floors. *Acta acustica united with acustica.* 2003 Mar 1;89(2):309-22.

[65] Ingelaere B, Wuyts D. Impact sound measurements on wooden floors. Project AH+, part 6. *In INTER-NOISE and NOISE-CON Congress and Conference* proceedings 2013 Sep 15 (Vol. 247, No. 1, pp. 6230-6238). Institute of Noise Control Engineering.

[66] Caniato M, Bettarello F, Fausti P, Ferluga A, Marsich L, Schmid C. Impact sound of timber floors in sustainable buildings. *Building and Environment.* 2017 Aug 1;120:110-22.

[67] Hynna P, Klinge P, Vuoksinen J. Prediction of structure-borne sound transmission in large welded ship structures using statistical energy analysis. *Journal of sound and vibration.* 1995 Mar 2;180(4):583-607.

[68] Burroughs CB, Fischer RW, Kern FR. An introduction to statistical energy analysis. *The Journal of the Acoustical Society of America.* 1997 Apr;101(4):1779-89.

[69] Hutton DV. Fundamentals of finite element analysis. *McGraw-Hill Science Engineering.* 2004.

[70] Łodygowski T, Sumelka W. Limitations in application of finite element method in acoustic numerical simulation. *Journal of theoretical and applied mechanics.* 2006;44(4):849-65.

[71] Brunskog J, Davidsson P. Sound transmission of structures. A finite element approach with simplified room description. *Acta acustica united with acustica.* 2004 Sep, *1;90(5):847-57.*

[72] London A. Transmission of reverberant sound through double walls. *The journal of the acoustical society of America.* 1950 Mar, *1;22(2):270-9.* doi: https://doi.org/10.1121/1.1906601.

[73] Brunskog J, Davidsson P. Kropp W, Rebillard E. On the air-borne sound insulation of double wall constructions. *Acta acustica united with acustica.*1999 Sep, *1;85(5):707-20.*

[74] Lin GF, Garrelick JM. Sound transmission through periodically framed parallel plates. *The journal of the acoustical society of America.* 1977 Apr, *1;61(4):1014-8.* doi: https://doi.org/10.1121/1.381386.

[75] Takahashi D. Sound radiation from periodically connected double-plate structures. *Journal of Sound and Vibration.* 1983 Oct, *22;90(4):541-57.* doi: https://doi.org/10.1016/0022-460X(83)90810-6.

[76] Skelton EA. Acoustic scattering by parallel plates with periodic connectors. *Proceedings of the Royal Society of London. A. Mathematical and Physical Sciences.* 1990 Feb, *8;427(1873):419-44.* doi: https://doi.org/10.1098/rspa.1990.0021.

[77] Skelton EA. Brunskog J. The influence of finite cavities on the sound insulation of double-plate structures. *The Journal of the Acoustical Society of America.* 2005 Jun, *1;117(6):3727-39.* doi: https://doi.org/10.1121/1.1904264.

[78] Shin, H. K.; Park, S. H.; Kim, K. W. Inter-floor noise classification using convolutional neural network *Plos one*.2020, *15*, e0243758. doi: https://doi.org/10.1371/journal.pone.0243758.

[79] Garg, N.; Dhruw, S.; Gandhi, L. Prediction of sound insulation of sandwich partition panels by means of artificial neural networks. *Arch. Acoust.* 2017, *42*, 643–651. doi: https://doi.org/10.1515/aoa-2017-0068.

[80] Buratti, C.; Barelli, L.; Moretti, E. Wooden windows: Sound insulation evaluation by means of artificial neural networks. *Appl. Acoust.* 2013, *74*, 740–745. doi:

https://doi.org/10.1016/j.apacoust.2012.12.001.

[81] Luo Z, Li T, Yan Y, Zhou Z, Zha G. Prediction of sound insulation performance of aramid honeycomb sandwich panel based on artificial neural network. *Appl. Acoust.* 2022 (190), 108656. doi: https://doi.org/10.1016/j.apacoust.2022.108656.

[82] Caniato M, Bettarello F, Ferluga A, Marsich L, Schmid C, Faustic P. Acoustic of lightweight timber buildings: A review. *Renewable and Sustainable Energy Reviews* 2017(80): 585-596. doi: https://doi.org/10.1016/j.rser.2017.05.110.

[83] Bader Eddin M, Ménard S, Bard Hagberg D, Kouyoumji J-L. Vardaxis, N.-G. Prediction of Sound Insulation Using Artificial Neural Networks—Part I: Lightweight Wooden Floor Structures. *Acoustics* 2022, 4, 203–226. doi: https://doi.org/10.3390/acoustics4010013.

[84] Bader Eddin M, Vardaxis NG, Ménard S, Bard Hagberg D, Kouyoumji J-L. Prediction of Sound Insulation Using Artificial Neural Networks—Part II: Lightweight Wooden Façade Structures. *Applied Sciences.* 2022 Jul 10; 12(14):6983. doi: https://doi.org/10.3390/app12146983.

[85] *ASTM.Committee E33 Subcommittees*; https://www.astm.org/COMMIT/SUBCOMMIT/E33.htm. Accessed: 2023-March-17.

[86] *ISO Committee*; International Organization for Standardization: Geneva, Switzerland. https://www.iso.org/committee/48558.html. Accessed on: 2023 March 07.

[87] Hoeller C. Review and Comparison of ASTM and ISO Standards on Sound Transmission in Buildings. *In INTER-NOISE and NOISE-CON Congress and Conference* proceedings 2018 Dec 18 (Vol. 258, No. 5, pp. 2338-2347). Institute of Noise Control Engineering.

[88] ISO.10140-4 Acoustics — Laboratory measurement of sound insulation of building elements — Part 4: Measurement procedures and requirements. *International Organization for Standardization*, 2021.

[89] *ISO.140-2*; Acoustics–Laboratory Measurement of Sound Insulation of Building Elements—Part 2: Measurement of Airborne Sound Insulation. International Organization for Standardization: Geneva, Switzerland, 2010.

[90] ISO.10140-5 Acoustics — Laboratory measurement of sound insulation of building elements — Part 5: Requirements for test facilities and equipment. *International Organization for Standardization*, 2021.

[91] *E989-06*; Standard Classification For Determination Of Impact Insulation Class (IIC). ASTM International: West Conshohocken, PA, USA, 2022.

[92] Francois C. Deep learning with Python.2108.

[93] Graupe, D. *Principles of Artificial Neural Networks*; World Scientific: Singapore, 2013.

[94] Anderson D, McNeill G. Artificial neural networks technology. *Kaman Sciences Corporation.* 1992 Aug 20;258(6):1-83.

[95] Schmidhuber, J. Deep learning. *Scholarpedia* 2015, *10*, 32832.

[96] Nielsen, M.A. *Neural Networks and Deep Learning*; Determination Press: San Francisco, CA, USA, 2015. doi: https://doi.org/10.4249/scholarpedia.32832.

[97] Sharma, S.; Sharma, S.; Athaiya, A. Activation functions in neural networks. *Towards Data Sci.* 2017, *6*, 310–316.

[98] Srivastava N. Improving neural networks with dropout. *University of Toronto.* 2013 Jan;182(566):7.

[99] Srivastava N, Hinton G, Krizhevsky A, Sutskever I, Salakhutdinov R. Dropout: a simple way to prevent neural networks from overfitting. *The journal of machine learning research.* 2014 Jan 1;15(1):1929-58.

[100] Smilkov, D.; Thorat, N.; Kim, B.; Viégas, F.; Wattenberg, M. Smoothgrad: Removing noise by adding noise. *arXiv* 2017, arXiv:1706.03825. doi: https://doi.org/10.48550/arXiv.1706.03825.

[101] Baehrens, D.; Schroeter, T.; Harmeling, S.; Kawanabe, M.; Hansen, K.; Müller, K.R. How to explain individual classification decisions. 2009 Dec 6. *arXiv preprint arXiv:0912.1128.* doi: https://doi.org/10.48550/arXiv.0912.1128.

[102] Shrikumar, A.; Greenside, P.; Shcherbina, A.; Kundaje, A. Not just a black box: Learning important features through propagating activation differences. *arXiv* 2016, arXiv:1605.01713. doi: https://doi.org/10.48550/arXiv.1605.01713.

[103] Simonyan, K.; Vedaldi, A.; Zisserman, A. Deep inside convolutional networks: Visualising image classification models and saliency maps. *arXiv* 2013, arXiv:1312.6034. doi: https://doi.org/10.48550/arXiv.1312.6034.

[104] Sundararajan, M.; Taly, A.; Yan, Q. Axiomatic attribution for deep networks. In Proceedings of the International Conference on Machine Learning, PMLR, Sydney, Australia, 6–11 August 2017; pp. 3319–3328.

[105] Ruder, S. An overview of gradient descent optimization algorithms. *arXiv* 2016, arXiv:1609.04747. doi: https://doi.org/10.48550/arXiv.1609.04747.

[106] Paszke A, Gross S, Massa F, Lerer A, Bradbury J, Chanan G, Killeen T, Lin Z, Gimelshein N, Antiga L, Desmaison A. Pytorch: An imperative style, high-performance deep learning library. *Advances in neural information processing systems.* 2019;32.

[107] Widenius, M.; Axmark, D.; Arno, K. *MySQL Reference Manual: Documentation from the Source*; O'Reilly Media, Inc.: Newton, MA, USA, 2002.

[108] Hair JF, Black WC, Babin BJ, Anderson RE. *Multivariate data analysis.* Eight Edition, Cengage: Learning EMEA. 2019.

[109] Warnock, ACC. Summary report for consortium on fire resistance and sound insulation of floors: Sound transmission and impact insulation data. *Institute for Research in Construction, National Research Council Canada.* 2005.

[110] *ISO.140-03*; Acoustics–Measurement of sound insulation in buildings and of building elements–Part 3: Laboratory measurements of airborne sound insulation of building elements. International Organization for Standardization: Geneva, Switzerland, 1995.

[111] *ISO.140-06*; Acoustics–Measurement of sound insulation in buildings and of building elements–Part 6: Laboratory measurements of impact sound insulation of floors. International Organization for Standardization: Geneva, Switzerland, 1998.

[112] Bradley, J. S.; Birta, J. A. *Laboratory measurements of the sound insulation of building facade elements*; Institute for Research in Construction, National Research Council Canada: Ottawa, ON, Canada, 2000.

[113] Leonard S, Bader Eddin M, Prichard M, Broyles J, Brown N, Ménard S. Trade-off Between Embodied Carbon and Acoustic Insulation for Mass Timber Floor Assemblies. In WCTE 2023 proceedings 2023 June 19.-22. Oslo, Norway, .

[114] Hassan OA. Building acoustics and vibration: theory and practice. *World Scientific Publishing Company*, 2009 Jun 24.

[115] Vardaxis NG, Bard D, Persson Waye K. Review of acoustic comfort evaluation in dwellings—part I: Associations of acoustic field data to subjective responses from building surveys. *Building Acoustics.* 2018 Jun;25(2):151-70.

[116] ISO.16283-1 Acoustics–Field measurement of sound insulation in buildings and of building elements–Part 1: Airborne sound insulation. *International Organization for Standardization*. 2014.

[117] ISO.16283-2. Acoustics–Field measurement of sound insulation in buildings and of building elements–Part 1: Impact sound insulation. *International Organization for Standardization*. 2015.

[118] Vardaxis NG, Bard D. Review of acoustic comfort evaluation in dwellings: Part II—Impact sound data associated with subjective responses in laboratory tests. *Building Acoustics.* 2018 Jun;25(2):171-92.

[119] Vardaxis NG, Bard D. Review of acoustic comfort evaluation in dwellings: Part III—airborne sound data associated with subjective responses in laboratory tests. *Building Acoustics.* 2018 Dec;25(4):289-305.

[120] Radkau J. *Wood: A History*; Polity: Cambridge, UK, 2012.

[121] Popovski M, Ni C. Mid-rise Wood-Frame Construction Handbook; FPInnovations: Vancouver, BC, Canada, 2015.

[122] Chatti S. 1Production of profiles for lightweight structures. BoD–Books on Demand; 2006.

[123] Rasmussen B, Machimbarrena M. Building Acoustics throughout Europe Volume 1: Towards a Common Framework in Building Acoustics throughout Europe. DiScript Preimpresion, S.L.: Madrid, Spain, 2014.

[124] *ISO.12354-2*; Building acoustics–estimation of acoustic performance of buildings from the performance of elements–part 2: impact sound insulation between rooms. International Organization for Standardization: Geneva, Switzerland, 2017.

[125] Chattopadhyay A, Manupriya P, Sarkar A, Balasubramanian VN. Neural network attributions: A causal perspective. *In International Conference on Machine Learning.* 2019 May 24 (pp. 981-990). PMLR.

[126] Abdel-Hamid O, Deng L, Yu D. Exploring convolutional neural network structures and optimization techniques for speech recognition. In *Interspeech*; Citeseer: Princeton, NJ, USA, 2013.

[127] Dede G, Sazlı MH. Speech recognition with artificial neural networks. In *Digital Signal Processing.*; 2010 May 1;20(3):763-8. doi: https://doi.org/10.1016/j.dsp.2009.10.004.

[128] Deng L, Hinton G, Kingsbury B. New types of deep neural network learning for speech recognition and related applications: An overview. In *In 2013 IEEE international conference on acoustics, speech and signal processing*; 2013 May 26 (pp. 8599-8603). IEEE. doi: https://doi.org/10.1109/ICASSP.2013.6639344.

[129] Thai L.H, Hai T.S, Thuy N.T. Image classification using support vector machine and artificial neural network. *Int. J. Inf. Technol. Comput. Sci.* 2012, *4*, 32–38. doi: https://doi.org/10.5815/ijitcs.2012.05.05.

[130] Mahmon NA, Ya'acob N. A review on classification of satellite image using Artificial Neural Network (ANN). *In 2014 IEEE 5th Control and system graduate research colloquium.* 2014 Aug 11 (pp. 153-157). IEEE. doi: https://doi.org/10.1109/ICSGRC.2014.6908713.

[131] Li Q, Cai W, Wang X, Zhou Y, Feng DD, Chen M. Medical image classification with convolutional neural network. *In 2014 13th international conference on control automation robotics & vision (ICARCV).* 2014 Dec 10 (pp. 844-848). IEEE. doi: https://doi.org/10.1109/ICARCV.2014.7064414.

[132] Dangeti, P. *Statistics for Machine Learning*; Packt Publishing Ltd.: Birmingham, UK, 2014.

[133] Ma C; Chen C, Liu Q, Gao H, Li Q, Gao H, Shen Y. Sound quality evaluation of the interior noise of pure electric vehicle based on neural network model. *IEEE Trans. Ind. Electron.* 2017, *64*, 9442–9450. doi: https://doi.org/10.1109/TIE.2017.2711554.

[134] Wang YS, Shen GQ, Xing YF. A sound quality model for objective synthesis evaluation of vehicle interior noise based on artificial neural network. *Mechanical Systems and Signal Processing.*2014 Mar 3;45(1):255-66.

[135] Mohamed AR, Dahl GE, Hinton G. Acoustic modeling using deep belief networks. *IEEE transactions on audio, speech, and language processing.* 2011 Jan 31;20(1):14-22. doi: https://doi.org/10.1109/TASL.2011.2109382.

[136] Di Loreto S, Serpilli F, Lori V, Squartini S. Sound quality evaluation of kitchen hoods. *Applied Acoustics.* 2020 Nov 1;168:107415.

[137] Serpilli F, Lori V, Di Loreto S. Speech recognition assessment in Italian pediatric schools using close-set speech tests: A case of study. *In INTER-NOISE and NOISE-CON congress and conference proceedings* 2020 Oct 12 (Vol. 261, No. 5, pp. 1768-1778). Institute of Noise Control Engineering.

[138] Sak H, Senior A, Beaufays F. Long short-term memory based recurrent neural network architectures for large vocabulary speech recognition. *arXiv preprint arXiv:1402.1128.* 2014 Feb 5.

[139] Nagaya, K.; Li, L. Control of sound noise radiated from a plate using dynamic absorbers under the optimization by neural network. *J. Sound Vib.* 1997, *208*, 289–298. doi: https://doi.org/10.1006/jsvi.1997.1201.

[140] Iannace, G.; Trematerra, A.; Ciaburro, G. Case study: Automated recognition of wind farm sound using artificial neural networks. *Noise Control. Eng. J.* 2020, *68*, 157–167. doi: https://doi.org/10.3397/1/376814.

[141] IANNACE G, Ciaburro G, Trematerra A. Using neural networks to detect wind turbine functioning conditions. *International Journal of Automation and Smart Technology.* 2020 Jun 1;10(1):145-52.

[142] Ciaburro G, Iannace G, Passaro J, Bifulco A, Marano D, Guida M, Marulo F, Branda, F. Artificial neural network-based models for predicting the sound absorption coefficient of electrospun poly (vinyl pyrrolidone)/silica composite. *Appl. Acoust.* 2020, *169*, 107472. doi: https://doi.org/10.1016/j.apacoust.2020.107472.

[143] Iannace G, Ciaburro G, Trematerra A. Modelling sound absorption properties of broom fibers using artificial neural networks. *Applied Acoustics.* 2020 Jun 1;163:107239. doi: https://doi.org/10.1016/j.apacoust.2020.107239.

[144] Bader Eddin M, Menard S, Bard D, Kouyoumji J.L, Vardaxis N.G. A Sound Insulation Prediction Model for Floor Structures in Wooden Buildings Using Neural Networks Approach. In *INTER-NOISE and NOISE-CON Congress and Conference Proceedings*; Institute of Noise Control Engineering: Reston, VA, USA, 2021. doi:

https://doi.org/10.3397/IN-2021-2619.

[145] Géron, A. *Hands-on Machine Learning with Scikit-Learn, Keras, and TensorFlow: Concepts, Tools, and Techniques to Build Intelligent Systems*; O'Reilly Media, Inc.: Newton, MA, USA, 2019.

[146] Labach A, Salehinejad H, Valaee S. Survey of dropout methods for deep neural networks. arXiv preprint arXiv:1904.13310. 2019 Apr 25. https://doi.org/10.48550/arXiv.1904.13310 Focus to learn more.

[147] Aggarwal, C.C. *Neural Networks and Deep Learning*; Springer: Berlin/Heidelberg, Germany, 2018; Volume 10. doi: https://doi.org/10.1007/978-3-319-94463-0.

[148] Mastromichalakis, S. ALReLU: A different approach on Leaky ReLU activation function to improve Neural Networks Performance. *arXiv* 2020, arXiv:2012.07564. doi: https://doi.org/10.48550/arXiv.2012.07564.

[149] Kingma D.P, Ba J. Adam: A method for stochastic optimization. *arXiv* 2014, arXiv:1412.6980. doi: https://doi.org/10.48550/arXiv.1412.6980.

[150] Tato, A.; Nkambou, R. Improving adam optimizer. 2018. Accessed on: 2021 November 09.

[151] Xu, J.; Li, Z.; Du, B.; Zhang, M.; Liu, J. Reluplex made more practical: Leaky ReLU. In Proceedings of the 2020 IEEE Symposium on Computers and Communications (ISCC), Rennes, France, 7–10 July 2020; IEEE: Piscataway, NJ, USA, 2020. doi: https://doi.org/10.1109/ISCC50000.2020.9219587.

[152] Rindel, J.H. *Sound Insulation in Buildings*; CRC Press: Boca Raton, FL, USA, 2017. doi: https://doi.org/10.1201/9781351228206.

[153] Blazier Jr WE, DuPree RB. Investigation of low-frequency footfall noise in wood-frame, multifamily building construction *The Journal of the Acoustical Society of America.* 1994 Sep;96(3):1521-32.

[154] Sipari P. Sound insulation of multi-storey houses—A summary of Finnish impact sound insulation results. *Building Acoustics.* 2000 Mar;7(1):15-30.

[155] Ljunggren F, Ågren A. Potential solutions to improved sound performance of volume based lightweight multi-storey timber buildings. *Applied acoustics.* 2011 Mar 1;72(4):231-40.

[156] Schoenwald S, Zeitler B, Nightingale TR. Influence of receive room properties on impact sound pressure level measured with heavy impact sources. *In EUROREGIO 2010 CONGRESS ON SOUND AND VIBRATION.* Ljubljana 2010 Sep.

[157] Reynders EP, Wang P, Lombaert G. Prediction and uncertainty quantification of structure-borne sound radiation into a diffuse field. *Journal of Sound and Vibration.* 2019 Dec 22;463:114984.

[158] Prato A, Schiavi A, Ruatta A. A modal approach for impact sound insulation measurement at low frequency. *Building Acoustics.* 2016 Jun;23(2):110-9.

[159] Hopkins C. Sound insulation. *Routledge.* 2012 May 31.

[160] Zhou J, Zhao Z. Apparent impact sound insulation performance of cross laminated timber floors with floating concrete toppings. *In INTER-NOISE and NOISE-CON Congress and Conference.* Proceedings 2021 Aug 1 (Vol. 263, No. 1, pp. 5203-5215). Institute of Noise Control Engineering. doi: https://doi.org/10.3397/IN-2021-3006.

[161] Uris A, Llopis A., Llinares, J. Effect of the rockwool bulk density on the airborne sound insulation of lightweight double walls. *Appl. Acoust.* 1999, *58*, 327–331. doi: https://doi.org/10.1016/S0003-682X(98)00065-6.

[162] Fora-Moncada A, Gibbs, B. Prediction of sound insulation at low frequencies using artificial neural networks. *Build. Acoust.* 2002, *9*, 49–71. doi: https://doi.org/10.1260/135101002761035735.

[163] Ottelin J, Amiri A, Steubing B, Junnila S. *Comparative carbon footprint analysis of residents of wooden and non-wooden houses in Finland*; Environmental Research Letters. 2021 Jun 22;16(7):074006.

[164] Bettarello F, Gasparella A, Caniato M. *The Influence of Floor Layering on Airborne Sound Insulation and Impact Noise Reduction: A Study on Cross Laminated Timber (CLT) Structures*; Applied Sciences. 2021 Jan;11(13):5938. doi: https://doi.org/10.3390/app11135938.

[165] Jayalath A, Navaratnam S, Gunawardena T, Mendis P, Aye L. *Airborne and impact sound performance of modern lightweight timber buildings in the Australian construction industry*; Case Studies in Construction Materials. 2021 Dec 1;15:e00632. doi: https://doi.org/10.1016/j.cscm.2021.e00632.

[166] Forss*é*n J, Kropp W, Brunskog J, Ljunggren S, Bard D, Sandberg G, Ljunggren F, *Å*gren A, Hallström O, Dybro H, Larsson K, Tillberg K, Sjökvist L-G, *Ö*stman B, Hagberg K, Bolmsvik *Å*, Olsson A, Ekstrand CG, Johansson M. *Acoustics in wooden buildings, State of the art 2008, Vinnova project 2007-01653*; Report 2008:16, SP Trätek (Technical Research Institute of Sweden), Stockholm, 2008.

[167] Pei S, Rammer D, Popovski M, Williamson T, Line P, van de Lindt JW. *An overview of CLT research and implementation in North America*; In: WCTE 2016, Vienna, Austria, August 22-25, 2016.

[168] Secchi S, Cellai G, Fausti P, Santoni A, Martello N. Z. Sound transmission between rooms with curtain wall façades: a case study *Build. Acoust.*2015, *22*, 193–207. doi: https://doi.org/10.1260/1351-010X.22.3-4.193.

[169] *ASTM.E966-04*; Standard Guide for Field Measurements of Airborne Sound Insulation of Building Facades and Facade Elements. ASTM International: West Conshohocken, PA, USA, 2010.

[170] Clark, D. M. Subjective study of the sound-transmission class system for rating building partitions *J. Acoust. Soc. Am.* 1970, *47*, 676–682. doi: https://doi.org/10.1121/1.1911950.

[171] Sign-to-speech translation using machine-learning-assisted stretchable sensor arrays. Nature Electronics.2020 Sep;3(9):571-8. doi: https://doi.org/10.1038/s41928-020-0428-6.

[172] Dijckmans, A.; De Geetere, L.; Wuyts, D.; Ingelaere, B. The effect of mechanical connectors on the sound insulation of structural insulating panels. *InINTER-NOISE and NOISE-CON Congress and Conference Proceedings.* 2018 Dec 18, *258*, *9*, 1261–1272.

[173] Demanet C, De Rozas M.J, Chene J.B, Foret R. 2011. European Round Robin Test for sound insulation measurements of lightweight partition. *Proceedings of InterNoise*; Osaka, Japan.

[174] Wszołek, G. and Engel, Z., 2004. Investigations of uncertainty of acoustical measuring instruments applied to noise control. *Archives of Acoustics*, 29(2).

[175] Sinha A. How Good is Wood? Facts and Myths Regarding Wood as a Green Building Material. In Wood is Good 2017; (pp. 443-450). *Springer, Singapore.*

[176] Pandey KK, Ramakantha V, Chauhan SS, Kumar AA. Wood is Good. *Springer: Singapore; 2017*.

[177] Yadav R, Kumar J. Engineered Wood Products as a Sustainable Construction Material: A Review. *Engineered Wood Products for Construction.* 2021 Aug 30. https://doi.org/10.5772/intechopen.99597.

[178] Hildebrandt J, Hagemann N, Thrän D. The contribution of wood-based construction materials for leveraging a low carbon building sector in Europe. *Sustainable cities and society.* 2017 Oct 1;34:405-18. doi: https://doi.org/10.1016/j.scs.2017.06.013.

[179] Švajlenka J, Kozlovská M. Construction Systems Based on Wood. *In Efficient and Sustainable Wood-based Constructions* 2022; *(pp. 17-34).* Springer, Cham.

[180] Riggio M, Alhariri N, Hansen E. Paths of innovation and knowledge management in timber construction in North America: a focus on water control design strategies in CLT building enclosures. *Architectural Engineering and Design Management.* 2020 Jan 2; *16(1):58-83.* doi: https://doi.org/10.1016/j.cscm.2021.e00632.

[181] Homb A, Guigou-Carter C, Rabold A. Impact sound insulation of cross-laminated timber/massive wood floor constructions: Collection of laboratory measurements and result evaluation. *Building Acoustics* 2017, *Mar;24* (1):35-52. doi: https://doi.org/10.1177/1351010X16682966.

[182] Singh SP, Kumar A, Darbari H, Singh L, Rastogi A, Jain S. Machine translation using deep learning: An overview. *In 2017 international conference on computer, communications and electronics (comptelix)* 2017 Jul 1 (pp. 162-167). IEEE. doi:

https://doi.org/10.1109/COMPTELIX.2017.8003957.

[183] Tian Y. Artificial intelligence image recognition method based on convolutional neural network algorithm. *IEEE access.* 2020 Jun 30. 8:125731-44. doi: https://doi.org/10.1109/ACCESS.2020.3006097.

[184] Nassif AB, Shahin I, Attili I, Azzeh M, Shaalan K. Speech recognition using deep neural networks: A systematic review. *IEEE access.* 2019 Feb 1. 7:19143-65. doi: https://doi.org/10.1109/ACCESS.2019.2896880.

[185] Jeon JH, Yang SS, Kang YJ. Estimation of sound absorption coefficient of layered fibrous material using artificial neural networks. *Applied Acoustics.* 2020 Dec 1. 169:107476. doi: https://doi.org/10.1016/j.apacoust.2020.107476.

[186] Genaro N, Torija A, Ramos A, Requena I, Ruiz DP, Zamorano M. Modeling environmental noise using artificial neural networks. *In 2009 Ninth International Conference on Intelligent Systems Design and Applications.* 2009 Nov 30 (pp. 215-219). IEEE. doi: https://doi.org/10.1109/ISDA.2009.179.

[187] Crispin C, Ingelaere B, Van Damme M, Wuyts D. The Vibration Reduction Index K ij: Laboratory Measurements for Rigid Junctions and for Junctions with Flexible Interlayers. *Build. Acoust.* 2006, Jun;13(2):99-111. doi: https://doi.org/10.1260/135101006777630427.

[188] Nilsson E, Ménard S, Bard D, Hagberg K. Effects of building height on the sound transmission in cross-laminated timber Buildings–Airborne sound insulation. *Building and Environment.* 2023 Jan 4:109985. doi: https://doi.org/10.1016/j.buildenv.2023.109985.

[189] Kylliäinen M, Talus L, Lietzén J, Latvanne P, Kovalainen V. Assessment of the low-frequency procedure in the field measurements of impact sound insulation between dwellings. *Applied Acoustics.* 2022 Jan 1;185:108399. doi: https://doi.org/10.1016/j.apacoust.2021.108399.

[190] Pajchrowski, G.; Noskowiak, A.; Lewandowska, A.; Strykowski, W. Wood as a building material in the light of environmental assessment of full life cycle of four buildings. *Construction and Building Materials.* 2014, 428-36.

[191] Gustavsson, L.; Sathre, R. Variability in energy and carbon dioxide balances of wood and concrete building materials. *Building and Environment.* 2006, 41(7):940-51.

[192] Sewell, EC. Transmission of reverberant sound through a single-leaf partition surrounded by an infinite rigid baffle. *Journal of Sound and Vibration.* May 1970;1;12(1):21-32.

[193] Broyles JM, Shepherd MR, Brown NC. Modified acoustic transmission metrics for early-stage design exploration using a computational case study of heavyweight floors. *Applied Acoustics.* 2022 Jul 1;196:108865. doi: https://doi.org/10.1016/j.apacoust.2022.108865.

[194] Leppington FG, Heron KH, Broadbent EG, Mead SM. Resonant and non-resonant acoustic properties of elastic panels. II. The transmission problem. *Proceedings of the Royal Society of London. A. Mathematical and Physical Sciences.* 1987 Aug 8;412(1843):309-37. doi: https://doi.org/10.1098/rspa.1987.0091.

ANNEX A: Laboratory sound insulation measurements for floor structures

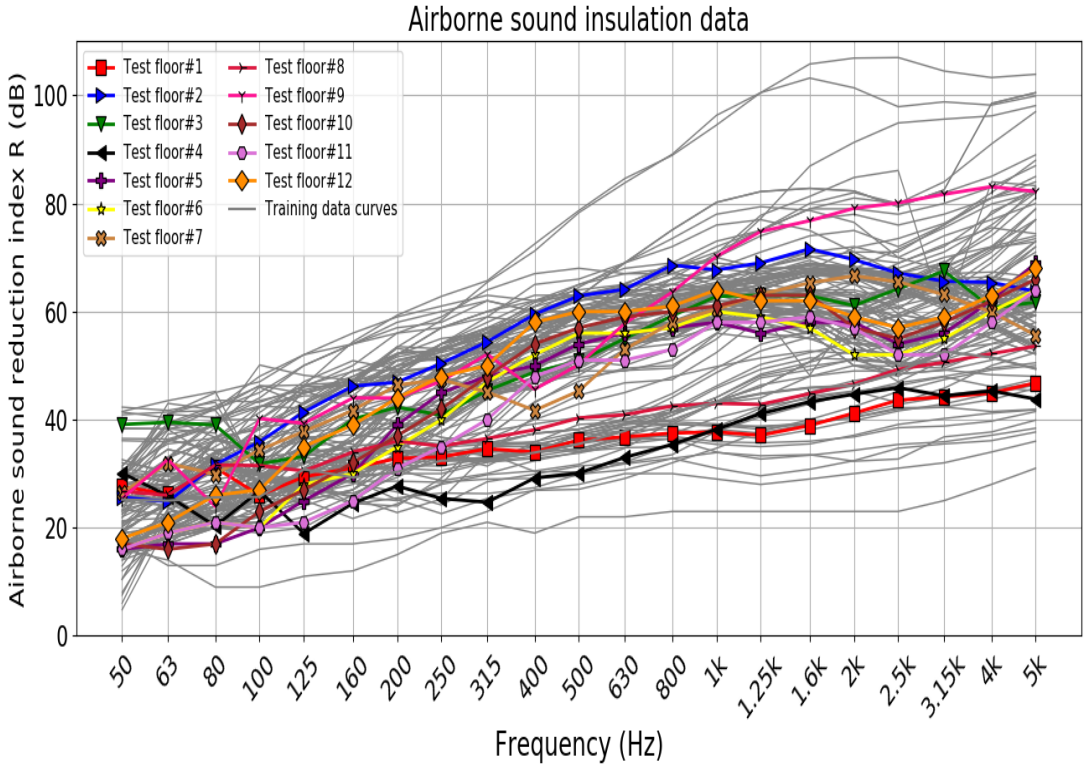

Figure A1: Standardized laboratory measurements for airborne sound reduction index for floor structures.

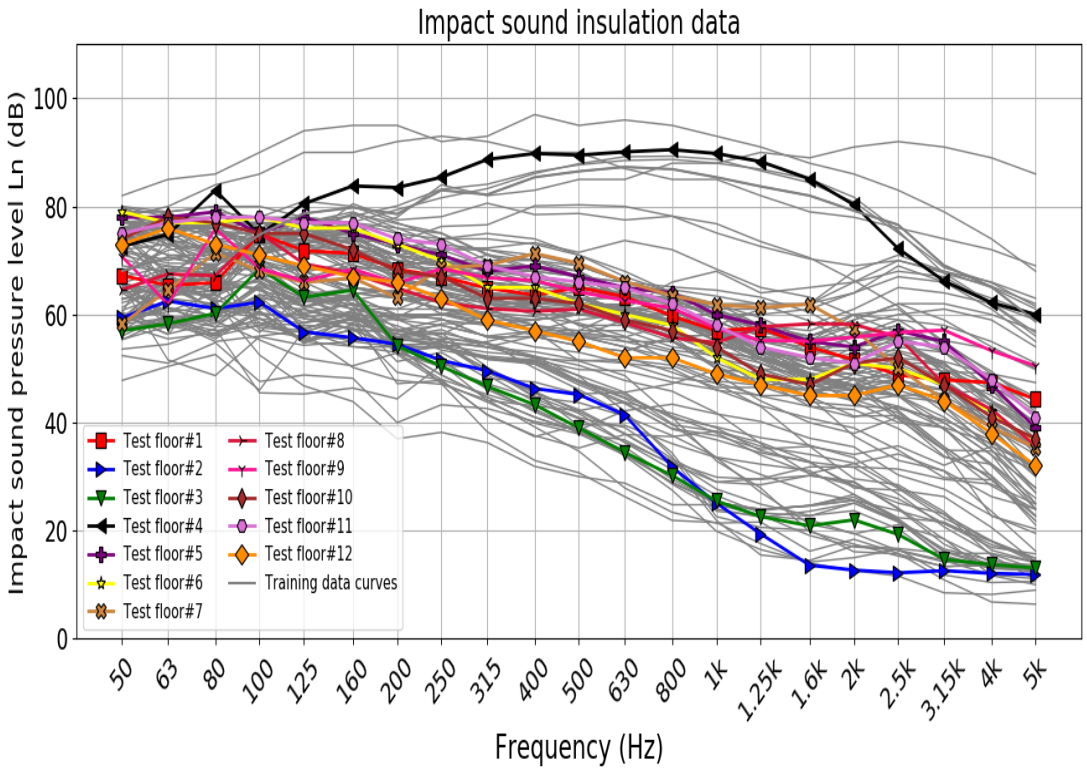

Figure A2: Standardized laboratory measurements for normalized impact sound pressure levels for floor structures.

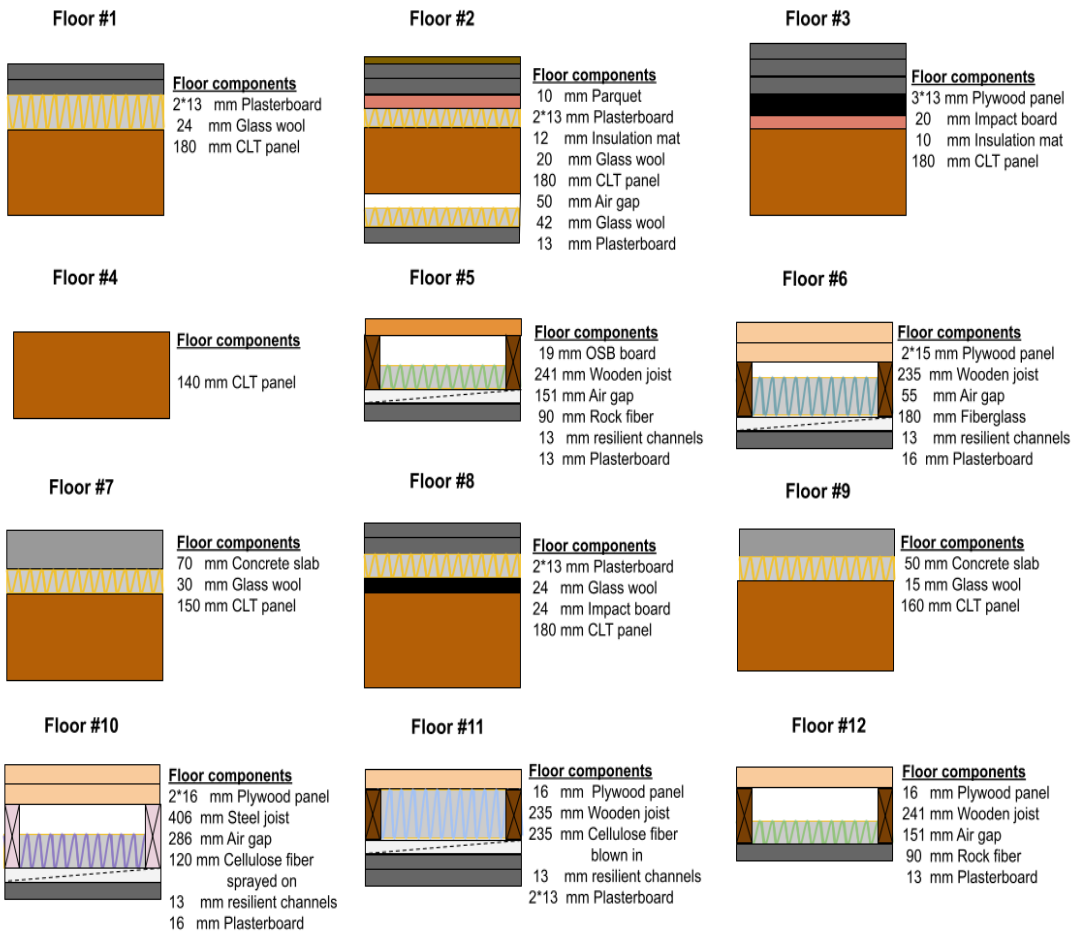

Figure A3: Test floor configurations used to evaluate the predictive accuracy of airborne and impact sound insulation curves based on laboratory measurements.

ANNEX B: Laboratory sound insulation measurements for façade structures

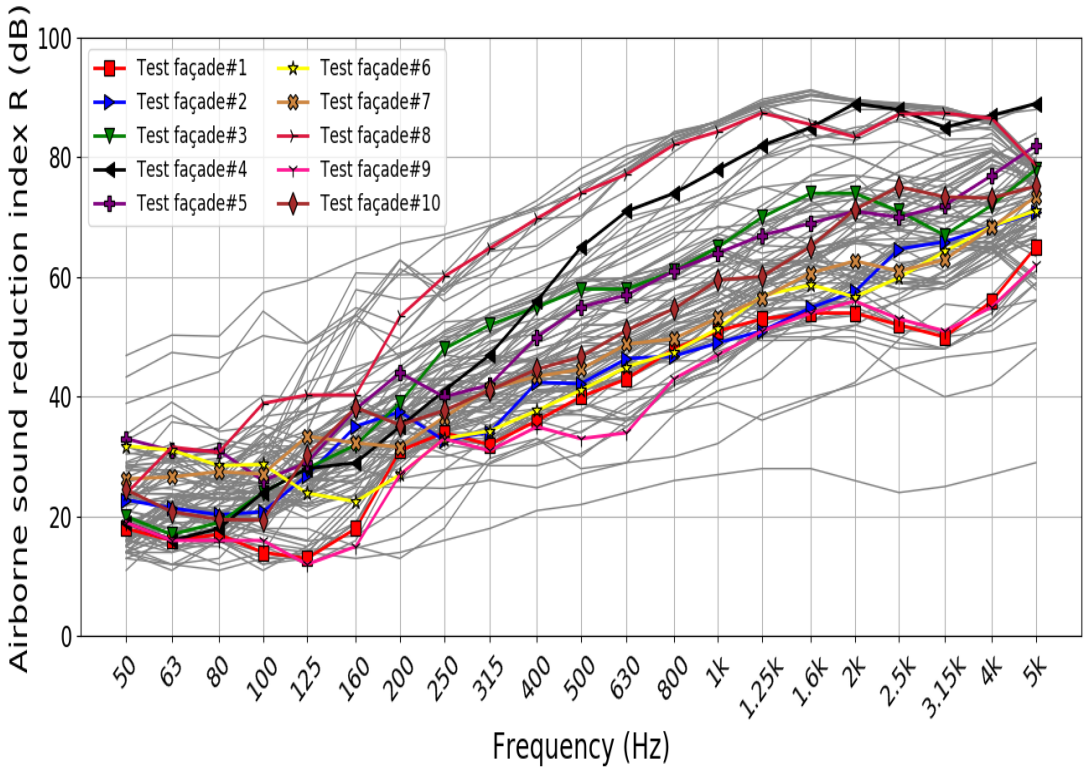

Figure B1: Standardized laboratory curves for airborne sound reduction index of façade walls.

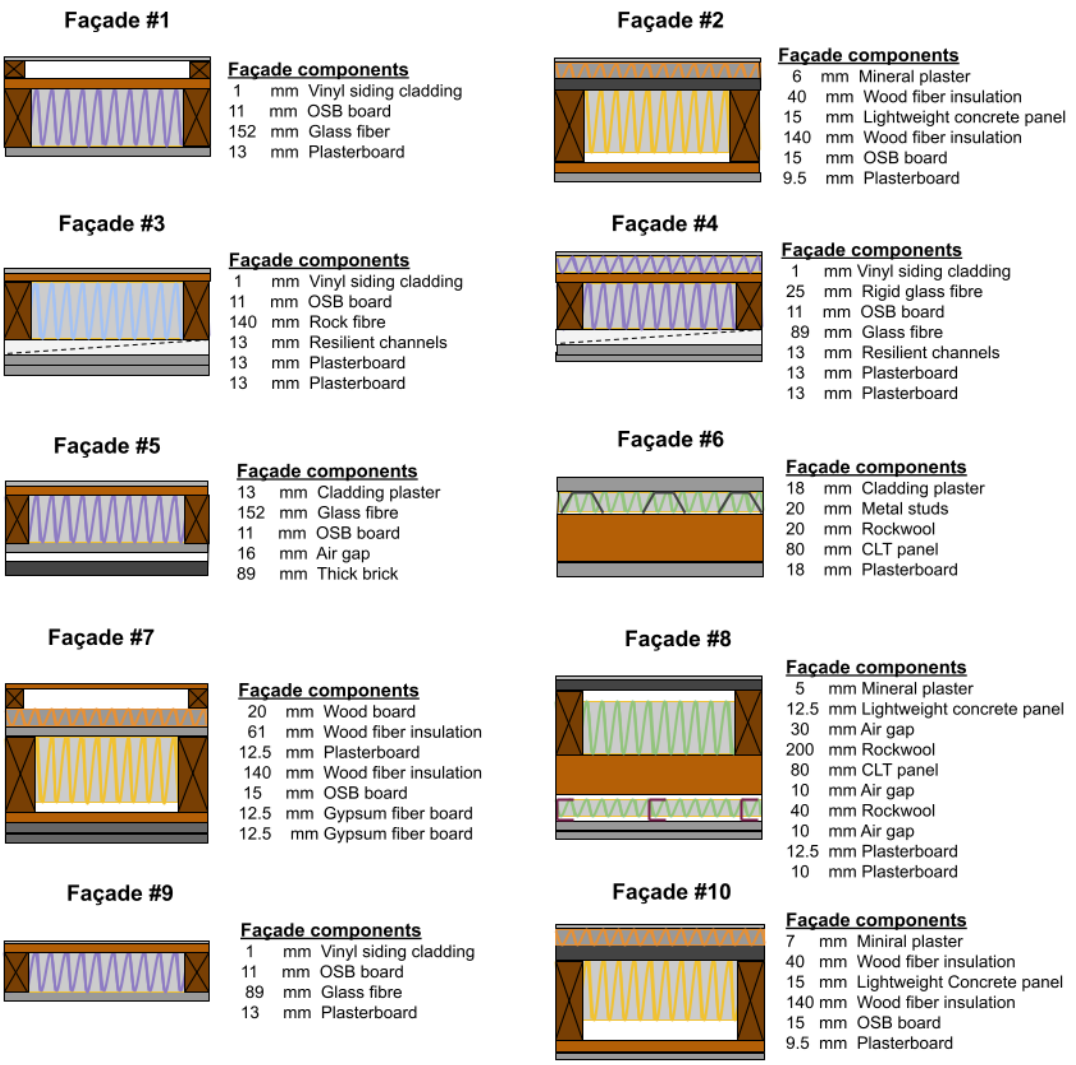

Figure B2: Structural components of the selected test façads for testing the ANN network.

ANNEX C: Field sound insulation measurements for floor structures

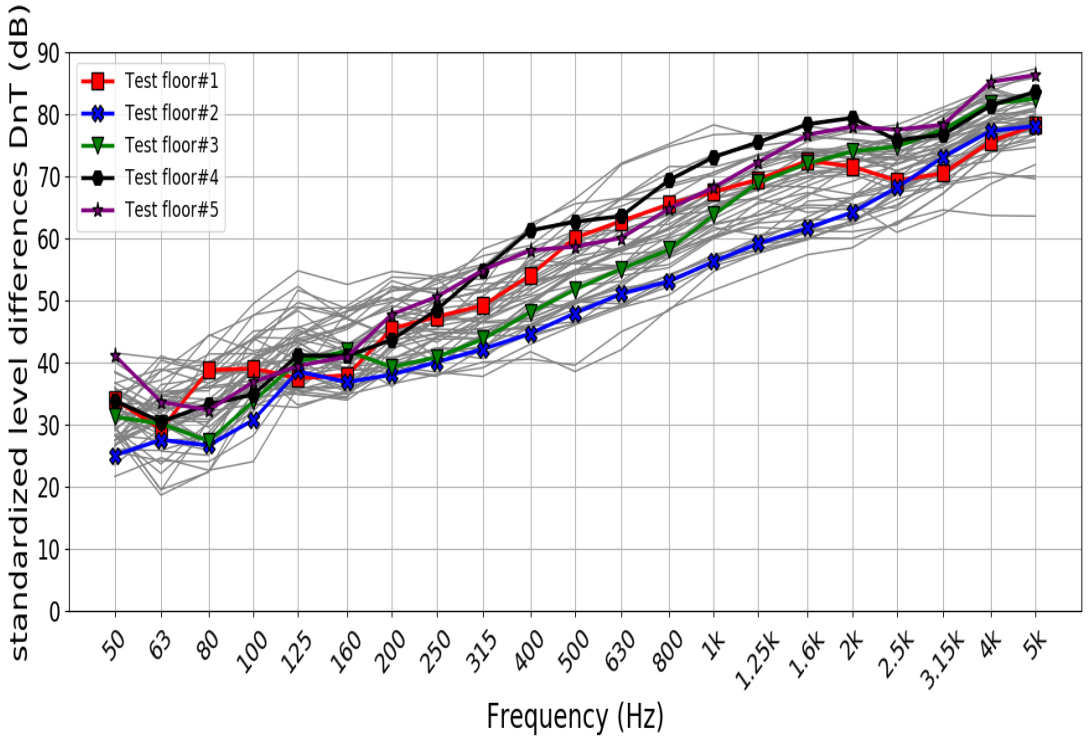

Figure C1: Field sound insulation measurements for standardized level deference curves. Curves in gray represent curves that are utilized to train and validate the network model.

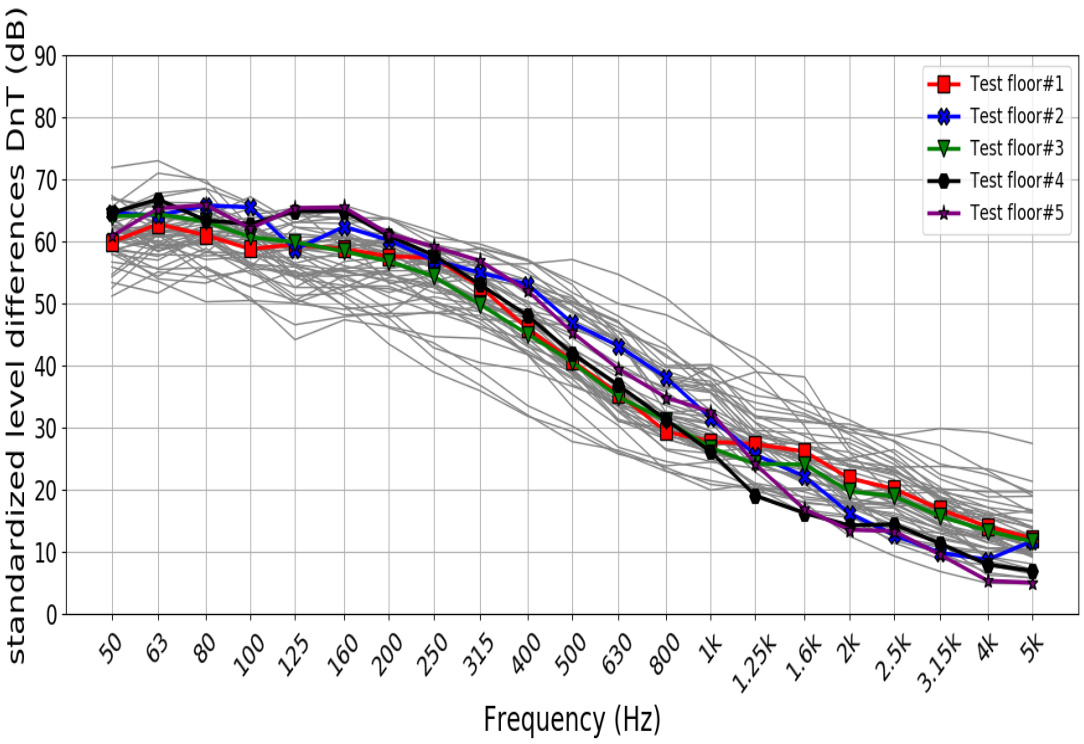

Figure C2: Field sound insulation measurements for standardized impact sound pressure level curves. Curves in gray represent curves that are utilized to train and validate the network model.

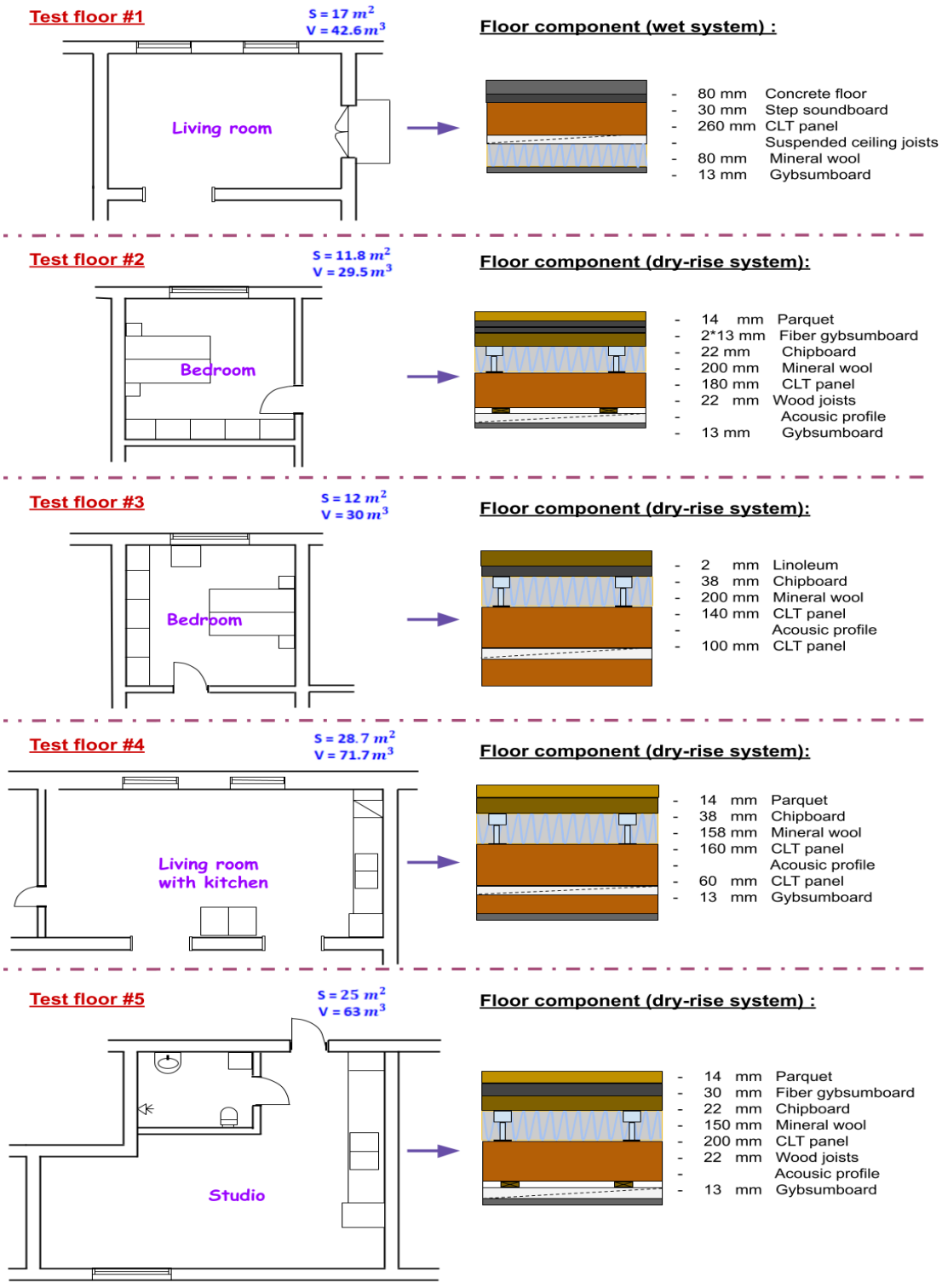

Figure C3: A schematic layout and section drawing of each test floor structure shows the function of each room, surface area (S), volume of the receiving room (V), and floor configurations.